Republic of Iraq
Ministry of Higher Education
and Scientific Research
University of Misan
Faculty of Engineering
Civil Engineering Department

Flexural Behavior of Tubular Continuous Ultra High Performance Concrete Beams

A Thesis
Submitted to The College of Engineering in The University of Misan in Partial Fulfillment of the Requirements for the Degree of Master of Science in Civil Engineering
(Structures Engineering)

By
Mohammad Shnawa Jasim
(B.Sc. in Civil Engineering, 2012)

Supervised By :
Dr.Nasser Hakeem Tu'ma

March 2022 A.D Rajab 1443 A.H

بسم الله الرحمن الرحيم

" فَتَعَالَى اللَّهُ الْمَلِكُ الْحَقُّ ۗ وَلَا تَعْجَلْ بِالْقُرْآنِ
مِن قَبْلِ أَن يُقْضَىٰ إِلَيْكَ وَحْيُهُ ۖ وَقُل رَّبِّ
زِدْنِي عِلْمًا "

صدق الله العلي العظيم

(القرآن الكريم - سورة طه - الآية ١١٤)

DEDICATION

To her who left my life and stay live in my heart and left the beautiful effect and she was wishing in her live to see this great moment ,(my mother) may god have mercy.

To the spontaneous soul …my father

To my great supervisor ….Dr.Nasser.Hakeem

To the icon of happiness…..my wife

To the pleasure of life …..my childreen

To my support in life …..my brother Haider

I offer you that humble work ….thank you so much

Certification of the supervisor

I certify that this thesis entitled "**Flexural behavior of tubular continuous ultra high performance concrete beams**", which is being submitted by **Mohammad Shnawa Jasim**,was made under my supervision at University of Misan /College of Engineering, in partial fulfillment of the requirements for the Degree of master of science in Civil Engineering (Structures).

Signature:
Name: Dr. Naser Hakeem Tu'ma
(Supervisor)

In view of the available recommendations, I forward this thesis for debate by the examining committee.

Signature:
Name: Asst. Prof. Dr. Samir Mohammed Chasib
Head of the Civil Engineering Department /University of Misan

ACKNOWLEDGEMENTS

In the name of Allah, the most gracious, the most merciful

All thanks and praise to ALLAH to give me the ability and the insisting on complete this work despite all the difficulties that have faced me .

To the person that shared the life with me with its sweet and its bitter and passing together all the difficulties of the study stages, my dear wife, to my soul (my kids).

All the words fail to express my immense gratitude to my advisor; Dr.Nasser Hakeem Tu'ma I. Said, for his guidance, encouragement and for the endless generosity and kindness he offered throughout his supervision of this research. Then thanks for Dr. Abbas Odah Dawwod, Dr. Saad Fahad ,Dr. Abdulkhaliq Abdulyima, Dr. Samir Mohammad

Also I wish to express my sincere thanks to the all staff of the undergraduate laboratories at Basrah University /Engineering College for their remarkable patience and for keeping all needed resources accessible during the long experimental work.

Special thanks are to all my friends in master stage espically Raad Saadoon, Majid Jafeer , Murtadhah Dafar , Fatma Sattar, for their assistant and support in the experimental work.

Finally I would like to express my sincere appreciation and thanks to everyone who helped me during the preparation of this thesis.

ABSTRACT

Service pathways are an important aspect of any structure. As a result, using structural elements with longitudinal holes is a good way to cover the demand for these paths while also providing other economic benefits. As a result, the hollow beams have two general structural and economic properties. The first is a benefit in terms of beam weight reduction. So, the current study aims to address this issue by reducing the amount of concrete while preserving and increasing its quality by choose a proper hole's dimension by calculations prepared for this purpose.

This study investigates the flexural behavior of continuous Ultra High Performance Concrete (UHPC)beams. Twelve tubular continuous supported beams were tested under two concentrated point loads at mid-spans. Three beams of each group were tubular, while the fourth beam was solid as a reference beam to comparison. The beams divided into three groups, the first group to investigate moment redistribution phenomenon, the second group to study the influence of steel fiber ratio change. The third group to know influence of reinforcement ratio change. Each beam had a total length (3000)mm, a clear of each span (1400) mm, a width (150) mm, and a depth (200)mm. The experimental work figures out when the first crack appeared, determine first crack load (Pcr). ultimate load (Pu), service deflection (Δs), maximum deflection (Δu), failure modes, load-deflection curves, cracks width , cracks patterns, ductility and strain distribution and determine the mechanical properties of UHPC and effect of heat curing where plays major role in improvement of mechanical properties by by manufacurated tank with three heater connect to electrical to curing the beams in the first three days.

Different tensile reinforcement ratios utilized, the elastic and experimental moments at failure were then compared to assess the ratio according to ACI code requirements. The experimental results proved that when used reinforcement ratio more than 0.5ρb caused an increased in (redistribution ratio > 20%) in both sagging regions (M^+)and hoggings region (M^-). Also the results showed that the hogging moment redistribution in the middle support is always 1arger than at mid-span and amount of moment redistribution was determined to be around 15%, which is 1ess than the 20% allowed by ACI-conditions.

The results exhibit improvement in first cracking load when increase steel fiber ratio from 1% to 1.5% and 2% at about 11.1% and 66.6% and increase in ultimate load at about 5.2% and 18.4%. Then when compared the tubular beam (1.5% steel fiber) with reference solid (1.5 % steel fiber) the increasing in ultimate failure load was(20%), in addition of increasing compressive strength. And the ultimate load was increased at about (2.6%,15.78%and 20.1%) as positive reinforcement ratio increased from 1% to 1.12% ,1.71% and 1% solid beam and when negative reinforcement increased from 0.78% to 1% ,1.4% and 0.78% solid beam respectively. The presence of longitudinal holes in continuous beams contributed to decreasing load carrying capacity, first crack load and deflections, by 5.2%, 18.2% and 13.5%. Despite the area ratio of the hole was (11.67%) from the whole area, therefore this ratio is proper to achieve flexural requirement and economical in the work.

LIST OF CONTENTS

LIST OF TABLES

LIST OF FIGURES

LIST OF SYMBOLS

A_s	Area of tensile steel (mm^2).
E_c	Modulus of elasticity of concrete (MPa).
E_s	Modulus of elasticity of steel (MPa).
$M_{u,exp}$	Experimental failure moment (kN.m).
M_e	Elastic moment (kN.m).
M_{exp}	Experimental moment (kN.m).
M_n	Nominal moment capacity (kN.m).
M_u	Factored moment at section (kN.m).
$N.A.$	Neutral axis depth (mm).
P_{exp}	Experimental failure load (kN).
$P_{u,a}$	Ultimate flexural load based on actual values (kN).
$P_{u,d}$	Ultimate flexural load based on design values (kN).
S_c	Crack spacing (mm).
b	Width of rectangular cross section (mm).
H	Height of rectangular cross section (mm).
c	Distance from extreme compression fiber to the neutral axis (mm)
c_b	Distance from extreme compression fiber to neutral axis at balanced strain condition (mm).

d	Distance from extreme compression fiber to centroid of tension reinforcement (mm).
d'	Controlling cover distance (mm).
d_b	Diameter of reinforcing bar (mm).
d_c	Thickness of concrete cover measured from extreme tension fiber to center of bar (mm).
f'_c	Specified compressive strength of concrete (MPa).
f_s	Allowable stress in steel reinforcement (MPa).
f_y	Yield strength of steel reinforcement bar (MPa).
f_r	Modulus of rupture in (MPa).
f_{cu}	Cube compressive strength in (MPa).
f_{sp}	Splitting tensile strength (MPa).
L	Length of tested beam (mm).
Sf	Silica fume content by cement weight
p	Applied load (kN).
p_{cr}	Cracking load (kN).
p_u	Ultimate applied load (kN).
t	Thickness of the cross-section (mm).
w	Maximum crack width (mm).
w_c	Crack width (mm).

α_1	The ratio of average stress of equivalent rectangular stress block to f'_c.
ε_c	Strain in concrete.
ε_{cu}	Ultimate strain in concrete.
ρ_b	Steel reinforcement ratio producing balanced strain conditions
ρ_{min}	Minimum reinforcement ratio for steel
σ_c	Concrete stress (MPa).
Vf	Volumetric steel fiber ratio
w/c	Water to cement ratio
w/b	Water to binder ratio
ϕ	Steel bar diameter (mm).
Δu	Maximum deflection (mm).
Δs	Service deflection (mm).

LIST OF ABBREVIATIONS

AASHTO	American Association of State Highway and Transportation Officials.
ACI	American Concrete Institute.
AFGC	Association Française de Génie Civil.
ASTM	American Society for Testing and Materials.
CSA	Canadian Standard Association.
CSH	Calcium silicate hydrate.
CSM	Crack sliding model.
EURO-CRETE	European Committee for Concrete.
GFRP	Glass Fiber Reinforced Polymer.
HRWRA	High-Range Water Reducers Admixture.
HSC	High Strength Concrete.
HT	Heat Treatment.
JSCE	Japan Society of Civil Engineers.
MR	Moment Redistribution.
RC	Reinforced Concrete.
RO	Reverse Osmosis.
RPC	Reactive Powder Concrete.
SF	Silica Fume.

SLS	Serviceability Limit State.
UHPC	Ultra High Performance Concrete.
ULS	Ultimate Limit State.
CFRP	Carbon Fiber Reinforced Polymers.
HPFRCC	High Performance Fiber Reinforced Cement Composite.
RCN	Reinforced Concrete and Normal spacing stirrups.
FHPS	Reinforced HPFRCC and special spacing stirrups.
PVC	Poly vinyl Chloride.
GI PIPE	Galvanized Iron Pipe.
LVDT	Linear Variable Differential Transformer

CHAPTER ONE: INTRODUCTION

1.1 GENERAL

Continuous concrete beams was considered as a statically indeterminate and utilized in structural designs when two or more span occur, common structural elements in all types of structures which along its length. These are often in the identical horizontal plane, and the spans between the supports are in one straight line It is provides resistance to bending when applied the load; at least one of the supports of it should be able to develop a reaction along the beam axis [1].

Continuous beams occur frequently in cast in situ construction when a single span of construction is connected to an adjoining span also commonly used in bridges. Bending moment of continuous beams does not confine to a single span just but it will affect the whole system. Also it is a structural component that gives resistance to bending when a load is applied. These beams are popularly used in bridges [2].

When continuous concrete beams are used over interior supports, they increase flexural rigidity by providing an alternated load path among the beams, because the continuity tends to decrease the top value moment on a beam and make it stiffer, this alternate load path leads to reduced moments and stresses at mid spans, resulting in shallower beams that are stronger than simply supported beams of equal span and with less deflection [3].

One of the examples of the continuous beam that forms from ultra-high performance concrete the bridge in Mexico. Yet NM Bridge No. 9706 is a very unique structure that won the New Mexico Chapter American Concrete Institute's super in Concrete competition in 2017. It is the first superstructure for a bridge in

the state made from UHPC, and consider the first bridge structure in the nation made from UHPC [4] as shown in Figure 1.1.

Figure 1.1: Two span bridge from UHPC in Anthony, New Mexico [4]

1.2 Advantages and Disadvantages of Continuous Beam

Any structural element in construction world has advantages and disadvantages, so what seeking about is the least affecting, therefore the comparison between the continuous beam and simply supported beam as follow [5] :

1. The continuous beams are produce moments in span are a lot lesser than simply supported beams which in turn results in smaller sections.

2. For the same span and section, the perpendicular load capacity of continuous beam is higher and the mid span deflection is lower.

3. Utilized moment-redistribution to attain an optimal section without congestion of reinforcement at supports and to attain an alternate load pathway .

4. The depth at a section can be lesser in same span because of the deflection and bending stress are lesser then provide economical in material.

5. It permit much larger spans or distance between supports.

6. The net bending moment is lower, in a continuous beam and due to negative end moments, mid span moment (in a simply supported beam) would be lesser; as a result of the design for the maximum bending moment (which would be lesser in continuous beams).

The other side there are disadvantages of continuous beam as follow[5] :

1. Reversal of moment because of seismic force requires suitable analysis and design.

2. Difficulties in construction mostly that deals with precast structure or member.

3.The shear force and max moment nearby the supports requires proper detailing of bar reinforcement.

4. Secondary stresses develop because the time dependent effect such as shrinkage, creep and variations of temperature .

1.3 Estimate Structure Elements with Tubular Core

In the present work, consider pipes and ducts are necessary to confirm essential in a buildings. Structural engineering was looked for an structural element that has a function of passing services in order to provide the complete comfort of the user by making the buildings equipped with all types of services. The hollow core in the elements passing services through it with different types of services (plumbing pipes, electrical ducts and cooling/heating ducts) as shown in in Figure 1.2, due to its properties as a structural function with concrete and economic and services function in reducing the element dead-weight and passing the services. One of the

positives of the development of this type of structural element will give an increase in structural strength and saving the weight with control the deflection [6].

Figure 1.2 Concrete-Hollow-Core [6]

This type of structural elements has several advantages :

- In addition to its structural function, it provides safe and isolated access to service pipelines and protects against environmental damages.
- Compared with the solid beam, this element has a greater economic benefit in terms of reducing the quantities of concrete to the presence of hollow core and also reduce the dead weight of the beam element.

The following disadvantages can be summarized as :

- On-site casting requires high precision and high-quality control unless the use of modern concrete free of coarse gravel for easy flow of the mixture in the composite mold.
- This type of structural element may costly as a result of the complex construction process but on the other hand, it is considered an economical to maintain the money related to service runs repairs, a hollow section was construct from cork material as shown in Figure 1.3.

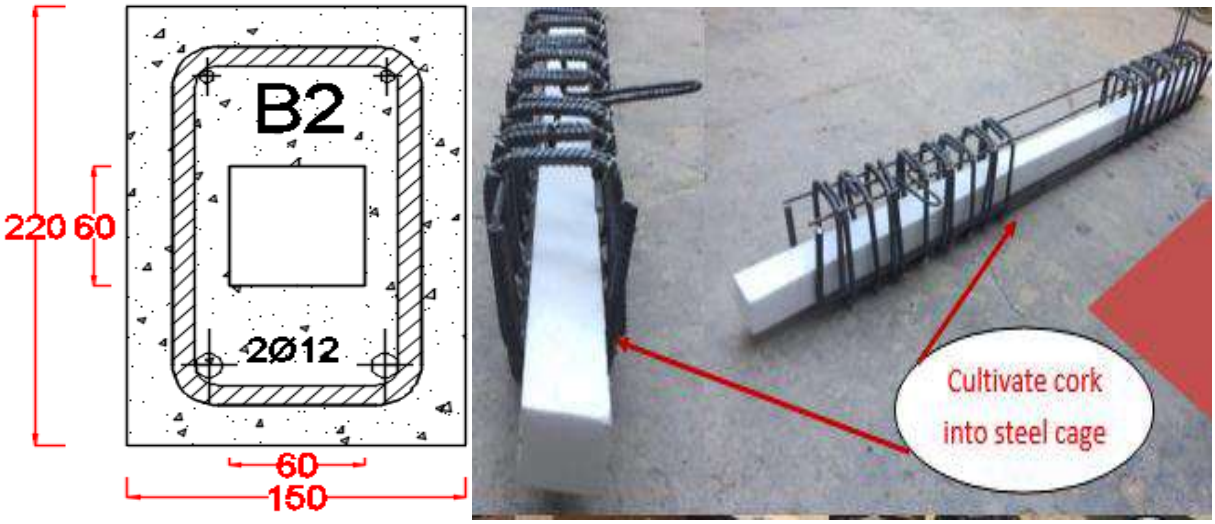

Figure 1.3 Study effect of hole longitudinal on behavior of beam [7]

1.4 Ultra High Performance Concrete

In the 1990s France, High Performance Concrete (HPC) was deemed to be the stiffest cement based material with a compressive strength of approximately (70 MPa) and a flexural strength at about (10 MPa), then begin development because the engineers are now using higher compressive strength limit in their designs, which led to the need for production of new concrete types that differ from ordinary concrete. Several experiments have been conducted to reduce the water content to a minimum and to add new plasticizers to increase the workability of the mixture without adding excess water. Other experiments have been performed to increase compressive strength by substituting a percentage of the cement used with pozzolanic materials such as silica fume. In addition to the use of these additives materials, the methods of curing the concrete after casting have been changed by developing new methods of treatment, including heat treatment used in ultra-high-performance concrete mixture (UHPC) and pressure treatment by pre-setting the concrete mix. Ultra-High Performance Concrete (UHPC) that can reach

compressive strengths higher than (200 MPa) and tensile strengths of about (50 MPa). UHPC's high durability, which fundamentally begin from its resistance against all kinds of corrosion, increases the design life of a project and reduces the maintenance cost. For example, UHPC has an extremely low permeability against chloride breakthrough high strength, high ductility, high durability, limited shrinkage [7].

UHPC is a mixture of cement, silica fume, fine sand, high range water reducer, water and steel fibers without coarse aggregate to enhance the homogeneity.

Richard and Cheyrezy(1995) [8] gave the following issues to develop RPC:

1. Utilized fine sand, without using gravel, to progress the concrete's consistency.
2. Existing the silica fume to increasing the pozzolanic reaction.
3. Getting the optimized granular mixture ,packing volume.
4. Increasing the compaction status by used pre-setting pressure.
5. Heat curing to amelioration the microstructure .
6. Utilized of steel fibers to promote the ductility.

1.5 Properties of UHPC

When compared UHPC with normal concrete will know the important properties that distinguish UHPC that consider leap in concrete technology world and the main properties of UHPC [9]:

- UHPC consider more homogeneous than normal concrete because of excellent packing density and confined used of coarse aggregate. The difference in size and strength between coares and fine aggregate is so tiny.
- Ultra-high performance concrete (UHPC) is a modern composite material with extremely good mechanical characteristics.

- UHPC shows ductile material conduct and its tensile effecting can be remarkably improved.
- Nanomaterial that found UHPC accelerate,s the hydration of cement, condenses the microstructure, increase strength, and then participate to its durability
- Low permeability.
- The compressive strength of UHPC is 10 times that of conventional concrete.
- UHPC 's density is optimized
- From the experience and past study that safety factor of UHPC is very high.
- UHPC show super abrasion resistance, approximately twice as resistant as ordinary concrete.
- The feature of UHPC identical to hard rock.
- UHPC often is made with fine sand, cement, high-strength steel fibers, a high amount of SF, and low w/c (w/c ratio less than 0.20).

1.6 Structures' Performance Determination

For structures of today, we're looking for material have four discriminatory characteristics: (strength, durability, workability, and affordability), the first three characteristics essentially comprise whole eight requirements of performance mentioned above, affordability means cost, when says high performance, refers to refinement in some or whole of those characteristics. Occasionally, one's has to give-up a little in the one to a little gain in other. Those four properties as follow:

1.6.1 Strength

High strength show material saving; then give two advantages the first is less weight and the second is less material because when exist less weight this lead to decreasing material demand according to much studies to investigate this effect[10].

1.6.2 Durability

When seeking about material that have durable and reduce maintenance effort this lead to increase the design life of the materials and the durability of UHPC effected by concrete's resistance to fluid penetration. UHPC shows good behavior in this field[10].

1.6.3 Workability

Concrete’s workability is board and subjective term describing how easily freshly mixed concrete could be mixed, placed, consolidated and finished with least damage of homogeneity. Workability is peculiarity that directly impacts strength, quality, appearance, and even labors’ costs.

1.6.4 Cost

The cost consider important actor to determine if the structures will be construct or no. The cost of production of UHPC is more than normal concrete approximately 3-10 times , therefore it utilized in important and vitality project.

1.7 Uses of UHPC

In the last years, UHPC enter in much working such as, artwork, precast elements, pedestrian bridges, and a few highway bridges in USA. Many different applications in Europe, Canada, Australia and Asia as shown in Table 1.1, specially constructed in transportation industry. Sherbrooke pedestrian bridge, was constructed in Quebec, Canada. The 197 foot long structure is a post tension open space truss as shown in Figure 1.4.

In 1997 UHPC's durability received a test when it was used replace steel beams that intended to replace in the cooling towers of the Cattenom power plant, in France. The environment is extremely corrosive and UHPC was pick out due its durability properties and the possibility of elimination the maintenance. Other transit applications include footbridges constructed in South Korea, Japan, France, and Germany. The Footbridge of Peace in Seoul, South Kore as shown in a Figure 1.5, is an arch-bridge with a span of 394 ft (120 m), arch height of only 49 ft , and a deck thickness varying anywhere between 1.2 in. and 4 in. In Japan, the Sakata-Mirai footbridge was completed in 2002 and demonstrated how a perforated webs in a UHPC. France utilized UHPC's fire resistant capabilities and high load carrying properties to construct an aesthetically pleasing yet, highly fire resistant footbridge at a Chryso Plant in Rhodia . Most recently, the Gärtnerplatz Bridge was completed in Kassel, Germany [10].

Table 1.1 Application of UHPC in Asia[11]

Name	Country	Year
Kuyshu Express way bridge	Japan	----
Riverside Senshu footbridge, Negaoka-shi	Japan	----
Sakata –Mirai footbridge ,Sakata	Japan	2002
Akakura Onsen	Japan	2004
Yukemuri pedestrian bridge	Japan	2004
Yamagata	Japan	2004
Tahara bridge Aichi	Japan	2004
Horikoshi Highway C-ramp Fukuoka	Japan	2005
Keio University footbridge Tokyo	Japan	2005
Toriska River Highway bridge Hokkaido	Japan	2006
Toyota City Gymnasimn footbridge Aichi	Japan	2007
Sungai Muar bridge	Malaysia	----
Papatoetoe footbridge	New Zeland	2005
Five pedestrian bridge, Auckland	New Zeland	2006
Seonyu Sunyudo footbridge Seoul	South Korea	2002
Kampung Linsum bridge	Malaysia	----
GSE bridge Tokyo Airport	Japan	2007
Tokyo Monorail	Japan	2006
Torisologawa bridge	Japan	2009
Akasaka Yogenzaka footbridge	Japan	2008

Figure 1.4 World's First UHPC bridge -Sherbrook Pedestrian Bridge [10].

Figure 1.5 UHPC 's applications around the world [11].

1.8 Research Objectives

The objectives of the current study is to identify the structural flexural behavior (tubular continuous reinforced UHPC beams) by applying two-point

flexural loads, and recording all the readings resulting from loading in terms of deflections, maximum load capacity and etc. This study effort to accomplish the following objectives:

1- Study effect of the presence of the hollow in the continuous concrete beam sections and compared with solid continuous beam by making longitudinal hole through using cork material.
2- Study effect of changing steel fiber ratio on the behavior of concrete section.
3- Explore effect of changing the longitudinal reinforcement ratios on the behavior of concrete section.
4- Studying moment redistribution in practical and compared with theory studying according to ACI-Code.
5- Explore the toughness, ductility index, stiffness and load-strain for different tubular continuous beams.

1.9 Outline of Thesis

Chapter one: Representing introduction, advantage of continuous beam and disadvantage, application of UHPC, study objective and outline of thesis.

Chapter two: Shows previous studies that related on the UHPC and moment redistribution of UHPC continuous beam**.**

Chapter three: Describing the experimental work of design of UHPC mix and continuous beam test begin from mix, casting and curing , mechanical properties of UHPC beam and study flexural behavior of tubular continuous beams.

Chapter four: Shows test of continuous beam and record the results of experimental work in sence of cracks, deflections, load capacity and the results discussion.

Chapter five: Provides a summary for this work and its conclusions with a specified proposal for future work.

CHAPTER TWO: LITERATURE REVIEW

2.1 General

UHPC is a ductile, high-strength material made from a mixture of powders (portland cement, silica fume, fine sand , high-range water reducer, water, and steel fiber. UHPC mixtures having compressive strength, flexural strength and modulus of elasticity of more than 100 MPa, 10 MPa and 50 GPa ; respectively have been developed (Acker and Behloul 2004)[12]. UHPC has several advantages, including the capacity to be essentially self-contained, building speed, and improved aesthetics, as well as superior corrosion, abrasion, and impact resistance, all of which translate to lower maintenance and a longer life term for the structure. Improved micro-structural features of the matrix give UHPC better durability qualities. In comparison to normal concrete, UHPC has a compressive strength of ten times. UHPC is gaining traction in a number of nations, with applications including bridges, construction, repair rehabilitation, architectural features, off-shore constructions, and overlay materials. The use of UHPC for bridges and bridge components may be found in a variety of countries, including the United States, France, Japan, Germany, Denmark, Australia, China, Italy, Austria, Canada, Malaysia, Czech Republic, Netherlands, Slovenia, Korea, Switzerland and New Zealand. UHPC with high compressive strength, and durability improving exemplify a concrete technology's quantum leap. UHPC material is offer interesting implementations diversity. It allows the economic buildings and sustainable to constructed with an exceptional slender design. Its ductility and strength make it definitive building material [7].

2.2 Historical Background and Development of UHPC

The goal in the early 1980s was to create fine-grained concretes with a very dense and "uniform cement matrix, which would prevent the formation of micro - cracks within the structure when it was loaded. They were dubbed "Reactive Powder Concretes (RPC)" because of the small grain size (less than 1 mm) and high packing density (due to the use of various inert or reactive mineral additives). (Richard and Cheyrezy 1995)[8]. Meanwhile, a wider range of formulas existed, and the name Ultra High Performance Concrete (UHPC) was coined to describe concretes with compressive strength up to 150 N/mm^2 over the world. It was largely employed in the security business for specialized applications like as vaults, "strong rooms," and defensive defense structures. The first research and development efforts aimed at using UHPC in construction began about 1985. Since then, other technical solutions have been developed sequentially or concurrently: UHPC precast elements that are heavily (conventionally) reinforced for bridge decks; in situ applications for the rehabilitation of deteriorated concrete bridges and industrial floors (Buitelaar 2004)[13]; ductile fiber reinforced fine grained "Reactive Powder Concrete" (RPC) like "Ductal" produced by Lafarge in France or Densit produced in Denmark (Acker and Behloul 2004)[12].With or without additional “passive” reinforcement it is used for precast elements and other applications like offshore bucked foundations. Furthermore, coarse-grained UHPC using artificial or natural high-strength aggregates has been created, for example, for highly loaded columns and extremely high-rise structures (Schmidt et al. 2003)[14]. Nowadays, a growing number of formulas are available, each of which can be tailored to match the unique needs of a certain design, construction, or architectural approach. The first prestressed hybride pedestrian bridge was built in Sherbrooke, Canada, in 1997, as was the replacement of steel portions of the cooling tower at Cattenom, and two 20.50 and 22.50 m long road bridges for

automobiles and trucks were built in Bourg-lès-Valence, France, in 2001 (Hajar et al. 2004)[15]. See Figure 2.1. The UHPC was reinforced with 2 to 3% vol. steel fibers of various types for these projects. The toll-gate of the Millau Viaduct in France is a stunning example of architectural design that takes advantage of UHPC's unique advantages "Construction is under underway. Figure 2.2, shows the exquisite roof, which is 98 meters long and 28 meters wide with a maximum thickness of 85 centimeters in the center and looks like a huge twisted sheet of paper (Resplendino 2004)[16]. UHPC's increased durability and mechanical qualities, particularly flexural strength, toughness, impact strength, fatigue resistance, and reduced vulnerability to cracking/spalling, have contributed to this achievement.

UHPC was divided into two classes: UHPC200 and UHPC800, with nominal compressive strengths of 200 and 800 MPa, respectively, and attributes listed in Table 2.1. Each class has its own fabrication procedures, properties, and can be utilized for a variety of structural and non-structural purposes. The materials used in both classes are the same (Portland cement, fine sand with particles ranging from 150 to 600 microns, silica fume, superplasticizer, steel fibers, and water). UHPC 200 can be produced and cast in a similar manner to conventional high performance concrete. The lower compressive strength (170MPa) results from curing the concrete at ambient temperature, whereas the greater compressive strength (230MPa) results from hot water or steam curing at 80-90°C for 48 hours after two days of pre-curing at ambient temperature. UHPC800 must be dried in the air at temperatures over 250°C. Before and during setting, the material is pressured. Steel powder can be used instead of quartz sand to achieve compressive strengths of up to 810 MPa.

In (Bouygues) company where they publish the first publication in 1994 developed UHPC200 which gives compressive strength up to 200 MPa, and in

1995, they publish second publication in which the concrete type UHPC800, which has a compressive strength up to 800 MPa, so there are two types of UHPC and each type has a different mixing method, different mixture ratios, different treatment methods, and different result properties. The characteristics and components of these two types explain in Table 2.2.

Table 2.1 Properties of UHPC produced by Richard and Cheryezy[8].

Property	**RPC200**	**RPC800**
Presetting	no pressurization	50 N/mm^2
Treatment by heat	20 - 90 ºC (for 48 h)	250 - 400 Cº
Compressive strength	170 - 230 N/mm^2	490 - 680 MPa (using quartz sand) 650-810 MPa.
Flexural strength	30 - 60 N/mm^2	45 - 141 N/mm^2
Young´s modulus	50 - 60 GPa	65 - 75 GPa

Table 2.2 Comparison between UHPC200 and UHPC800[8].

	UHPC 200				UHPC 800	
Composition	Non-Fibered		Fibered		Silica Fume	Steel aggregate
Portland Cement	1	1	1	1	1	1
Silica Fume	0.25	0.23	0.25	0.23	0.23	0.23
Sand 150-600 *mm*	1.1	1.1	1.1	1.1	0.5	-
Superplasticizer	0.016	0.019	0.016	0.019	0.019	0.019
Steel fiber 12mm	-	-	0.175	0.175	-	-
Steel fiber L=3mm	-	-	-	-	0.63	0.63
Steel agg. 800 mm	-	-	-	-	-	1.49
Water	0.15	0.17	0.17	0.19	0.19	0.19
Compacting pressure	-	-	-	-	50MPa	50MPa
Heat curing temp.	20	90	20	90	250-400	250-400

Figure 2.1 Sakata-Mirai Pedestrian Bridge in Japan, 2002[11].

Figure 2.2 Toll-Gate Millau Viaduct in France[11].

2.3 Effect of Heat Treatment (curing) on UHPC beam's properties

In order to improve the concrete mix properties, so in this type of concrete thermal treatment is used after the casting process. It increases the compressive, flexural and tensile strength as well as increase the durability and resistance of chloride ion penetrability. The amount of increase in these properties depends on the quantity of temperature and the of heat treatment during because the thermal treatment reduces the permeability of the concrete mix. The use of heat treatment and the delay of vapor deposition have a positive effect on the behavior of concrete by decreasing the creep of concrete, because the previous researchers found that the increase of temperature and the thermal curing period leads to formation of (C-

S-H) in large quantities, which is responsible for increasing the adhesion between cement and aggregate, which leads to increase the concrete strength.

Jungwirth et al. 2002 [18], investigate the effect of using 90° heat treatment on tesile strength and compression strength of the UHPC mixture and compared the results with 20° C water treatment for samples. The mixture proportions were used (638 kg/m^3 of cement, 239 kg/m^3 silica fume, 1085 kg/m^3 furnace slag sand, 157 kg/m^3 metallic fibers with l/d 25/0.16, w/c of 0.23 and 23.7 kg/m^3 of superplasticizer). The usage of a 90 °C heat treatment increased compressive strength from 120 to 180 MPa and flexural strength from 25 to 45 MPa, according to the findings.

Canadian Highway Bridge Desig Code et al. 2019[17], heat treatment(HT) and high homogeneity of materials because of using a extra fine aggregate (sand) only, participate to eliminated initiation of extensive the soon age cracks those're UHPC's major disadvantage. Those lead to get superior UHPC's mechanical properties, like very, high tensile and compressive strengths, high ductility, high modulus of- elasticity, and fatigue strength will be high too.

2.4 Previous Studies in Moment Redistribution in Continuous Beams

Scott and Whittle et al. 2005[26], at the service limit state, the redistribution of moment has been examined (SLS). After testing 33 two-span beams, it was discovered that a significant amount of moment redistribution occurs at the service limit state. The real stiffness at the service limit state differs from what was assumed when the moment for the final limit state was calculated. It's due to modifications in the reinforcement layout along the member. The studies also indicate that the reinforcing arrangement (big vs. small bars) was not a significant determinant in moment redistribution.

Mostofi Nejad et al. 2007[21], a parametric research was carried out on moment redistribution in continuous RC beams with equal spans under uniform stress. Using ductility demand and ductility capacity principles, the governing equation for the permissible percent of moment redistribution was first derived. The impacts of several parameters on moment redistribution were then explored, including concrete compressive strength, the amount and strength of reinforcing steel, the magnitude of elastic moment at the support, and the ratio of the length to the effective depth of the continuous beam. According to the findings, while the permissible moment redistribution in continuous reinforced concrete beams based on current code requirements is not in a safe margin in some scenarios, it is conservative in the majority of cases.

Maghsoudi et al,2009[20] the moment redistribution and flexural behavior of a carbon-fiber-strengthened continuous reinforced high-strength concrete beam (HSC) were examined. They came to the conclusion that as the number of CFRP layers is raised, the ultimate strength, ductility, moment redistribution, and ultimate strength of CFRP sheets decrease. For the studied specimens, an analytical model for moment–curvature and load capacity was constructed and employed. The experiment and predicted values were found to be in good agreement**.**

M.Reza et al. 2010[10], in UHPC the subject of flexural redistribution was studied. Four beams, each measuring roughly 50 in x 4 in x 4in, were put to the test. Two focused loads were given at around the middle of two spans supported at three places in the experiments. The amount of moment redistribution from the center support into the spans was determined to be around 14%, which is less than the 20% allowed by ACI 318–08 building code requirements for conventional concrete.

Bagge et al.2014[23], the influence of longitudinal and transverse reinforcement ratios, as well as concrete strength, on moment redistribution in RC beams was examined. Even at modest stress levels, the experimental examination revealed significantly nonlinear structural behavior of the tested beams, with moment distributions that differed from linear elastic analysis. The longitudinal reinforcement arrangement had a significant impact on the evolution of moment redistribution and the degree of moment redistribution at the ultimate limit state (ULS), whereas the transverse reinforcement ratio had a minor impact up to the longitudinal reinforcing steel yielding, with the concrete strength slightly reducing the degree of moment redistribution.

ACI 318-14[25], a maximum of 20% of the negative moment at the support should be redistributed into the span. The increase in positive moment areas is caused by a decrease in factored negative moment. Redistribution of moment is limited to 20% in the ACI 318–14 for both positive and negative moments. The following ACI 318–14 articles deal with flexural redistribution:

1 – Except where approximate moment values are used, factored moments calculated by elastic theory at sections of maximum negative or maximum positive moment in any span of continuous flexural members for any assumed loading arrangement may be reduced by not more than $1000\varepsilon_t$ percent, with a maximum of 20%.

2 – When (t) is equal to or greater than 0.0075 at the part where the moment is reduced is it necessary to redistribute the moments.

3 – For all other sections inside spans, the lowered moment will be utilized to calculate redistributed moments. After redistribution of moments for each loading configuration, static equilibrium must be maintained.

Visintin et al. 2018[22], the redistribution of moment in ultra-high performance fiber reinforced concrete beams was explored. The findings of the experiment reveal that the observed moment redistribution was bigger than the code predictions for beams with the hinge created at the support. The observed moment redistribution was less than the codes predicted for the beam where the hinge developed under the load sites. As a result, the findings revealed that current design standards for UHPFRC beams may not always provide a conservative prediction of moment redistribution.

Frank Küsel et al. 2019[19], investigated to learn about the effect of steel fibers on moment redistribution in reinforced concrete beams. The findings of 15 two-span continuous beams, each with a different combination of steel fibers and reinforcing bars, showed considerable moment redistribution prior to plastic behavior. In terms of moment redistribution, a 1.5% fiber content corresponded to a flatter post-peak moment-curvature relationship. The addition of fibers resulted in lower deflections, with fiber effectiveness improving as the reinforcing ratios were increased.

R. Ehsani et al. 2019[24], investigated the ductility and moment redistribution of The specimens have a rectangular cross section of 250 mm (height) 200 mm (width) and are continuous across two spans of 1800 mm each, with two concentrated equal statically monotonic loads (from zero to failure) applied at the mid-span of each beam. Two of the beams were regular concrete with two alternative stirrup configurations in the middle support (hogging) and mid span (sagging) areas, while the other two beams were companion but constructed entirely of HPFRCC composites.

In comparison to a reference beam, the use of HPFRCC layers in section beams and a reduction in stirrup spacing boosted the ultimate load, ductility ratio, plastic

hinge properties, and moment redistribution capability of these beams. In comparison to the RCN beam, FHPS had the highest load carrying capability of 42 percent. In comparison to the reference beam, the FHPS beam had the highest moment redistribution values of roughly 23.31 percent and the highest displacement ductility ratio of 1.8. Without local shear cracks, sufficient shear strength is obtained in HPFRCC beams. This allows for the development of plastic hinges in beams and the formation of a plastic hinge zone.

2.5 Modulus of elasticity of UHPC

In order to simplified the process of quality control of the concrete structure, so many international codes and researchers have developed equations that connect compressive strength with the modulus of elasticity through scalar factors. Table 2.3 shows the recommendations for the UHPC modulus of elasticity.

Table 2.3 Compressive Strength and (E) Relationship.

References	Equations related fc' with E_c
ACI 318[27]	E=4700 $\sqrt{fc}'$ in SI units for (normal strength and normal weight concrete) E= $w_c^{1.5}(0.043)\sqrt{fc}'$ (w_c is the unit weight concrete(1500-2500) kg/m) .. In case UHPC [59] w_c=2480 → E=5311 $\sqrt{fc'}$
Kakizaki et al [56]	E=3650*$\sqrt{fc'}$ in SI units for fc′ (83-138)Mpa
ACI 363R-92 [28]	E=3320*$\sqrt{fc'}$ +6900 for high strength concrete fc′ ≥ 83MPa
Ma et al [57]	E=525000* $\sqrt{\frac{fc}{10}}$ for UHPC with no coarse aggregate
FHA [29]	E=46200*$\sqrt{fc'}$ for fc′ ≥193MPa
AFGC[31]	E=50 GPa
JSCE[30]	E=50 GPa
Gowriplan[33]	E=50 GPa

Samir[34]	E=4572*$\sqrt{fc'}$ for fc′ (79-119)MPa
Maha [35]	E=[(S_1-S_2)/(ε_2= -0.00005)] , S_1= Stress with 40% of ultimate -load,;MPa S_2=Stress with longitudinal -strain (0.00005);MPa ε_2= longitude strain `produced by stress ,$S2$
Mahesh[36]	E=3.65*$\sqrt{fc'}$ (Mahesh found E_c of UHPC increased with time especially when using thermal treatment)

2.6 Nominal Bending Moment Capacity of UHPC Beams

There are no many international codes mention the nominal capacity of the (UHPC) sections, but some codes and some researchers proposed equations to estimate the capacity of the section. The difference between these equations is in the simplification of the stress block of compression and tension, some equations simplify the actual stress block to (a rectangle) stress block and some of them simplify the actual stress block to (a triangle and a square) stress block.

Nasser et al. 2016 [37], carried out the theoretical nominal moment based on JSCE and simplify actual stress block to the rectangular stress block.

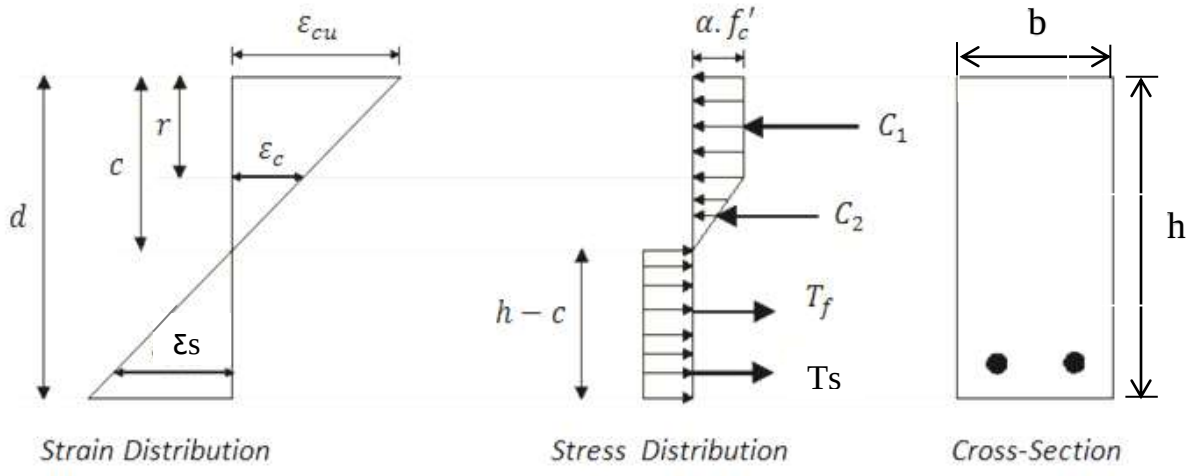

Figure 2.3 Stress-strain distribution by Hakeem [45].

$C_1 = \propto . f'_c . b . r \quad , \quad r = \left(1 - \frac{\varepsilon_c}{\varepsilon_{cu}}\right) * c = \left[1 - \frac{\propto . f'_c .}{\varepsilon_{cu} . E_c}\right] * c$

$c = \frac{\varepsilon_{cu}}{\varepsilon_{cu} + \varepsilon_{FRP}} * d \implies c = \frac{\varepsilon_{cu}}{(\varepsilon_{cu} + \frac{f_{FRP}}{E_{FRP}})} d$ sub (r,c) in C1

$$C_1 = \propto . f'_c . b . \left[1 - \frac{\propto . f'_c}{\varepsilon_{cu} . E_c}\right] * \frac{\varepsilon_{cu}}{\varepsilon_{cu} + \frac{f_{FRP}}{E_{FRP}}} * d \quad \ldots\ldots\ldots (2\text{-}1)$$

$C_2 = \frac{1}{2}(c - r) * \propto . f'_c . b$, sub (r) ,(c) in C2

$$C_2 = \frac{1}{2} * \frac{(\propto . f'_c)^2}{\varepsilon_{cu} . E_c} . b . \frac{\varepsilon_{cu}}{(\varepsilon_{cu} + f_{FRP})} * d \quad \ldots\ldots\ldots\ldots (2\text{-}2)$$

$T_f = 0.4 * \sqrt{f'_c} * b . (h - c)$,sub (c) in Tf

$$T_f = 0.4 * \sqrt{f'_c} . b . [h - \frac{\varepsilon_{cu} . d}{\left(\varepsilon_{cu} + \frac{f_{FRP}}{E_{FRP}}\right)}] \quad \ldots\ldots\ldots (2\text{-}3)$$

$$T_{FRP} = A_{FRP} \, x f_{FRP} \quad \ldots\ldots (2\text{-}4)$$

$(\sum T = \sum C)$

$$\propto . f'_c . b . \left[1 - \frac{\propto . f'_c}{\varepsilon_{cu} . E_c}\right] . \frac{\varepsilon_{cu} . d}{\left(\varepsilon_{cu} + \frac{f_{FRP}}{E_{FRP}}\right)} + \frac{1}{2} . \frac{(\propto . f'_c)^2}{\varepsilon_{cu} . E_c} . b . \frac{\varepsilon_{cu}}{\left(\varepsilon_{cu} + \frac{f_{FRP}}{E_{FRP}}\right)} . d = A_{FRP} *$$

$$f_{FRP} + 0.4 * \sqrt{f'_c} . b . [h - \frac{\varepsilon_{cu}}{\left(\varepsilon_{cu} + \frac{f_{FRP}}{E_{FRP}}\right)} . d]$$

By Multiplying by $(\varepsilon_{cu} + \frac{f_{FRP}}{E_{FRP}})$

$$\propto . f'_c . b . \varepsilon_{cu} . d \left(1 - \frac{\propto . f'_c}{\varepsilon_{cu} . E_c}\right) + \frac{1}{2} . \frac{(\propto . f'_c)^2}{E_c} . b . d = 0.4 . \sqrt{f'_c} . b . h . \left(\varepsilon_{cu} + \frac{f_{FRP}}{E_{FRP}}\right)$$

$-0.4 . \sqrt{f'_c} . b . \varepsilon_{cu} . d + A_{FRP} . f_{FRP} (\varepsilon_{cu} + \frac{f_{FRP}}{E_{FRP}})$ after simplified we get :

$$\propto . f_c' . b . \varepsilon_{cu} . d \left(1 - \frac{\propto . f_c'}{\varepsilon_{cu} . E_c}\right) + \frac{1}{2} . \frac{(\propto . f_c')^2}{E_c} . b . d = 0.4 . \sqrt{f_c'} . b . h . (\varepsilon_{cu}) + 0.4 . \sqrt{f_c'} . b . h . (\varepsilon_{cu})$$

$$-0.4 . \sqrt{f_c'} . b . \varepsilon_{cu} . d + A_{FRP} . f_{FRP} (\varepsilon_{cu} + A_{FRP} . \varepsilon_{cu} . \frac{{f_{FRP}}^2}{E_F} \quad \ldots\ldots\ldots (2\text{-}5)$$

$$M_n = C_1 * (c - \frac{r}{2}) + \frac{2}{3} * C_2 * (c - r) + \frac{1}{2} * T_f * (h - c) + f_{FRP} * A_{FRP} * (d - c) \ldots (2\text{-}6)$$

Danha et al.2012[38], simplify the actual stress block to rectangular and triangular stress block:

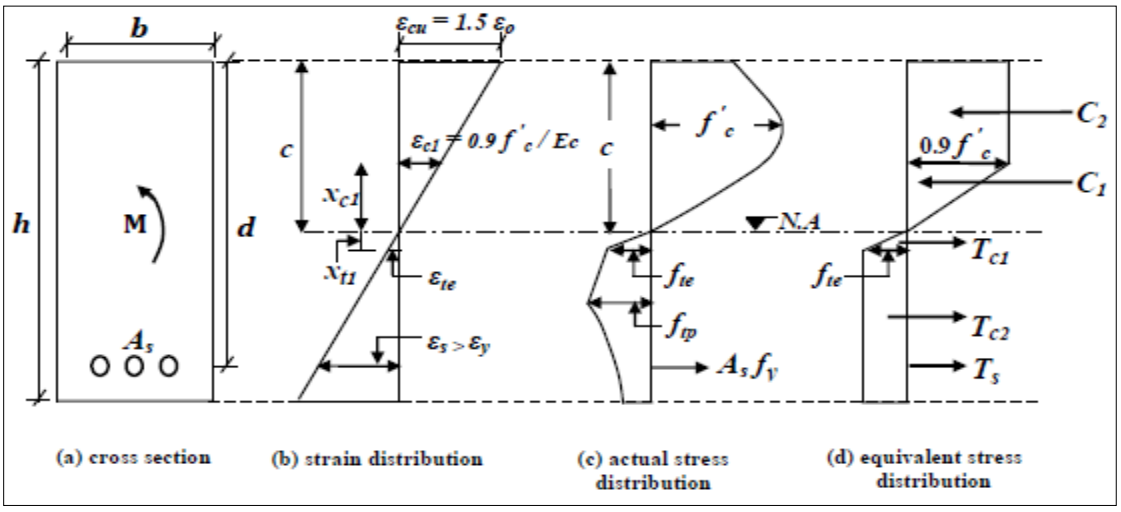

Figure 2.4 Stress-strain distribution by Danha[46]

Suad et al. 2008[39], simplify the actual stress block to rectangular and triangular stress block:

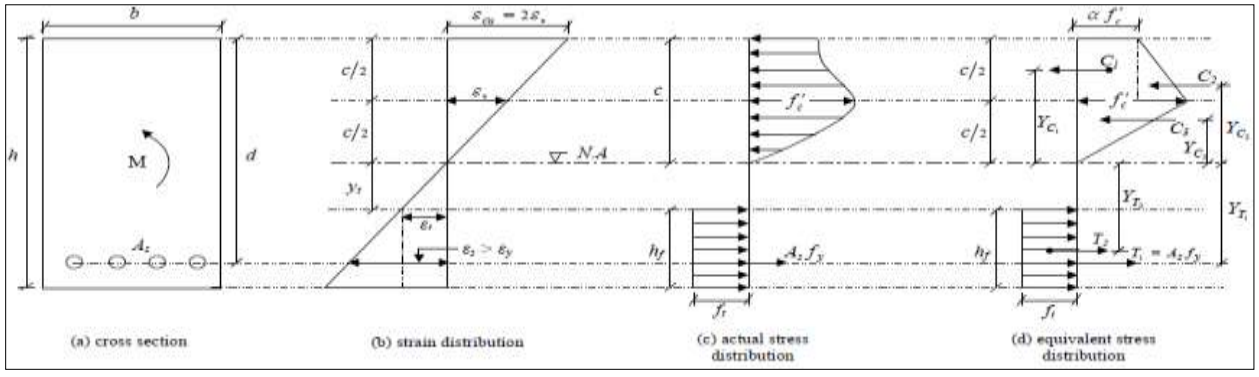

Figure 2.5 Stress-strain distribution by Suad[47].

Hekmet et al. 2014 [40], simplify actual stress block to rectangular stress block:

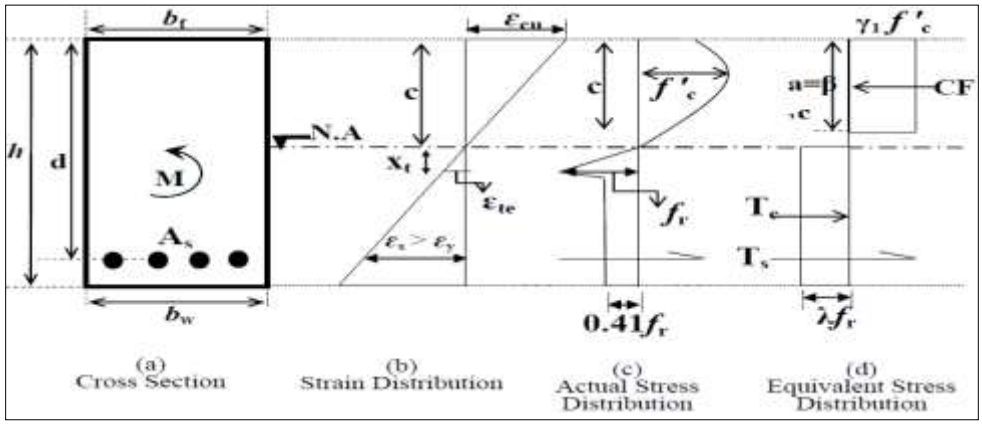

Figure 2.6 Stress-strain distribution by helmet[48].

Philip et al. 2010 [41], simplify actual stress block to rectangular stress block:

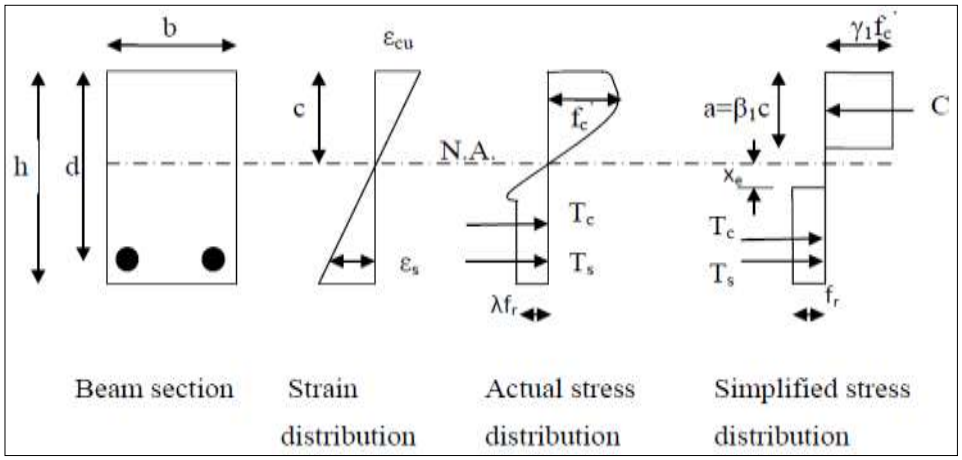

Figure 2.7 Stress-strain distribution by Philip[49].

After computing the total compressive forces and total tensile forces from the simplified stress blocks, then make equilibrium between the tensile forces and compressive forces to find the depth of compressive block and the neutral axis, then determining the nominal moment by summation moments around the neutral axis producted by all tensile and compressive forces and the summary in Table (2.4).

Table 2.4 The proposal equations to prediction the nominal moment.

Researcher	Nominal moment equation
Nasser[37]	Mn = α1.α.fc'.b.a.(C-a/2)+ 0.4 *√fc' *(h-C)*b*(h-C)/2+ As *fy *(d-c)
Danha [38]	Mn=0.45$f'c$ b ($c^2 - \frac{xc1^2}{3}$)+ 0.5 f_{te} b ($h^2 + c^2 - 2hc - \frac{xt1^2}{3}$) + As Fy (d-c)
Suad [39]	Mn=$\frac{1}{4}\left(\frac{5}{6}\alpha + 1\right)\left(\frac{c}{d}\right)^2 f\ b\ d^2 + As\ fy\ d\ \left(1 - \frac{c}{d}\right)$ + [$\frac{1}{2}(\frac{h}{d})^2$- $(\frac{h}{d})(\frac{c}{d})$ + $\frac{1}{2}$(1- $\frac{\varepsilon c^2}{4\varepsilon 0}$) − $(\frac{c}{d})^2$]$f\ b\ d^2$
Hekmet [40]	Mn = [γ1 f'c β1 bw c^2 . (1 - $\frac{\beta 1}{2}$) + bw λ fr ($\frac{h^2}{c}$ -hc+$\frac{c^2}{2}$) + As fy (d - c)] x 10^{-6}
Philip [41]	Mn = $\gamma 1 f c' \beta 1 c^2 b(1-\frac{\beta 1}{2}+ f y As(d-c)+ \frac{frb}{2}$ (h − c)^2− xe^2)

2.7 Longitudinal Opening in Beams

In general, the presence of openings in the concrete beam is an important subject, take the attention of the researchers.

Murugesan et al. 2016 [42], investigate the influence of the longitudinal circular hole on the flexural strength of reinforced concrete beams, by testing thirteen beams with dimensions (1.700, 150, 250) mm. All tested hollow RC beams had one hole with (25, 40 or 50) mm diameter longitudinally. The longitudinal holes fabricated using a frictionless PVC pipe and fixed reinforcements cage in the molds before casting. The parameters the research shown in Figure 2.8. The results showed that the first crack load depended on the distance begin from the center of the hole to the horizontal centroidal axis of the cross-section. The holes with the higher diameter reduced the moment of inertia higher than others and the resulting reduction in the cracking moment strength.

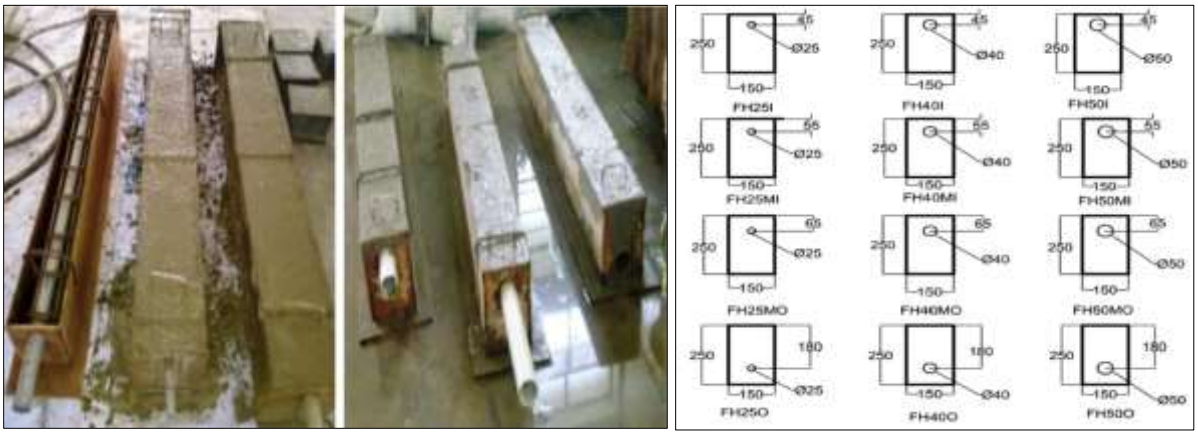

Figure 2.8 The parameters of the casted beams by Murugesan [50].

AL-Maliki et al. 2013[43], studied the behavior of five non-prismatic RC beams with deferent hollow shapes and materials. All beams have dimensions of (150x260x1170) mm with the hollow core of (50 x 50) mm square steel or (50mm) diameter of circular PVC. The beams are tested in simply supported ends and subjected to two points load. The results demonstrate that the presence of a hollow core in the beam section has led to the decreasing in stiffness and to an increase in deflections and strains. The square steel pipe has led to an increase in load capacity and to the decreased in deflections compared with circular PVC pipe.

Ahmad et al. 2014[44], they investigated the behavior of six (solid and with opening) beams with dimensions (length 1m, height 0.18m, width 0.12m), simply support. The tested load was (partial uniformly distributed). Four beams were containing longitudinal opening with varied section (80mm x 40mm) and (40mm x 40mm).Their parameters were, size of opening, stirrups effect, and stirrups orientation. The result is showed the existence of hollows are reduction the loads carrying capacity, and increased the deflections, stirrups are decreased whole deformations at whole phases of loading, especially after the initial cracking, and the ductility is raised when the hollow ratio reduced or stirrups increased-by-about-50%.

G. Balaji et al. 2019[45], this investigation examines the Flexural behaviour of reinforced concrete hollow beams under a gradually applied two-point load. The deflection at the ultimate stage is experimentally examined and compared with RC hollow beams. And we are concentrating material optimization by introduction of hollow portion using PVC pipe and GI pipe at tension zone in RC control beams. This experimental investigation includes casting and testing of five reinforced concrete beams having a size of the flexural strength of hollow beams with single openings is greater compared to hollow beams with the double opening. Hollow beams arehaving greater ductility when compared to the control beam tested hollow beams and control beam were failed by flexure failure as shown in Figure 2.9.

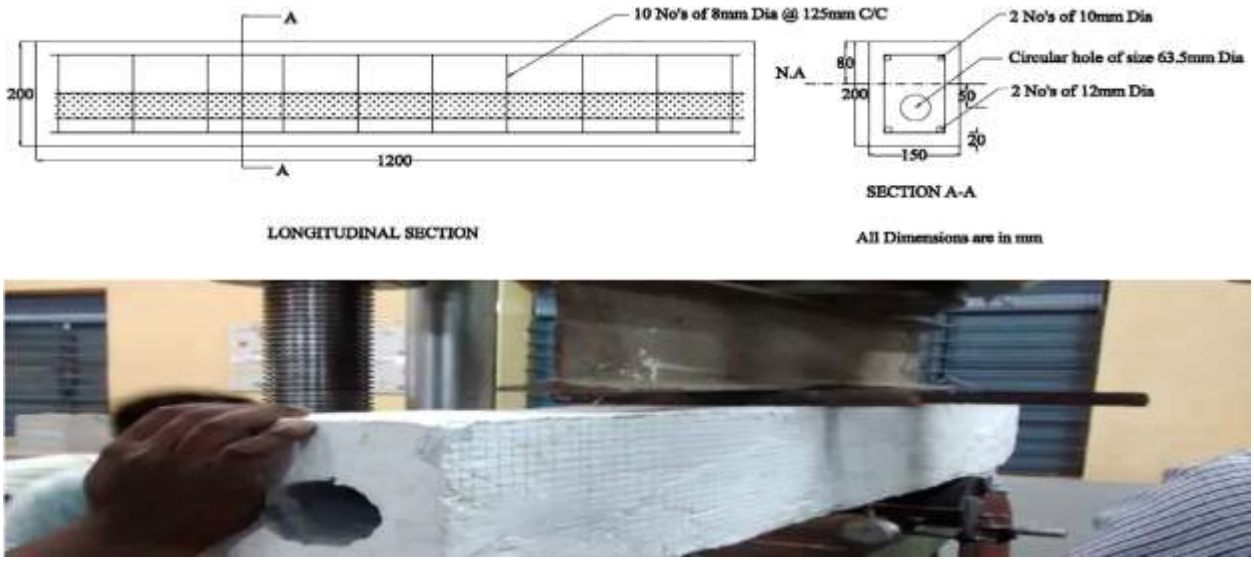

Figure 2.9 Circular hole in beam by G. Balaji [53].

Mustafa Özakça et al. 2020[46], in this work, 14 reinforced concrete solid and hollow beams were tested under four-point bending test to evaluate the flexural behavior of hollow concrete beams. The experimental program focused on two main variables which are the size reduction percentage and the inclusion of steel fiber. In addition, the longitudinal reinforcement ratio and the presence of lateral

stirrups were also within the investigated parameters. Four solid beams in addition to 10 hollow beams with central square holes with side lengths of 60, 80, and 100mm were fabricated to evaluate the test parameters.

Figure 2.10 Negrelli-Pedestrian Bridge, Main Railway Station-London[11].

Mazin B. Abdulrahman et al. 2019[47], investigate the structural behavior and strength of reinforced reactive powder concrete beams with a hollow section subjected under two point concentrated loading ten beams with dimensions (150mm width×200mm height×1000 mm length), eight of them are hollow beams and two solid beams were cast and tested up to failure. The major parameters adopted in the current research includes the hollowness ratio (10% and15%), hollow location (at top or at bottom), and hollow shape (circle or square) results showed that the strength capacity of hollow beam when the hollow lies in the bottom is much higher than for top hollow, and the square hollow will lead to more.

Mazin concluded that hollow in beam decrease the first cracking load and ultimate load capacity and have the ability to change the failure mode. As well as the number of cracks was larger in the hollow sections than in the solid ones under loading. Increase the ratio of hollowness from (10% to 15%) led to a decrease in the first cracking loads and the ultimate loads while increasing the deflection of these beams. The square section hollow leads to a more decrease in beam strength compared with the circular one. This is due to stress concentration and initiation of

cracks at square corner. It was shown that the strength capacity of the hollowed beam when the hollow lies at bottom position is much higher than of the top position. Presence of hollow in beams leads to a change in the failure mechanism of the solid beams from flexural failure to a combined flexural- shear failure for the hollowed beams.

2.8. Concluding Summary

From the reasons to investigate the present search were less mentioned in previous studies and from the distinctive features of the search are type of beam(continuous beam), tubular section , type of materials (UHPC) and study moment redistribution phenomenon. The inclusion of redistribution of moments requires knowledge of the moment curvature relationship, and maximum tensile and compressive strain in the reinforcement and the concrete respectively. The results conclusions and opinions expressed in the historical survey emphasize the importance of considering the following factors that affect redistribution:-

- Type of loading condition.
- Strength of concrete.
- Amount and type of tensile reinforcement.
- Moment curvature gradient
- Rotational capacity of the plastic hinges of members subjected to fiexural loads.

CHAPTER THREE: EXPRIMANTEL WORK

3.1 General

This chapter shows the experimental work to investigate the flexural behavior of continuous UHPC beams that have a longitudinal hole (tubular), in term of flexure at capacity, crack strength, crack pattern, deflection, stiffness, ductility and toughness. The beams were divided into three groups and each group had four beams to study the flexural behavior of tubular continuous beams with different parameters. The experimental program is divided into two part, part one contains casting of samples (cube, cylinder and prism) to investigate the mechanical properties of UHPC. For the production of the Ultra-High-Performance Concrete (UHPC) mixture, several concrete mixtures were used at different proportions and curing the specimens by heat treatment to obtain a target compressive strength at about 150 MPa. Part two represent casting twelve continuous beams to study the effect of some of the parameters that effecting on flexural strength were cast. The test was done under two point load in mid of distance for each span to study the changing of bar reinforcement ratio, steel fiber ratio change effect and finally and the important property in continuous beams is moment redistribution . Table 3.1,Table 3.2 and Table 3.3 are describe the detail of group one that shows the study of moment redistribution and group two that shows the effect of change steel fiber content and group three that shows the effect of steel reinforcement ratio change. The steps of mixing, casting, testing and curing of the specimens can be illustrated as shown in flow chart (3-1):

Table 3.1 Show group one to study moment redistribution.

Beam	Cross section (hxb)mm	Hollow dimension (hxb)mm	Stirrup at supports (mm)	Stirrup at mid span (mm)	Steel fiber content %	Positive reinforcement quantity(As^+)	M^+ (kN.m)	P Flexural (kN)	Negative reinforcement quantity(As^-)	M^- (kN.m)	P Flexural (kN)
MXB-1	200x150	70x50	Ø 10@50	Ø 10@100	2%	2 Ø 12 +1 Ø 16 (427mm^2)	60.1	520	2Ø 12 +1Ø 10 (304.7 mm^2)	75.3	470
MXB-2	200x150	70x50	Ø 10@50	Ø 10@100	1.5%	2Ø 10+ 1Ø 8 (207.3 mm^2) p<0.5 pb	49	430	2Ø 8+ 1Ø 10 (179 mm^2)	63.1	418
MXB-3	200x150	70x50	Ø 10@50	Ø 10@100	2%	2 Ø 10 +1Ø 16 (358 mm^2) p>0.5pb	57.5	492	3 Ø 10 (235 mm^2)	71.5	440
RE.M	200x150	Solid	Ø 10@50	Ø 10@100	2%	2 Ø 10 +1Ø 16 (358 mm^2) p>0.5pb	51	492	3 Ø 10 (235 mm^2)	63.4	440

Table 3.2 Show group two to study effect of steel fiber ratio change.

Beam	Cross section (hxb)mm	Hollow dimension (hxb)mm	Stirrup at supports (mm)	Stirrup at mid span (mm)	Steel fiber content %	Positive reinforcement quantity(As^+)	M^+ (kN.m)	P Flexural (kN)	Negative reinforcement quantity(As^-)	M^- (kN.m)	P Flexural (kN)	$\frac{M^-}{M^+}$
MXB-4	200x150	70x50	Ø 10@50	Ø 10@100	1 %	2 Ø 12 +1 Ø 10 (304 mm^2)	63.1	530	2 Ø 10 + 1Ø16 (358 mm^2)	65	540	1.03
MXB-5	200x150	70x50	Ø 10@50	Ø 10@100	1.5 %	2 Ø 12 +1 Ø8 (276 mm^2)	61	480	2 Ø 10 + 1Ø16 (358 mm^2)	65	540	1.06
MXB-6	200x150	70x50	Ø 10@50	Ø 10@100	2 %	2 Ø 16 +1 Ø 10 (480 mm^2)	65	532	3 Ø 16 (603 mm^2)	69	550	1.06
RE.S	200x150	Solid	Ø 10@50	Ø 10@100	1.5 %	2 Ø 12 +1 Ø8 (276 mm^2)	61	480	2 Ø 10 + 1Ø16 (358 mm^2)	65	540	1

Table 3.3 Show group three to study effect of reinforcement ratio change.

Beam	Cross section (hxb)mm	Hollow dimension (hxb)mm	Stirrup at supports (mm)	Stirrup at mid span (mm)	Steel fiber content %	Positive reinforcement quantity(As^+)	M^+ (kN.m)	P Flexural (kN)	Negative reinforcement quantity(As^-)	M^- (kN.m)	P Flexural (kN)	$\frac{M^-}{M^+}$
MXB-7	200x150	705x50	Ø 10@50	Ø 10@100	2 %	2 Ø 16 +1 Ø 12 (515 mm^2)	60.1	530	3 Ø 16 (603 mm^2)	69	540	1.06
MXB-8	200x150	70x50	Ø 10@50	Ø 10@100	2 %	2 Ø 12 +1 Ø8 (276 mm^2)	49.6	480	3 Ø 12 (336 mm^2)	49	470	0.98
MXB-9	200x150	70x50	Ø 10@50	Ø 10@100	2 %	2 Ø 12 +1 Ø 10 (304 mm^2)	57.6	470	2 Ø 10 + 1Ø16 (358 mm^2)	51	440	0.88
RE.B	200x150	Solid	Ø 10@50	Ø 10@100	2 %	2 Ø 12 +1 Ø 10 (304 mm^2)	57.6	470	2 Ø 10 + 1Ø16 (358 mm^2)	51	440	0.88

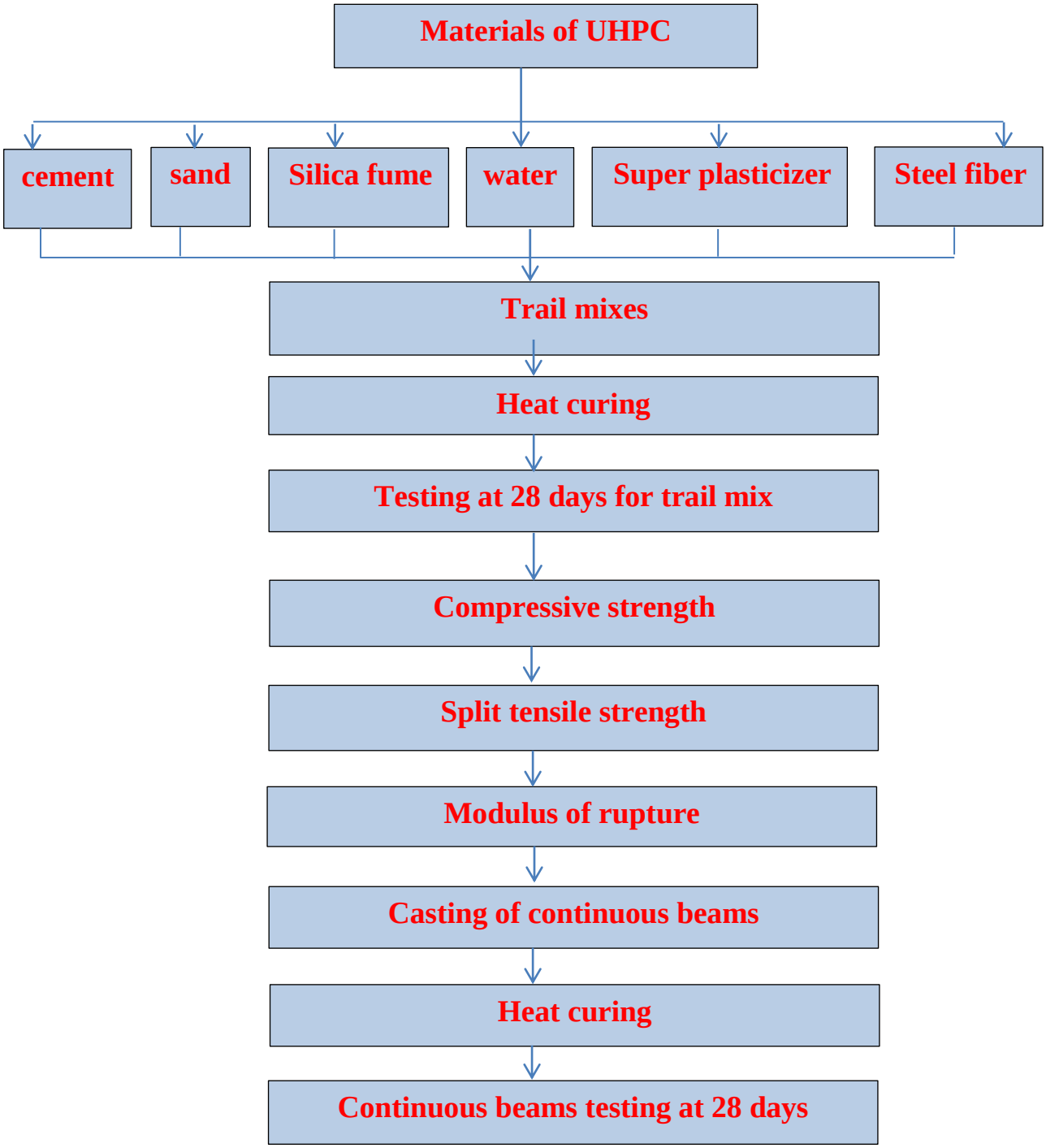

Flow chart 3.1 Programs of the experimental work.

3.2 Continuous Beam Specimens

In this stud, all the sample have the same total length (L) of 3000 mm with two span each span has distance (Ln) equal to (1400 mm) center to center of the support. The overall depth is (200 mm) and the width is (150 mm) with a longitudinal hole in dimensions (70 x50 mm) in depth and width respectively.

Twelve continuous beams were tested under two point loads and the reinforcement detailing of the beams are shown in Figure 3.2. Three beams are tubular by made longitudinal hole by cork material put in mid distance of transverse section and the fourth beams are solid beam consider the reference beam to comparison. All beams are reinforced by using stirrup(**Ø10** mm) at 100mm c/c to avoid shear failure. The ends of all beams extend 100mm beyond the supports. The concrete cover was 25mm.

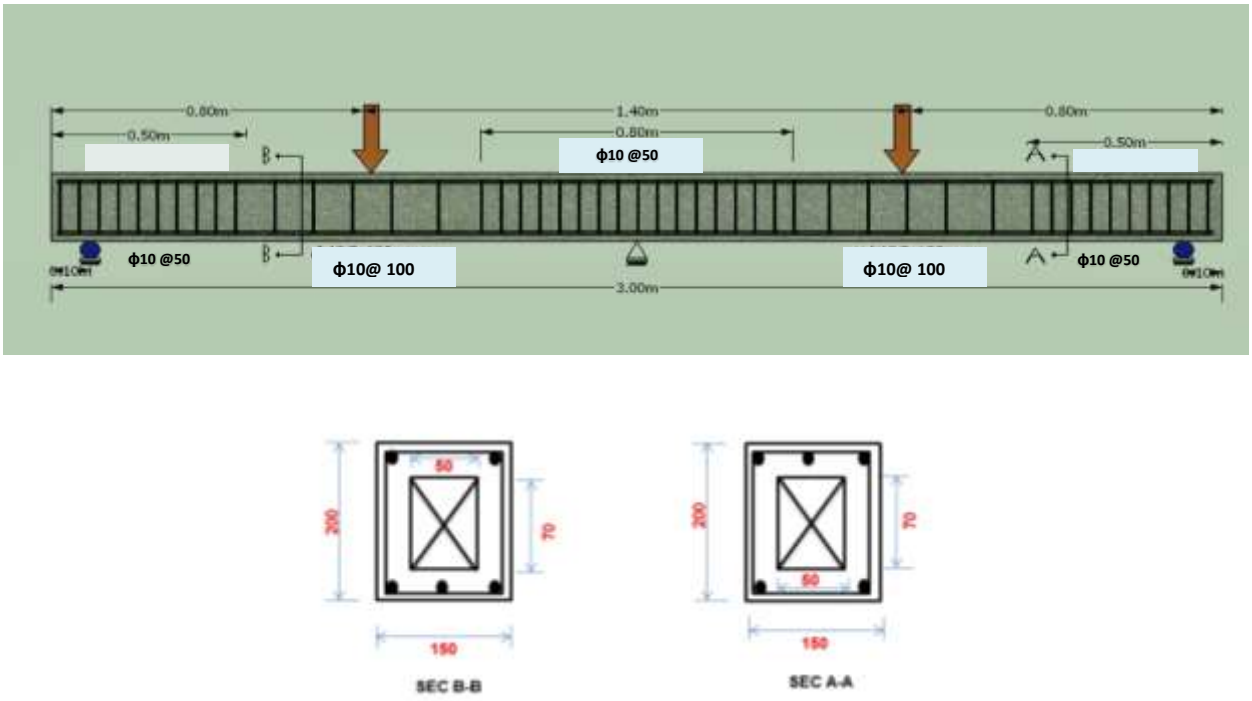

Figure 3.2 Layout of tested beam.

3.3 Trial mixes for UHPC

Many trial mixes were performed in this work until reaching the suitable performance with requirement of UHPC. The percentage of material was as follow the silica fume as percentage of cement weigh, water and superplasticizer is a proportion of cementitious material (cement and silica fume); and steel fiber as a proportion of flume mixing. The trail mix number (3) was taken as a reference mix proportions for structural member (beams) as shown in Table 3.4.

Table 3.4 Trial mixes properties.

Mix. No.	**Cement kg/m^3**	**Sand kg/m^3**	**Silica fume kg/m^3**	**Super-plastizer %**	**W/C %**	**Water kg/m^3**	**S.F %**	**Fc' for 28 days MPa**
1	1000	1000	250	3	0.22	275	0.0	66.5
2	1000	1000	250	3	0.2	250	1	80
3	1000	1000	250	3	0.2	250	2	143.2
4	1000	1000	250	3	0.2	250	1.5	91.6
5	950	1050	225	3	0.25	293.75	2	102.7

3.4 Construction Materials of Ultra High Performance Concrete Specimens:

3.4.1 Cement

The type of cement that utilized in all the mixtures of this work was ordinary Portland cement (CARASTA). The physical and chemical properties of cement were also examined in Amarah Technical Institute laboratory to check its specification before its utilized, Its chemical composition and physical properties are given in Tables (3.5) and (3.6), respectively. This conformed to Iraqi Standard Specification **No. 5:1984** [49].

Table 3.5 Physical test results of cement.

Physical properties	**Test result**	**Limits of Iraqi Specification No.5/1984**
Soundness (Autoclave method)	0.03	0.8 (max)
Setting-time utilizing Vicat's instrument Initial (min.) Final (hr.)	(81) (3.0)	(45) Minimum (10) Maximum
Compressive strength at: (3days MPa) (7days MPa)	(17.2) (21)	(12) Minimum (19) Minimum
Specific Surface Area (Blaine Method).(m2/kg)	410	(230) Minimum

Table 3.6 Chemical test results of cement.

Oxide composition	**Content by weight %**	**Limit of Iraqi Specification No.5/1984**
Lime (CaO)	62.1	--
Silkone oxide (Sio2)	20.1	--
Alumina (AL_2O_3)	4.3	--
Iron oxide (Fe_2O_3)	4.8	--
Lime saturation (L.S.F)	0.81	0.66-1.02
Sulphate (SO_3)	2.6	2.8 (max.)
Loss on ignition (L.O.I)	2	4.0 (max.)
Magnesium oxide (Mgo)	3.3	5.0 (max.)
Insoluble Residue	0.6	1.5 (max.)
Free Lime	3.5	4.0 (max.)

3.4.2 Fine Aggregate

The fine aggregate (sand) that is utilized for UHPC production must be within certain sizes that differ from ordinary sand. The gradation that utilized in this work sand#4 has extra fine gradation (0.3mm - 0.6mm). It was produced by Don Construction Products Ltd. DCP (Appendix A), and available in the local markets in the form of bags weighing 25kg and big bags weighing (1000) kg. The sand was shown in Figure 3.3.

Figure 3.3 utilized Sand type.

3.4.3 Water

The tap water was used by Reverse Osmosis (RO) was utilized in the cast of the whole of the trial mixtures and the continuous concrete beams. The w/c ratio (0.2%) was utilized as a constant parameter in this study.

3.4.4 Silica Fume

Silica fume is a very effective pozzolanic material and an ultrafine material with spherical particles less than 1 μm in diameter. The average is about

0.15 µm. This makes it approximately 100 times smaller than the average cement particle. It found in form of bags, weighing 20kg. Figure 3.4 and Table 3.7 are showed the results of silica fume test. The ratio of silica fume (0.25%) is utilized as a constant in this study. Table 3.7 typical properties of microsilica, more details can be found in Appendix (A). Table 3.8 ”Chemical and Physical Requirements of MicroSilica ASTM C 1240-15 [50].

Figure 3.4 Silica Fume.

Table 3.7 Typical properties.

Property	**Value**
State	Sub-micron powder
colour	Gray to medium gray powder
Specific gravity	2.10 to 2.4
Bulk density	500 to 700 kg/m^3

Table 3.8 Chemical and physical properties for Micro-Silica
ASTM C1240-15 [50]

Chemical properties		
Oxides composition	**Oxides content %**	**ASTM C1240-15% limit**
SiO2	92.5	Min. 85
Al2O3	0.75	< 1
Fe2O3	0.49	< 2.5
CaO	0.87	< 1
SO3	0.88	< 1
L.O.I	5.3	Max. 6
Cl	0.1	< 0.2
K2O+Na2O	1.76	< 3
Physical properties		
Property	**Result**	**ASTM C1240-15**
Strength activity index	108	≥ 105%
Moisture content	0	≤ 2%
Specific surface area m^2/gm	16.5	> 15

3.4.5 Hyperplast PC260 (HRWRA)

The relationship between water content and compressive strength of mixtures is inverse relationship by correct calculations. In other words, the reducing in water percentage in the concrete mixture which plays a big role in obtaining UHPC. The addition of super-plasticizer to concrete mixture allows the reduction of w/c ratio without negatively effecting on mixture workability. The superplasticizer PC260, produced by (DCP) company in India utilized was complies with (ASTM C494) [51] type (A&G). Figure 3.5, and its technical

description was showed in Table 3.9. The superplasticizer ratio (3%) used as a constant in present study.

Figure 3.5 Superplasticizer PC260.

Table 3.9 Technical properties of PC260.

Technical properties @ 25 ˚C	
Color	Yellowish to brownish liquid
Freezing point	≈ -7 ˚C
Specific gravity	1.1 ± 0.02
Air entrainment	Typically less than 2% additional air is entrained above control mix at normal dosages.

3.4.6 Steel Fibers

Steel fiber that used is straight and golden type as shown in Figure 3.6. It's available in local markets in form of sacks weighing (20–25 kg). Steel fibers that utilized have 0.2 mm diameter, and 13 mm length with aspect ratio 65 . Table 3.10 shows the characteristics of steel fiber.

Table 3.10 Properties of steel fiber.

Description	**Straight**
Length	13 mm
Diameter	0.2 mm
Density	7800 kg/m^3
Tensile Strength	2600 MPa
Aspect Ratio	65

Figure 3.6 Utilized steel fiber.

3.4.7 Steel Bars Reinforcement

Four size of deformed steel reinforcement bars are used for all specimens manufactured by Ukraine state in diameter (ϕ16mm) , (ϕ12mm). Size applied as longitudinal reinforcement and as addition bar in compression region reinforcement and ϕ10 and ϕ8 mm bars size as negative region reinforcement and as (closed

stirrups) transverse reinforcement and the ratio are variable according to each groups as shown in Figure 3.7. The tests were carried out as shown in Figure 3.8 and Table 3.11 shows the results of tested bars.

Table 3.11 Properties of variable steel bar reinforcement.

Nominal bar diameter (mm)	Yield strength (MPa)	Ultimate strength (MPa)	Elongation %
16	577	687.4	10.4
12	494.4	583.5	11.8
10	516.5	624.3	14
8	476.2	642	29

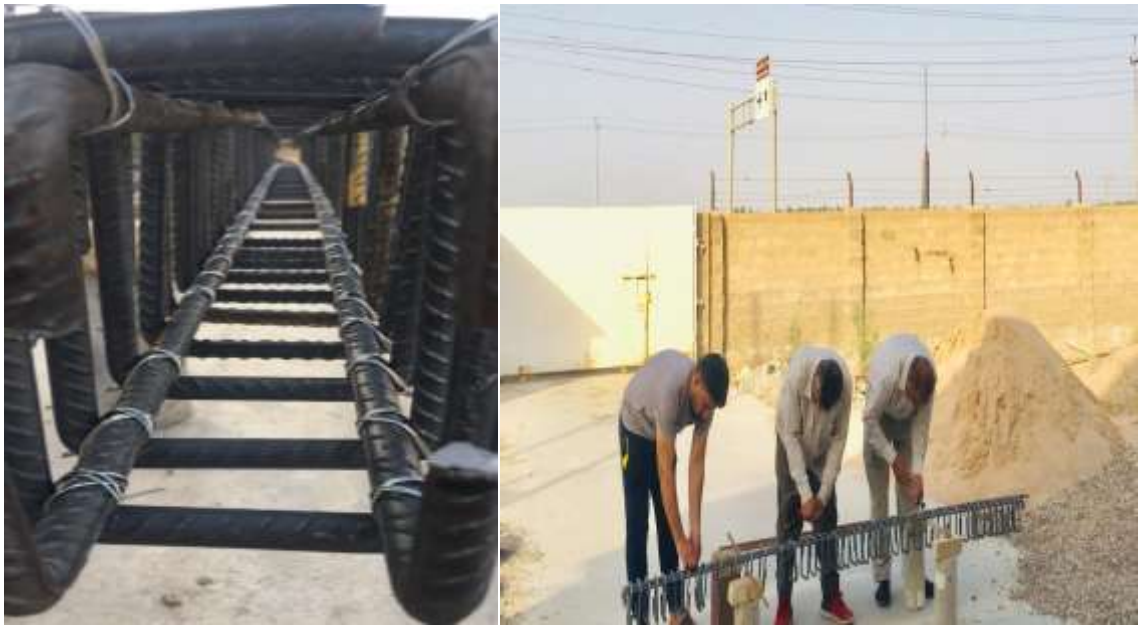

Figure 3.7 Beam Reinforcement.

Figure 3.8 Testing Machine of Steel Reinforcement.

3.5 Molds

Molds made of wood were used for casting the continuous beam specimens ad shown in Figure 3.9.All sides were fixed together by screws. Stander steel molds were used for casting the cylinders ,cubic and prisms.

Figure 3.9 Wood mold and steel molds for cubes, cylinder and prism

3.6 Longitudinal Hole Making

The longitudinal hole was made by cork material as dimensions (70x50) mm which installed by cut small steel bar. For obtaining a longitudinal hole (hollow core), the cork material was packed with adhesive tape to increase its resistance to crashing during the casting process. To obtain a hollow opening section in the longitudinal direction, the cork was connected using a tiny steel sticky **(**Ø6)mm, and silicone glue is used to connect it with the plywood mold. Figure 3.10 shows the process details of using cork in fabricating the hollow core.

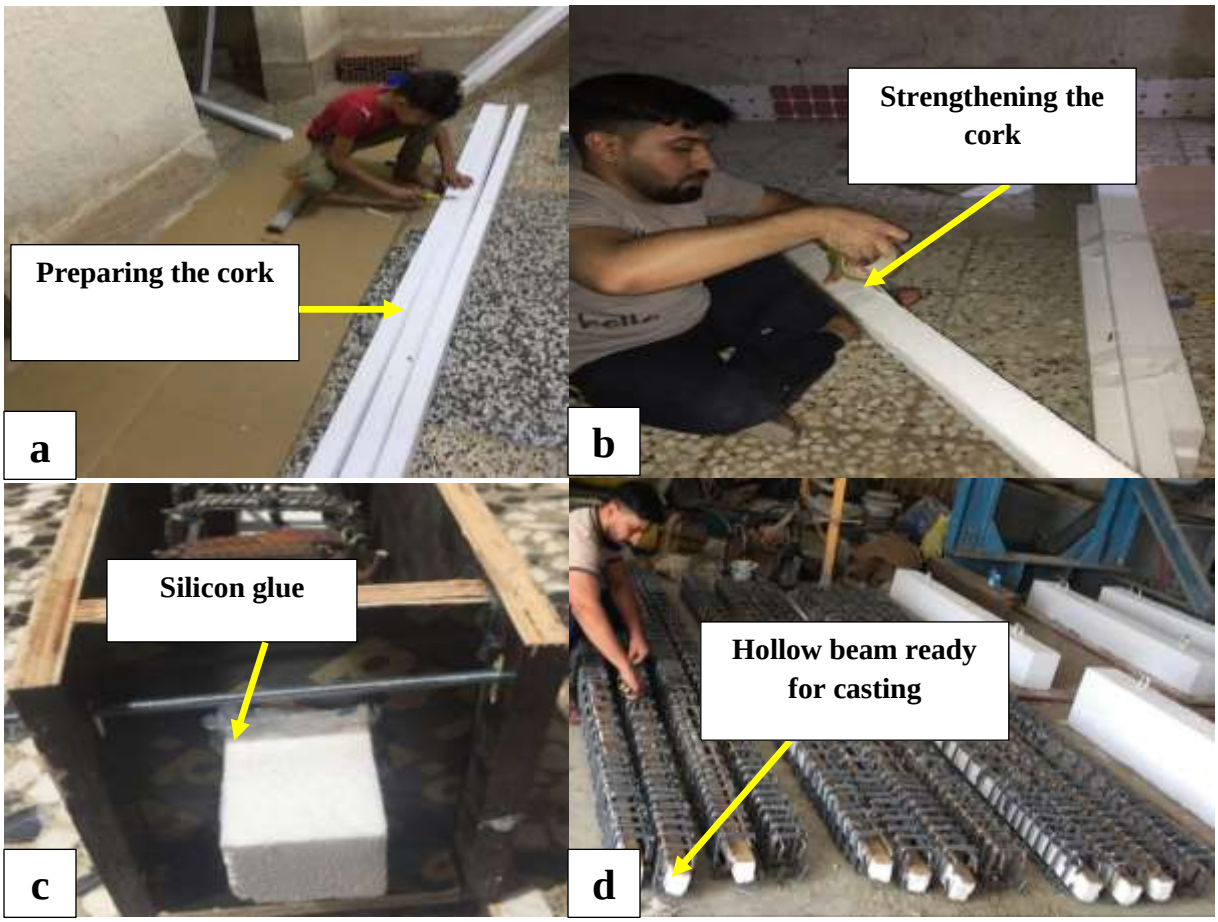

Figure 3.10 Longitudinal hole making stages.

3.7 Design for flexural strength

The basic aim from the present study is to investigate the flexural strength of the continuous beam and chosen the suitable method to deal with it in the new type of concrete that is UHPC.

3.7.1. Combined Method

The equations mentioned at chapter two (2-1 to 2-6) are utilized in the calculation of the main longitudinal reinforcement [37], with deduct the openings from each compressive and tensile areas, and utilized the force in the tensile steel bar. The method was organized in excel sheet, appendix-A-.

3.8 Concrete Mixing

In this study the UHPC trial mixes were mixed by utilizing pan mixer as shown in Figure 3.11. The processes of UHPC trial mixture were in strides as summarized below:

1. Cement and silica fume (cementitious materials), were mixed for dry state for about (3 minute) with slow motion of mixer to disperse the silica fume particles throughout the cement particles .
2. Sand was added slowly over cementitious, with continue mixing the dry materials with slow motion of mixer for another (5 minute).
3. The super plasticizer (PC 260) is dissolved in water and the solution of water and super plasticizer is gradually added mixed together, and added half of resulted liquid to admixture slowly and continue mixing for (5min.) with increase the speed of mixer to medium motion.
4. Half of remaining liquid was added slowly to admixture, and continue mixing for another (3min.).
5. The steel fibers were added slowly (to prevent forming of steel fiber balls) to mixture about (5 minute). Continued mixing for one minutes to mix steel fibers

well with other components. In total, the mixing of one batch requires approximately (21minutes). The time mixture of current research adopted on the procedure of an (a State of art- on development of reactive powder concrete)[61].

Figure 3.11 (a)Mixing machine, (b)Preparing the materials.

3.9 Casting Procedure

The steel reinforcement was put in its required placement in the mold as shown in Figure 3.12. All specimens were loaded with the mix. Every layer was compacted by external vibrator to reduce the air vacumes and to obtain well compacted concrete. The upper face of the molds was upload the samples were demolded marked and another cured .Figure 3.13 shows the casting of the beams .

Figure 3.12 The steel bars in required position.

Figure 3.13 Casting of the specimens.

The following samples were casted to define the properties of the hardened UHPC:

1: 50mm x 50 mm x 50mm cubes for compressive strength (6 cubes).

2: 100mm diam. x 200 mm long cylinder for compressive strength (6 cylinders).

3: 100 x 100 x 400mm prisms for modulus of rupture (3 prisms).

4: 100mm diam. x 200mm long cylinder for splitting tensile strength (3 cylinders).

5: 150mm diam. x 300 mm long cylinder for modulus of elasticity (3 cylinders).

3.10 Curing

For UHPC specimens, All samples were cured after 24 hours by placing the sand on the samples so that they are fully covered as shown in the Figure 3.14. In addition, the cubes, cylinders and prism were submerged in the water as show in Figure 3.15.

Figure 3.14 Sand cover for specimens

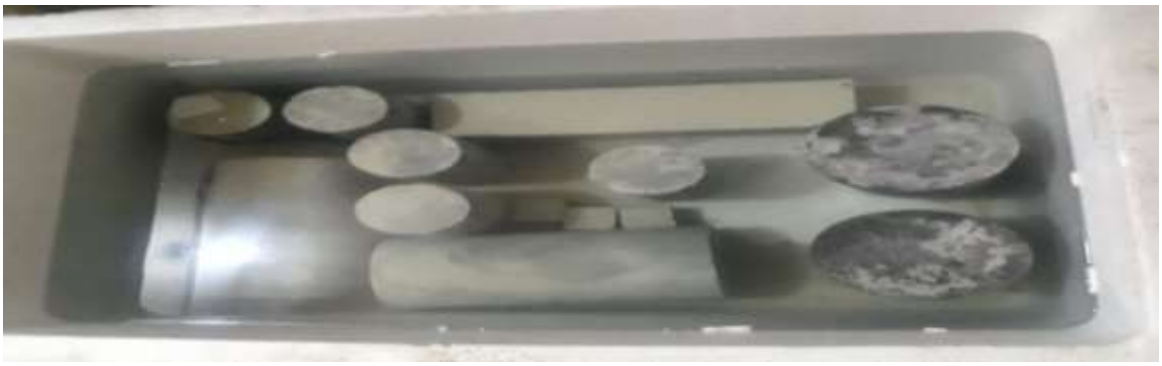

Figure 3.15 Curing of cube , cylinder and prism.

The tank with water connect the three heater to electrical reference to reach the degree of temperature about (± 5 (80^0))for three days [61] then in normal temperature degree of room. After that they cooled gradually left to 28 days as shown in Figure 3.16.

Figure 3.16 Heat treatment tank for specimens.

3.11 Testing for Mechanical Properties of UHPC

To specify the main mechanical properties of Ultra-High-Performance Concrete mix, three tests are performed to study a three mechanical properties (compressive strength, splitting tensile strength and modulus of rupture). These tests were done according to the specifications of the American Society for Materials Testing (ASTM). All these tests were done at the University of Misan and Basrah -Faculty of Engineering laboratory.

3.11.1 Compressive Strength

The compressive test was achieved according to ASTM C39/C39M- 05[54]. Cylinders by 100 x 200 mm and cubes (50) mm dimensions for UHPC specimens using hydraulic testing machine at a loading rate of 0.9KN per second, as shown in Figure 3.17 average of three samples for each mix were taken to study the compressive strength and accordance to ACI 318M-14[34] the mean of three cylinders readings was taken at the age of 28 days. Graybeal [61] studied the effect of shape and size of specimens of UHPFRC with strength from 80-200

MPa. The shape effect had no more than 8 percentage difference. In general, the ratio between cubes strength to cylinder strength of 100 mm in length and diameter, respectively, are equal to one.

Figure 3.17 Compressive Strength Test.

3.11.2 Modulus of Rupture

It was a material property which is defined as a stress of material under flexural test just before yield, it also known as a fracture strength. According to (ASTM C78/C78M-15a) [56], the test was doing by using prism specimens with dimension (100mmx100mmx400mm). Using flexural strength testing machine as shown in Figure 3.18. The test was performed by using three points of loading by a machine with 63 kN capacity, which is manufactured by COSQC. The results of tests are calculated by equation (3-1). The results obtained in the present work and the modulus of rupture get it as follow:

$$f_r = \frac{3pl}{2bd^2} \qquad \text{..... (3-1)}$$

where:

f_r= the modulus of rupture (MPa).

P = the ultimate failure load (N).

l = the Span length between the supports, (center to center) (mm).

b = prism cross section width (mm).

d= prism cross section depth (mm).

Figure 3.18 Modulus of Rupture Test.

3.11.3 Splitting Tensile Strength (fsp)

Three several methods of testing, but the most common is the Brazilian method which is the indirect tensile strength test conforming to ASTM C 496-04[55]. This method was used in the study, by testing three cylinders with a diameter of 100 mm and length of 200 mm placed horizontally in the universal ELE Machine with a capacity of 2000 kN to apply the load vertically along the length of the cylinders. as shown in Figure 3.19. The splitting tensile strength was calculated from the following formula:

$$f_{sp} = \frac{2P}{\pi dL} \qquad \text{.....(3-2)}$$

Where:

f_{sp}: splitting tensile strength (MPa)

P: maximum applied load (N)

d: diameter of cylinder (mm)

L: length of cylinder (mm)

Figure 3.19 Splitting Tensile Strength.

3.11.4 Static Modulus of Elasticity (Ec)

According to ASTM C469/C469M-14 , cylindrical specimens of 150 x 300 mm dimensions used to calculated the Ec as shown in Figure 3.20 and Eq.(3-4). The main parameter that affected on the flexural behavior is the modulus of elasticity of concrete E_c of the concrete . The test results of three tested cylindrical specimens, previously instrumented with strain gauges, were considered in calculation of concrete modulus of elasticity .The first one measurements by Hooke's Law and the second way was carried out by the below equation according to ASTM C469 [55] Standard:

$$\boldsymbol{E_c = \frac{S_2 - S_1}{\varepsilon_2 - 0.000050}} \text{ .....} \qquad \textbf{(3-3)}$$

Where E_c is chord modulus of elasticity in MPa, (Approximated to the nearest 300 MPa), S_2 is stress corresponding to 40% of ultimate load, S_1 is stress corresponding to a longitudinal strain (ε_1) of 50 millionth, and ε_2 is longitudinal strain produced by stress S_2.

.

$$\boldsymbol{E_c = [(\sigma_2 - \sigma_1)/(\varepsilon_2 - 0.0005)] x\, 10^{-3}} \text{ .....(3-4)}$$

Where:

Ec= modulus of elasticity (GPa)

σ_2= stress corresponding to 40 % of ultimate load (MPa).

σ_1= stress corresponding to longitudinal strain of 0.00005 (MPa).

$\boldsymbol{\varepsilon}_2$= longitudinal strain produced by stress σ_2.

Figure 3.20 Static Modulus of Elasticity.

3.12 Measuring Devices

The tools used in the work to measure (deflections, strains, crack width, load, crack projection, crack patterns) during the testing of each beam specimen are listed below:

3.12.1 Hydraulic Jack

All beams were tested as a continuous beams using one point loading for each span. The beams were testing by exercising the standardized electrohydraulic global testing machine with the ultimate range ability of 2000 kN, in the structural

laboratory of the civil engineering department, college of engineering, university of Basrah as shown in Figure 3.21.

Figure 3.21 Universal Testing Machine.

3.12.2 Deflection Measurement

The mid spans deflections were measured by strain gauge at the each mid spans of the beams sensibility at any load step, two types dail gauge the first was used laser strain gauge as shown in Figure 3.22 and the second was mechanical dial gauge as shown in Figure 3.23.

Figure 3.22 Laser Deflection Measurement (LVDT).

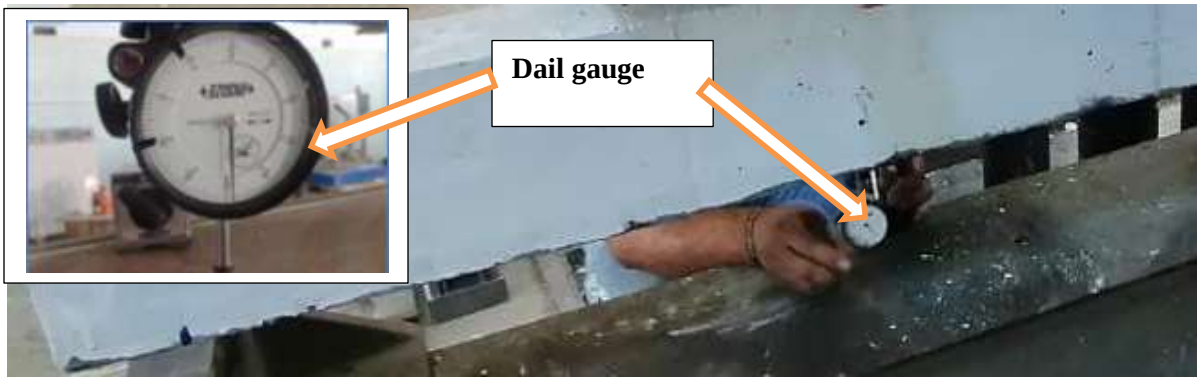

Figure 3.23 Mechanical Deflection Measurement.

3.12.3 Crack Width Measurement

Crack meter is a device used to measure the width of the incision, where all of its pointer (accuracy) is about 0.005mm as shown in Figure 3.24 show crack meter.

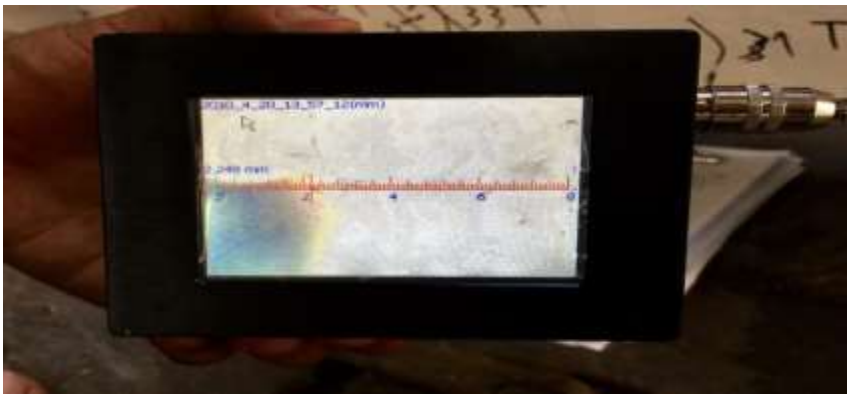

Figure 3.24 Crack width instrument.

3.12.4 Strain Measurement

The strain was measured by using strain gauges. As a result of their superior measurement properties, all the strain gauges used in this study were placed near two point load on the spans in compression and tension zones of the beam specimen. These strain-gauges were placed on a side surface of the beam specimen in the mid-span. Two concrete strain gauges used for the beam specimen. One placed in the upper edge on the extreme compression zone of concrete to find the

compressive strains of concrete during the loading process. The other placed in the bottom edge in the tension zone of concrete to find the tensile strains of the UHPC during the loading process. PFL-30-11-3L [57] strain gauges were used, (PF) refers to the gauge series (polyester foil gauge) and (L) refers to pattern configuration (single), (30) indicate to the length of the strain gauge is 30mm, (11) is compensation material ppm/Cº. (3L) indicates the length of the existing wire with the strain gauge is 3 meters as shown in Figure 3.25.

Figure 3.25 The strain gauge types used in this research.

3.12.5 The Process of Installation the Strain Gauges

The process of setting up the strain gauges are shown in Figure 3.26 where summarized as the following steps :

1- Surface preparation :

After complete the process of determining where the position of strain gauge should installed. The surface of the material must be cleaned from all rust, grease,

paint. Aslightly more extensive area of the strain gauge bonding area should be smoothed by using abrasive paper 80 to 120 for concrete.

2- Little cleaning :

The area was cleaned using a cleaner solution where strain gauge glued.

3- Setting up the strain gauge :

After completing the preparation of the strain gauge glued area, the strain scale is determined by a pencil. Special adhesive (CN adhesive series), was imported from Japan. A sufficient amount of adhesive is placed on the base of the strain gauge and usually using one drop of CN adhesive was applied. The adhesive one drop is then distributed on the strain gauge base by using the adhesive nozzle. Then place the sheet of strain gauge above the strain gauge and press by thumb with constant pressure for a period ranging from (60-120) seconds depending on the temperature of the room and the humidity of the air.

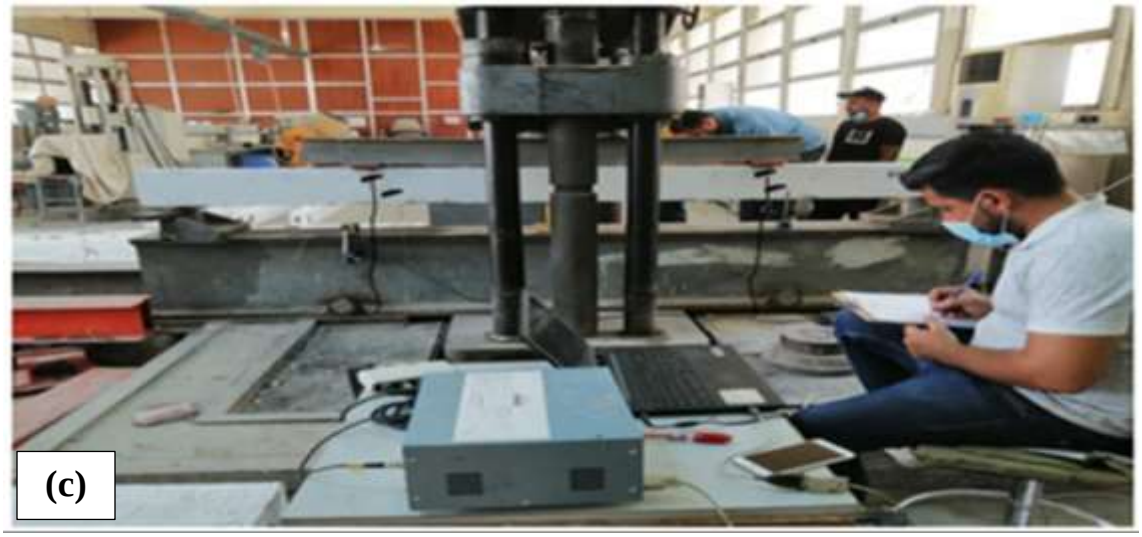

Figure 3.26 Steps of installation strain gauge on beams.

3.13 The Work Principle of the Strain Gauges

The process of measuring strains by using the strain gauges can be summarized as when the material is exposed to external force, physical deformations are produced, and these deformations cause changes in the electrical resistance of the exposed material. When the strain gauge is connected to the material, and the material is exposed to the external force that leads to generating strains that cause a change in the electrical resistance of the materials so that the strain will read the resistance changes. Due to this variation in electrical resistance, the strain is generated proportional to variation[57].

$$\boldsymbol{\varepsilon} = \frac{\Delta L}{L} = \frac{\Delta R/R}{K} \quad \ldots\ldots\ldots\ldots\ldots\ldots \quad (3\text{- }5)$$

ε is strain measured, R is a resistance of the gauge.

ΔR is resistance change due to the strain.

K is a gauge-factor existing on the package

3.14 Testing Procedure

After the end of curing period of the specimens, the specimens were extracted from the treatment tank at the age of 28 days. The beams are painted in white color to facilitate the vision cracks during the testing of the cracks as shown in Figure (3.30) that are appearing during the loading process. Each beam was tested individually and placed inside the frame of the testing machine for testing .The length of continuous beams was 3000mm, while a clear distance for each span 1400 mm between the center line of the supports. Two dial gauge was placed in the middle of each span of continuous beam and glued to the bottom face of the beam to record the mid-span deflection. Concrete strains were measured using strain gauges and supports in the correct places in compression and tension zones. Strains were reading by data logger, and crack's width were recorded at the end of each loading increment as shown in Figure 3.27.

The load was raised progressively and in each 50 kN step, deflection was listed. And the supports were roller from the ends and the middle support was hinged also crack propagation was nomination on the beam during the loading and maximum crack width was measured approximately using crack meter device which are shown in Figure 3.28.

Figure 3.27 Beams under test.

Figure 3.28 Record width of cracks.

3.15 Strain Tool Measurment

In this work, the Data Logger device was used for reading the strains measured by strain gauges in the beam specimens as shown in Fig.(3.29).

Figure 3.29 Data logger device.

Figure 3.30 Paint the beams.

CHAPTER FOUR: RESULTS AND DISCUSSION

4.1 General

This chapter includes the experimental results of twelve specimens to know their flexural behavior under effect of static loads. An experimental program was carried out to verify the mix design with basic available materials. The beams were tested in university of Basrah college of engineering's laboratory. Load-deflection behavior for each tested continuous beam's group was given with its identical sketched picture of continuous beam during the test. For tested continuous beams, sketching had been done to record load –deflection curves ,first crack, crack pattern, strain distribution and ultimate load at different load steps.

The first group included an experimental study for moment redistribution property of continuous UHPC beam. The second group studied the change of steel fiber ratio. The third group studied the change of longitudinal reinforcement ratio. All beams have the same geometric and mechanical properties.

4.2 Experimental Results of Mix Design

The experimental results are divided into two part, part one contains the mechanical properties of UHPC and the second part represent the behavior of continuous beams by study some parameters.

Name of material	Cement (Kg/m^3)	Sand (kg/m^3)	Water (kg/m^3)	Super plasticizer (kg/m^3)	Silica fume (kg/m^3)	Steel-fiber (kg/m^3)	Fiber-volume fraction Vf (%)
UHPC	1000	1000	200	37.5	250	156	2

4.2.1 Mechanical Properties of UHPC

To determine the mechanical properties of UHPC, control specimens were tested. The mechanical properties contained compressive strength (f'_c), splitting tensile strength (f_{sp}), modulus of rupture (f_r) and modulus of elasticity (E_c). Cylinders dimensions (100 x 200) mm used in determining compressive strength (f'_c) and splitting tensile strength (f_{sp}). Cylinders with (150 x 300) mm were used to study modulus of elasticity for UHPC also, cubes dimensions 50 mm to get compressive strength (f_{cu}) while prisms specimens (100 x 100 x 400) under two concentrated load at third span point to get the modulus of rupture (fr) and flexural tensile strength as shown in Figures (4.1) to (4.3).

Figure 4.1Modulus of elasticity test.

Figure 4.2 Cylinder compressive test.

Figure 4.3 Cube Compressive Test.

4.2.1.1 Flexural for Tensile Strength

The Figure 4.4 and Table 4.1 are showed results of modulus of rupture of the prism. The results of tests were calculated by Equation (4-1) that mentioned in (C78/C78M − 15a) [56].

$$f_r = \frac{3PL}{2bd^2} \qquad \text{……..(4-1)}$$

where:

(f_r): flexural strength (modulus of rupture MPa)

(P): ultimate failure load N

(L): clear span c/c 400 mm

(b): width of prism 100 mm

(d): depth of prism 100 mm

Figure 4.4 Modulus of rupture test device.

Table 4.1 Flexural Testing Results.

Modulus of rupture (f_r) MPa	14.13	16.14	18.05
Test load (N)	23584.99	24693.14	26840.8
Average stress MPa	16.1		

4.2.1.2 Splitting Tensile Strength

The splitting tensile strength for UHPC mixture carried out by testing of 100x200 mm cylindrical samples according to (ASTM C496M-11)[55]. Figure 4.5 and Table 4.2 are showed the results of test. The splitting tensile strength was calculated by Equation (4-2).

$$f_{sp} = \frac{2P}{\pi dL} \qquad \text{.....(4-2)}$$

Where:

f_{sp} : splitting tensile strength (MPa).

P : maximum applied load (N).

d : diameter of cylinder (mm).

L: length of cylinder (mm).

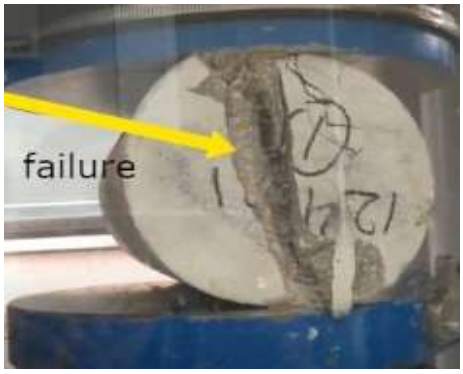

Figure 4.5 Splitting strength test.

Table 4.2 Splitting tensile strength testing results.

Splitting strength(f_{sp}) MPa	10.2	12.2	14.1
Test load (kN)	445.6	445.8	445.9
Average MPa	12.1		

4.2.1.3 Compressive Strength

Compressive strength test of UHPC was according to (ASTM C39/C39M −15a) [54]. Mixtures of compressive strength are measured after 28-days of curing. The compressive strength data listed in Table 4.3.

Table 4.3 Compressive strength testing results.

Mix	Cube compressive strength of 28- days (MPa)			Av. MPa	Cylindrical compressive strength of 28- days MPa			Av. MPa
1	135.1	132.3	140.1	135.83	-----	-------	------	------
2	134.5	133.7	139.3	135.8	119.3	118.5	123	120.2
3	141	138.3	145.4	141.6	124	135.4	130.3	130
4	129	125.4	131.4	128.6	108	115.4	112.8	112
5	121	105.3	110.3	112.2	------	------	-------	------

4.2.1.4 Modulus of Elasticity

Table 4.4 Modulus of elasticity testing results.

Modulus of elasticity (E) (GPa)	39.5	41.2	42
Average GPa	40.9		

4.3 Experimental Setup of Continuous Beams

The continuous beams tested under two point loads to study the flexural behavior. The applying loads accomplished by utilizing a hydraulic jack. The hydraulic jack was calibrated to provide required load. Strain gauges used to measure of deflection at two points at mid span for each span used for reading concrete strains that installed on the side of the concrete beam at its compressive and tensile fibers as shown in Figure 4.6. All strain gauges connected to a digital data logger to display the result strains during the loading. Testing of continuous

beams carried out in the structural laboratory of Basrah university college of engineering.

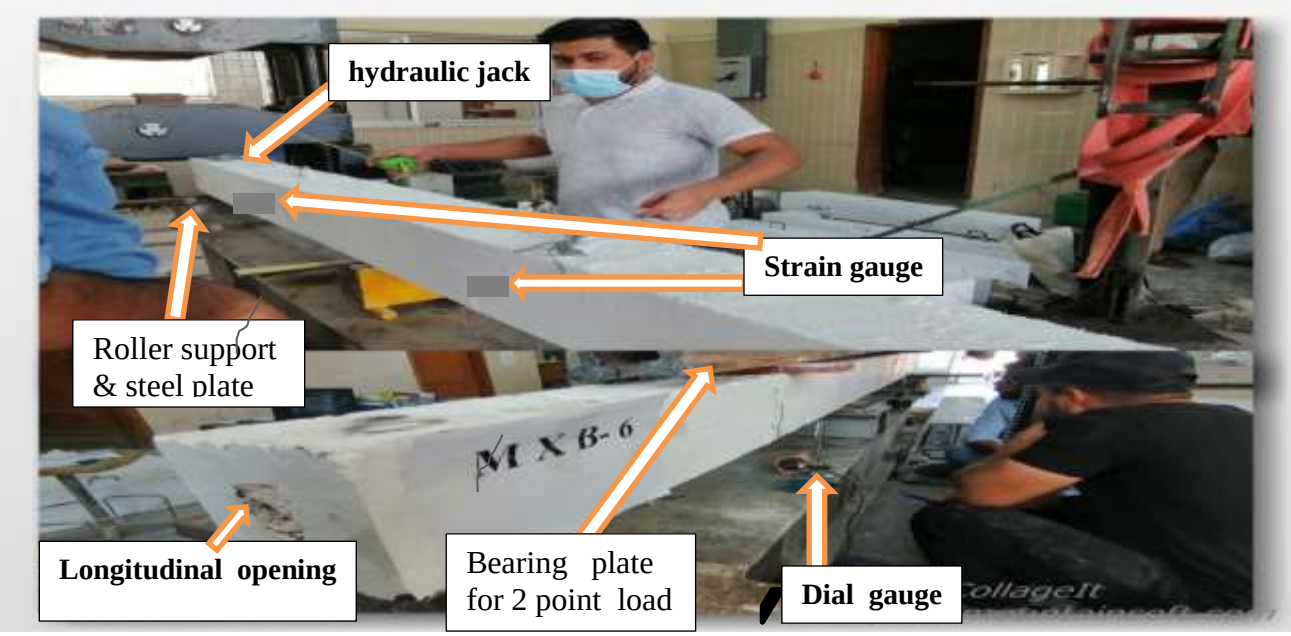

Figure 4.6 Test Setup of the experimental study of continuous beam.

4.3.1 Loading Procedure

Firstly the load was applied for preparation and then carried out the test. Loadings were progressively increased from 0 kN to failure with increasing of 10 kN as shown in Figure 4.7 All cracks were disclosed and were marked, and recorded loading value of first crack.

Figure 4.7 Record the results.

4.3.2 Result of Measurements

Results of deflection determined by used two dial gauges. The relation of load deflection of continuous beams recorded constantly during. The results of load deflection relation for all groups are showed that when load increases the deflection increases. In another word the continuous beam that has the greater failure load in the group has the greater deflection due to the directly relationship between the load and deflection.

4.4 Experimental Result of Tested Beam

1- The first cracks manifested in tension part at interior support or at mid of left and right span in the early stages of loading and known as cracking load.
2- The cracks manifested in tension part became wider and replicate toward compression part with increased load.
3- Further loading from the instrument made the crack to propagate and spread faster until happened failure case.
4- Presence longitudinal opening in continuous beam give compatible finding especially capacity property.

4.5 Behavior of tested beams

The continuous beams was tested by study some of parameters and its effect:

4.5.1 Effect of Steel Fiber Ratio Change

This group consists of four beams (three continuous beams were tubular and the fourth beam is solid). The aim of this group was to indicate the increasing of steel fiber competent of increasing the ultimate load capacity and ductility of beams .The experimental results denoted that the UHPC (1% S.F), UHPC (1.5% S.F), UHPC (2% S.F) and UHPC (1.5% S.F solid) enhance and give an increase in the flexural ultimate capacity at about (36.3%), (45.5%), (50) and (55%); respectively

with an increase in number of cracks (more warning before failure) as compared with UHPC (1% S.F), and the results indicated the significant effect on the capacity of the ultimate load. When the load was applied to these beams specimens, the first crack was formed at about (23.68%, 25%, 33% and 33.33%) of the ultimate load for beams (MXB-4, MXB-5, MXB-6, RE.S) respectively.

For (MXB-4) beam, the first crack registered at load (90 kN) at mid of right span and the beam fail at ultimate load equal (380 kN) and the type of failure was flexural failure.

For (MXB-5) beam, the first crack showed at load (100 kN) at mid of left span and the beam fail at ultimate load equal (400 kN) and the type of failure was flexural failure.

For (MXB-6) beam, the first crack noticed at load (150 kN) at mid of right span and the beam fail at ultimate load equal (450 kN) and the type of failure was flexural failure.

For (RE.S) beam, the first crack was observed at load (160 kN) at mid of left span and the beam fail at ultimate load equal (480 kN) and the type of failure was flexural failure.

In the solid beams (1.5% S.F), the experimental results showed that an increase in the first cracking and ultimate loads at about (60 % and 20 %), (77.7% and 26.3) and (6.66% and 6.67%); respectively with an increased in number of cracks (more warning before failure) as compared with MXB-5(1.5 S.F.) , MXB-4 and MXB-6.

The crack pattern for MXB-4, MXB-5, MXB-6 and solid as reference beam are shown in Figure 4.8 to Figure 4.11.

Figure 4.8 Crack pattern of MXB-4 (1% S.F).

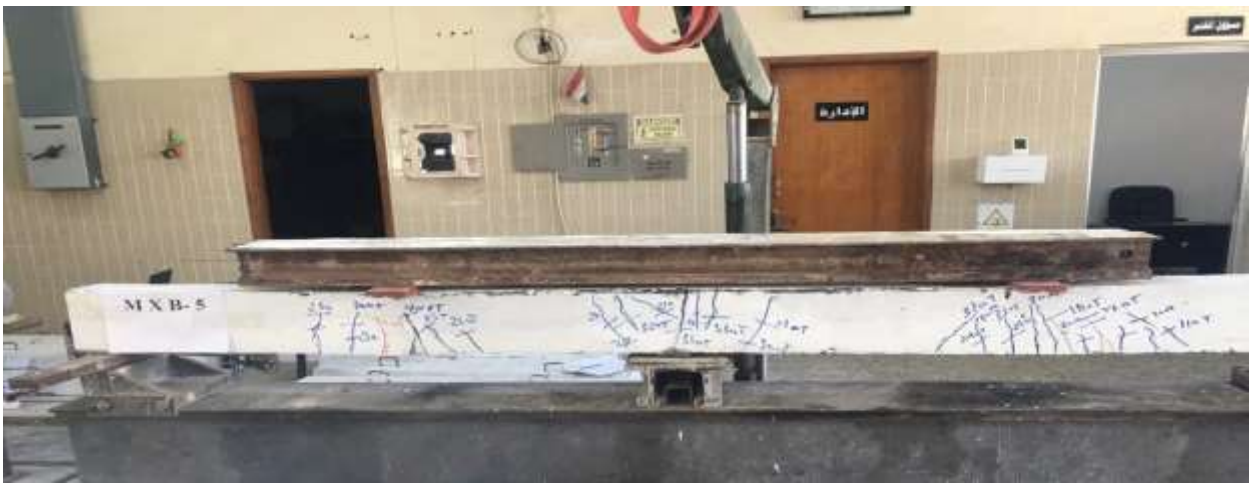

Figure 4.9 Crack pattern of MXB-5 (1.5% S.F).

Figure 4.10 Crack pattern of MXB-6 (2% S.F).

Figure 4.11 Crack pattern of solid beam-RE.S (1.5%S.F).

Table 4.5 Summary of results for group two.

Group No.	Beam designation	First crack load (kN) (Pcr)	Ultimate load (kN) (Pu)	Pcr/Pu %	Mid span deflection (mm) at ultimate load
2	MXB-4	90	380	23.68	14.23
	MXB-5	100	400	25	13.1
	MXB-6	150	450	33	12.6
	RE.S	160	480	33.33	11.8

4.5.2 Effect of Longitudinal Reinforcement Bars Ratio

Three ratios of longitudinal tensile reinforcement were used to study the flexural behavior of beam and mode of failure. This group consists of four continuous beams three beams are tubular beams and the fourth is solid to comparison, the ratio of beams are MXB-7(ρ^{-}=0.0171 & ρ^{+}=0.0141**)**, MXB-8 (ρ^{-}=0.0112 & ρ^{+}=0.0101), MXB-9 (ρ^{-}=0.01 & ρ^{+}=0.0078), RE.B(ρ^{-}=0.01 & ρ^{+}=0.0078).

The experimental results showed that when using high ratio of bar reinforcement, it was noticed that the longitudinal steel reinforcement had not significant effect on the first cracking load but significant effect on the ultimate load capacity.

It was observed that the ultimate load was increased by (12.82% and 15.78%) when positive and negative tensile reinforcement ratio was increased from (1% and 0.78%) for beam MXB-9 to (1.12% and 1.01%) for beam MXB-8, and (1.71% and 1.41%) for beam MXB-7, respectively and the ultimate was increased by (21.05%) for solid beam RE.B when utilized same amount of positive and negative tensile reinforcement with MXB-9. The increase in the ultimate loads related to the fact that increasing tensile reinforcement ratio leads to increase tensile force. Therefore, the resisting bending moment capacity of beam increases and this leads to increase the ultimate load.

In MB-7(ρ^{+}=0.0171 & ρ^{-}=0.0141) first crack was observed at an applied load (120 kN) at both side and the beam reached an ultimate load (440 kN) with flexure failure mode's.

In MXB-8 (ρ^{+}=0.0112 & ρ^{-}=0.0101)first crack was observed at an applied load (110 kN) at both side and the beam reached an ultimate load (390 kN) with flexure failure mode's.

In MXB-9 (ρ^{+}=0.01 & ρ^{-}=0.0078) first crack was observed at an applied load (100 kN) at both side and the beam reached an ultimate load (380 kN)with flexure failure mode's.

In RE.B (ρ^{+}=0.01 & ρ^{-}=0.0078) first crack was observed at an applied load (180 kN) at both side and the beam reached an ultimate load (460 kN) with flexure failure mode's as shown in Figures (4.12 to 4.15).

Figure 4.12 Crack pattern of MXB-7.

Figure 4.13 Crack pattern of MXB-8.

Figure 4.14 Crack pattern of MXB-9.

Figure 4.15 Crack pattern of RM-B (solid).

Table 4.6 Summary of results for group three.

Group No.	Beams designation	First crack load (kN) (Pcr)	Ultimate load (kN) (Pu)	Pcr/Pu %	Mid span deflection (mm) at ultimate load
3	MXB-7	120	440	27.27	8.1
	MXB-8	110	390	28.2	9.3
	MXB-9	100	380	26.3	11.1
	RE-B	180	460	39.13	8.5

During the testing, each beam showed a different behavior when reaching the ultimate load, except in the initial phase of loading, which showed an elastic behavior. By increasing the loads, both dial gauge and load-cell stopped slightly, which indicates internal micro crack occur after increasing the loads, non-linear behavior began which is an indicator that tested beams reach its plastic phase. The bending cracks in all beams started to increase and took a vertical direction towards the two loading points. Since cracks have a steady growth process with increased loading. However, the extension of cracking was interrupted by the presence of tensile stresses provided from the presence of steel fibers in UHPC mixture and steel reinforcement. Other flexural cracks appeared almost in the mid-span of the beams and increased. Then the inclined cracks (shear cracks) began to appear gradually and directed towards the supports and at the loading points. At the end of loading, the existing cracks began to grow and extended rapidly to the compressive zone of the concrete. Concrete crushing near the loading points was minimal due to the properties of Ultra-High-Performance Concrete (UHPC) and its high compressive strength.

4.6 Load Versus Mid Span Deflection Results

After the curing process of beams was finished, the beams were painted in white color and the load was applied in the center of the beam specimens by increasing the pressure of hydraulic jack. Two dail gauges were measured deflections during the test. The Figure 4.16 show measuring of results of load – deflection relation for all tested continuous beams in the first group. The general experimental behavior of the tubular continuous beams noticed during the test that can be summarized as follows; when increased the applied load the first crack occurs in the tension zone and give an indication that the concrete loss its tensile strength. therefore, the applied loads increased until increase in the dial gauge reading occur that give us an indication that bar reinforcement has been yielded. The increasing in applied loads led to crushing the concrete at compression fiber.

The main final cracks were at mid supports zone and under point load in both mid span for all tested beams, including the control beam (solid beam) and showed an indication that all the tested beam fails in flexural failure.

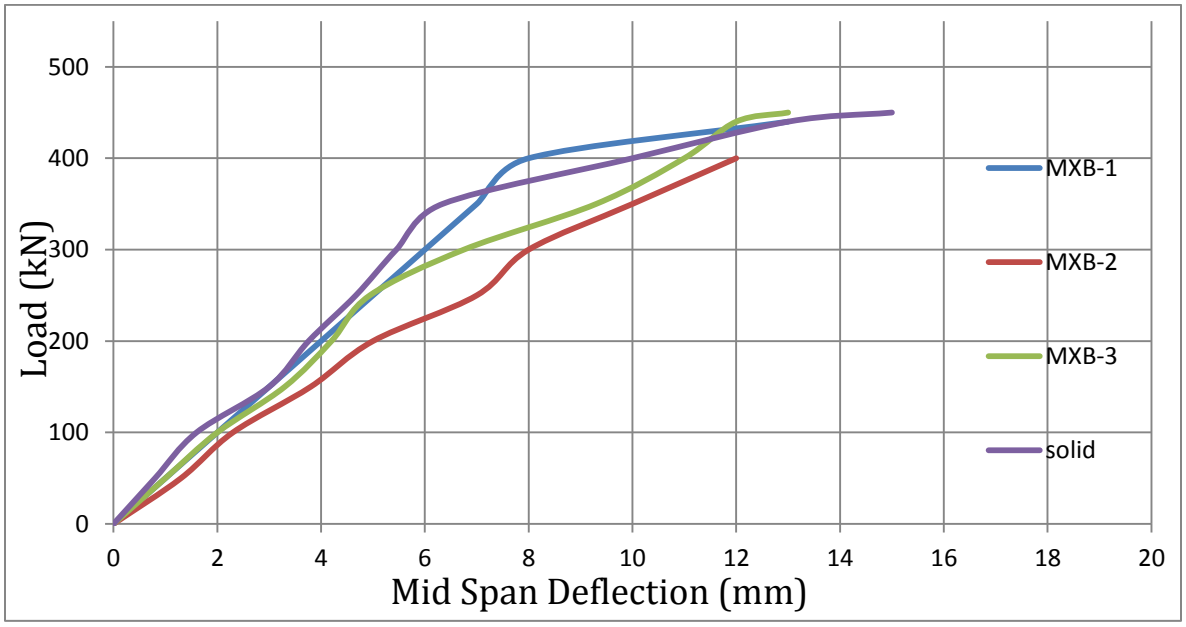

Figure 4.16 Load –mid span deflection curve of first group.

As shown in Figure 4.17, it was noticed that the beams with UHPC and when increased the steel fiber ratio enhanced the flexural behavior and gave more stiffness as well as the deflection of beams at the ultimate load (380 kN) was (14.23 mm), while the continuous beams MXB-5 ,MXB-6 and RE.S record increase in flexural stiffness and decrease in deflection about (7.94% ,11.45% and 17.07%), respectively and the deference between the reference beam and MXB-5 that have same steel fiber ratio is (9.9%). This can be attributed to the high resistance of the beams with UHPC (high compressive strength), and this causes high applied loads, which the deflection to increase. Moreover, the presence of steel fiber, makes the beams ductile and deflection decrease.

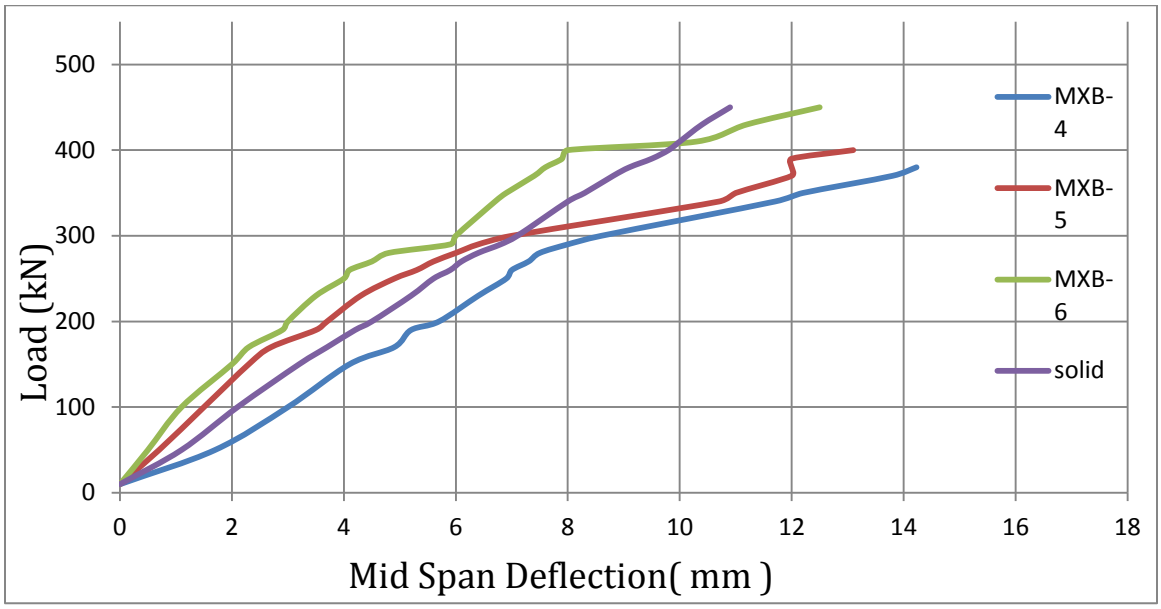

Figure 4.17 Load –mid span deflection curve of second group.

The Figure 4.18 show the load-deflection for group three. When the positive and negative longitudinal bar steel ratio increased from (1% and 0.78%) for beam MXB-9 to (1.12% and 1.01%) for beam MXB-8, and (1.71% and 1.41%) for beam MXB-7, the deflection in mid-span at ultimate stage increased by (19.35) %and (37.03)%. And the important point when utilized solid continuous beam it is

observed that the difference was (23.4%) as compared with MXB-9, every beam had same amount of bar reinforcement and steel fiber ratio, it can also be seen from the Figures below that the load-deflection curve of beam MXB-9 (beam with low longitudinal steel ratio) are steeper than similar curves belonging to beams MXB-8 and MXB-7.

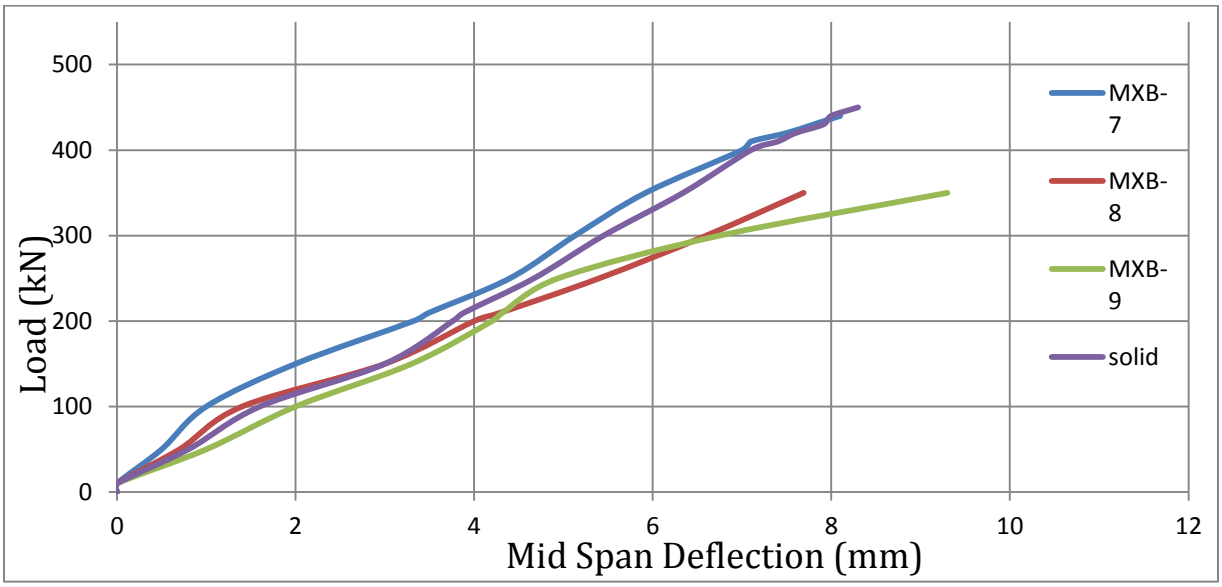

Figure 4.18 load –mid span deflection of third group.

4.7 Crack Width

Crack width was measured by modern crack meter tool for all tested continuous beam and also recorded the development of the first crack with applying load. The first crack does not always give the maximum crack width. Figure 4.19 and Figure 4.20 show the effect of longitudinal reinforcement ratio, steel fiber ratio, respectively.

In general , at the low loading level , the beams were free from any cracks, and all tested beams behaved in an elastic manner . As the load was increased and tensile stress resulted from the applied load exceeding the tensile strength of the concrete ,cracks were formed . Continuous beams failed in the flexural mode, the

first crack was formed at the bottom face of the beam near the mid span region for each span.

New cracks were appear when the loading level was further increased .for the beam made from UHPC ,the cracks appeared at the bottom face, while the top face did not more cracks.This is related to the high strength of the concrete.

It was found that when the steel fiber ratio increased by (1- 2)% the number of cracks increased by 30.6% compared with UHPC(1%), and the number of cracks increased by 25 % when increased longitudinal bar reinforcement ratio from to (ρ^{+}= 0.0112) to (ρ^{+}= 0.0171). Also the number of cracks increased when used solid continuous beam. The crack width decreased as the longitudinal ratio and steel fiber increased. Table 4.7 presents the maximum crack width and total number of cracks for the tested beams.

Table 4.7 Maximum crack width and number of cracks.

Beams Detail	**First crack**			**Total number of-cracks at failure**
	p_{cr}(kN)	**Crack-width average (mm)**	**Max. crack width (mm)**	
MXB-4	90	0.05	0.4	35
MXB-5	100	0.05	0.45	38
MXB-6	150	0.03	0.4	41
RE.S	160	0.01	1.2	45
MXB-7	120	0.02	0.5	52
MXB-8	110	0.05	0.6	45
MXB-9	100	0.04	1	55
RE.B	180	0.03	0.3	50

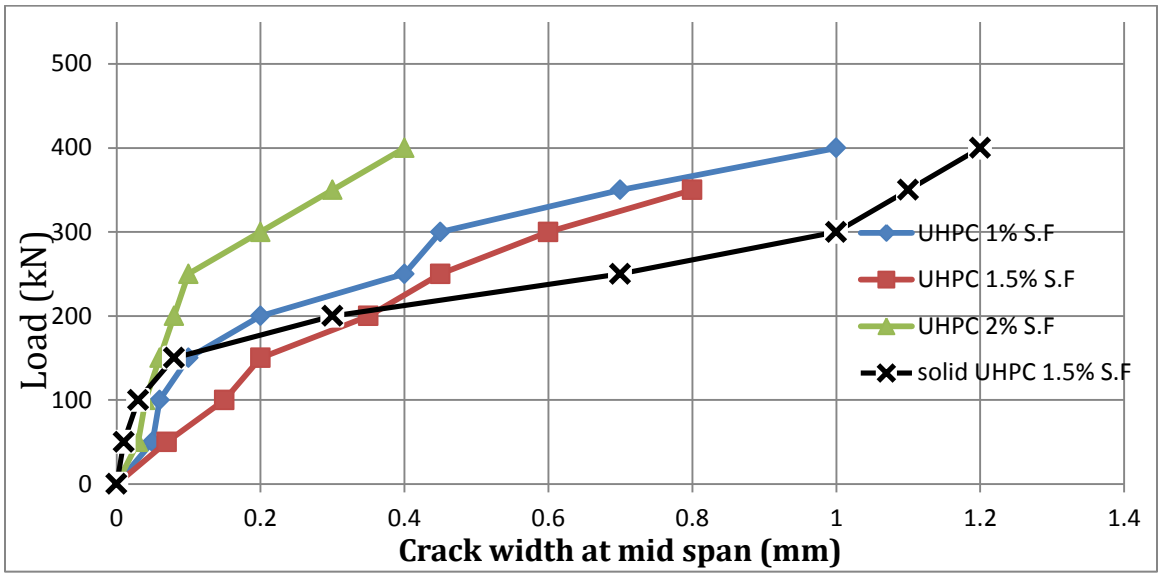

Figure 4.19 Development of crack width for second group.

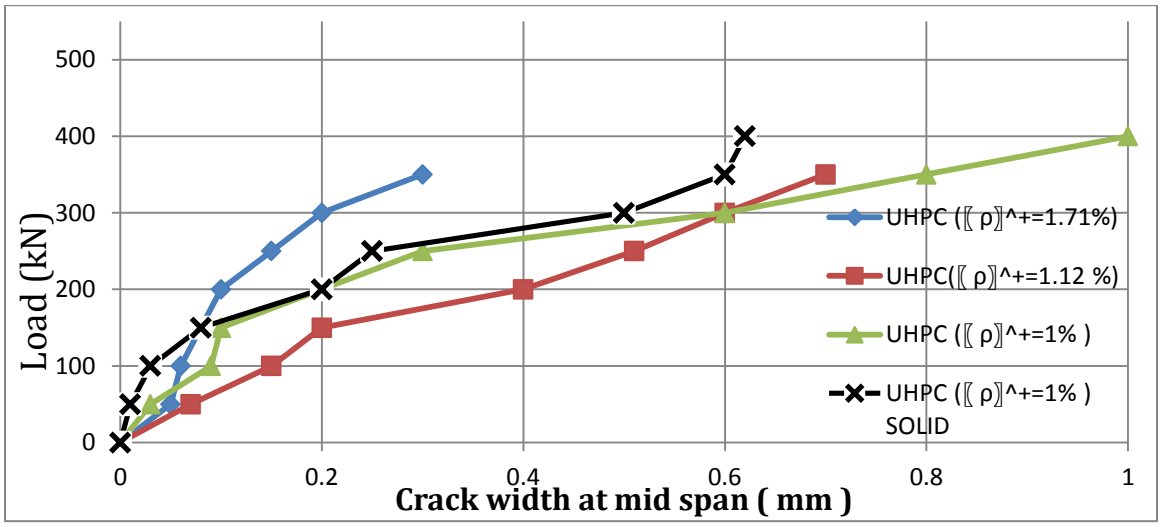

Figure 4.20 Development of crack width for third group.

4.8 Ductility Ratio

Ductility is one of the most important properties that should be taken into account in the designs of structures exposed to a large number of inelastic deformations resulting from different loading conditions. Beam ductility is defined as its ability to resist inelastic deformation without any reduction in its load carrying capacity up to failure. In other expression, the ductility can be simplified

as the ratio between the deformation at ultimate stage to yield deformation or it can be calculated by dividing the maximum deflection (Δu) on the yield deflection (Δy). From the load deflection curves, the deflection at yield limit indicated by intersect into two lines ; line of best fit as a tangent line and horizontal line passed through the ultimate line, as shown in Figure 4.21.

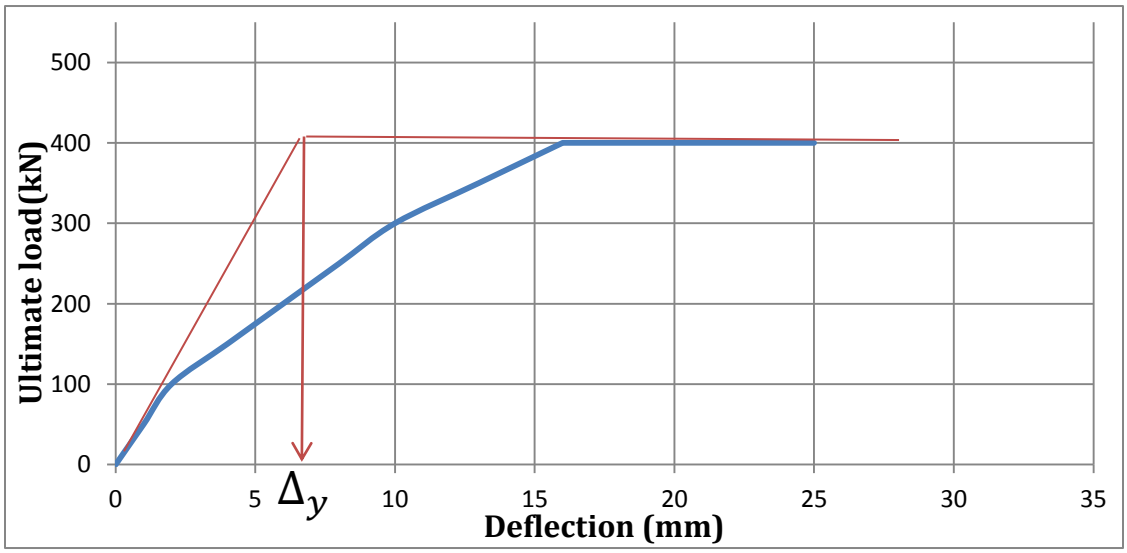

Figure 4.21 Indication of yield limit for Elasto – Plastic behavior.

The ductility ratio for tested beam shown in Table (4.8), noted that the UHPC had a ductile behavior more than normal concrete beams. Also, the results showed that increasing in steel fiber from(1% to1.5% to2%) lead to an increase in ductility at about (7.1%) and (13.36%); respectively. When compared with reference solid beam (RE.S) with MXB-5 that have same amount of steel fiber the result showed increase in ductility by (23.89%) in RE.S.

Table 4.8 Ductility ratio for the tested beams.

Group NO.	Beams Characterization	Deflection (mm)		Ductility ratio Δ_u/Δ_y
		Δ_y	Δ_u	
1	MXB-4	6.4	14.23	2.223
	MXB-5	5.5	13.10	2.381
	MXB-6	5.0	12.60	2.520
	RE.S	4.0	11.80	2.950
2	MXB-7	7.0	8.10	1.150
	MXB-8	7.7	9.30	1.200
	MXB-9	7.8	11.10	1.420
	RE.B	6.0	8.50	1.400

But three containing the beam that had highest longitudinal steel reinforcement ratio(MXB-7) has less ductility factor by (4.3%) than (MXB 8) and (23.47%) than (MXB 9). This means that the section that contains more longitudinal reinforcement has a greater ultimate load (Pu=440 KN). So, It reaches yield stage lately, where the elastic phase is greater than the plastic phase, which causes an increase in yield deflection value (Δy) lead to decrease the ductility factor ($\mu = \Delta u / \Delta y$). In addition when compared reference solid beam (RE.B) with tubular continuous beam (MXB-9) the result showed the decreased in ductility was very low (1.4%) this point proved the advantage and economical when utilized of longitudinal hole in continuous beam.

4.9 Toughness Capacity for The Tested Continuous Beams (Energy Absorption)

Energy absorption capacity can be calculated through the load-deflection curve. The area under the curve represents the value of energy absorption capacity. Figure 4.22 shows the energy absorption of group No.2, the increase in steel fiber ratio of continuous beams from 1% to 1.5% to 2% will increased energy absorption

by (5.2%) and (19.95%) respectively. The toughness of MXB-5 decreased by (0.3%) when compared with solid reference beam RE.S that had same amount of steel fiber (1.5%), this can give indication of benefit and activity of longitudinal hole.

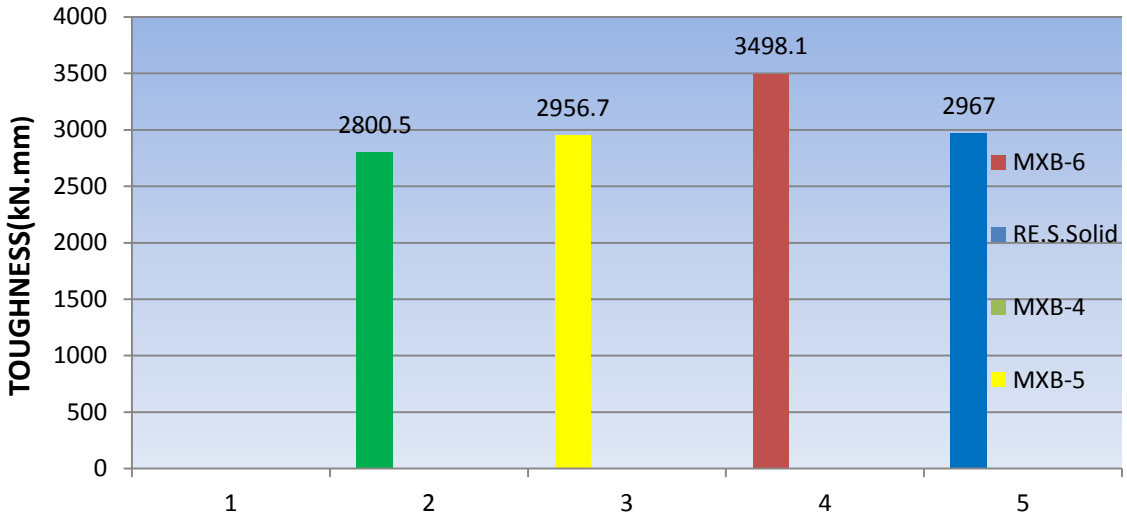

Figure 4.22 Toughness capacity for group two (change S.F. ratio).

As shown in Figure 4.23 show the energy absorption of group No. 3, the increase in steel bar reinforcement from 1% to 1.12% to 1.71% will increased energy absorption by (46.4%) and (21.44%) respectively and (34%) when compared solid RE.B with MXB-9 that have same amount of bar reinforcement. From the result show that when increased steel fiber ratio and bar reinforcement ratio increased toughness of continuous beam and show also can utilized longitudinal opening in selected dimensions in the present work.

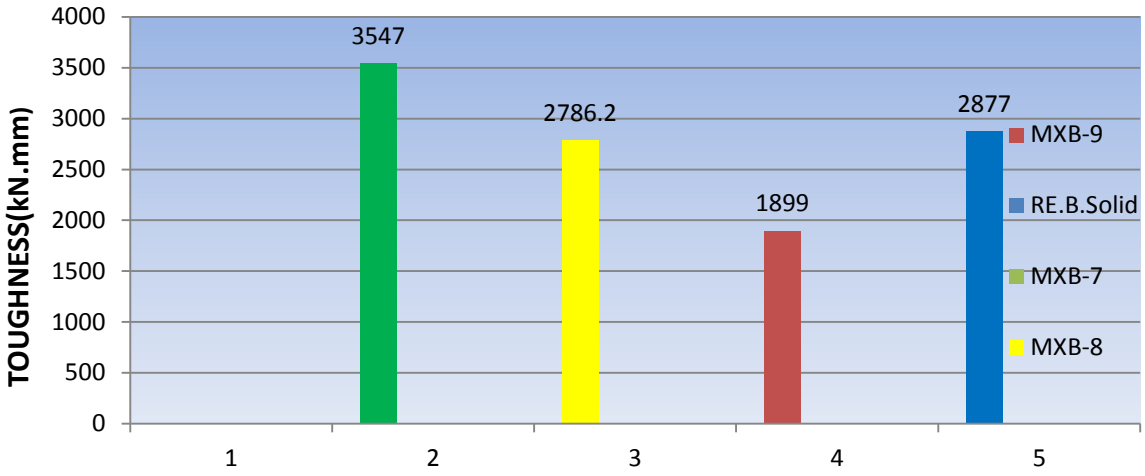

Figure 4.23 Toughness capacity for group three (change ρ ratio).

4.10 Stiffness Comparison for The Tested Beams

Stiffness can be defined as the required load for causing one-unit of deflection. The value of the stiffness can be calculated by dividing the ultimate load on the maximum deflection in the tested beam and called secant stiffness that will study. In general, the beam that has a higher ultimate load and less deflection will have a higher stiffness value. The stiffness values at ultimate loads of the tested beams are presented in Figure 4.24 to 4.25.

For group No.2 and as shown Figure 4.24**,** it noted that in the second group that when increase ratio of steel fiber from 1% to 1.5% to 2% increase stiffness by(12.45%) and (22.15%) and when compared reference beam with MXB-5 show the decreased in stiffness in tubular continuous beam was (24.87%).

In group No.3 as shown in Figure 4.25 It can notice that the tubular continuous beam (MXB 7) that has the higher longitudinal reinforcement give the higher stiffness than (MXB 8) and (MXB 9) by 22.83% and 37% respectively. This indicates that stiffness tubulr continuous beams increases when it is longitudinal reinforcement ratio increases and when compared reference beam with MXB-9 show the decreased in stiffness in tubular continuous beam was (36.78%). Finally

noticed in every group when compared between tubular beams and solid beams that represent reference beam stiffness for solid beams higher than tubular beams.

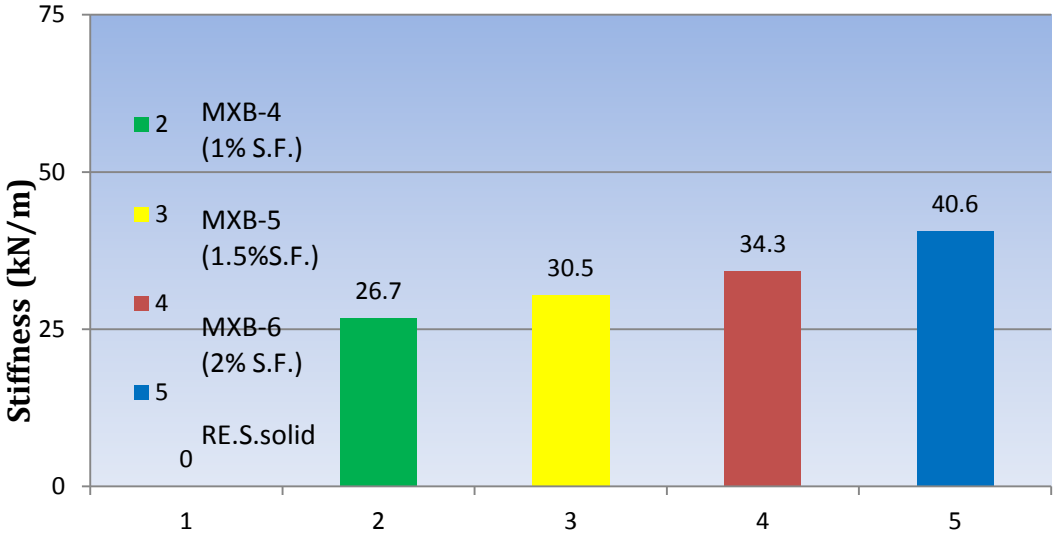

Figure 4.24 Stiffness values of the group two beams.

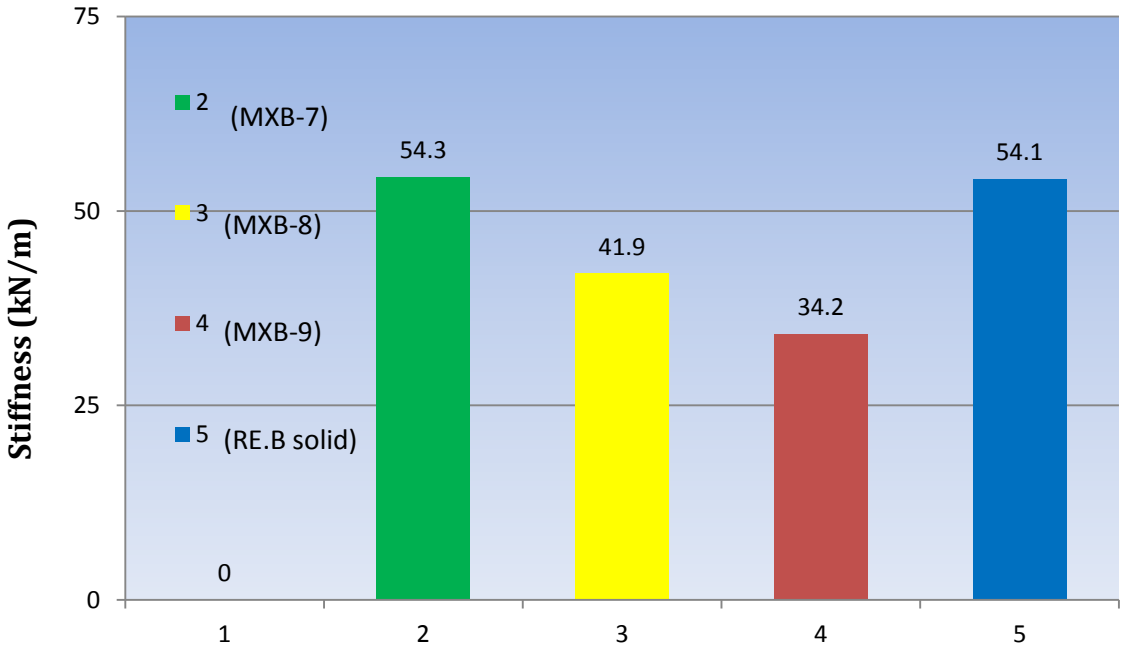

Figure 4.25 Stiffness values of the group three beams.

4.11 Concrete Strain Distribution

The strains in the concrete of tested continuous beams were measured by four strain gauges in right and left mid span. The maximum concrete strain can be expected in the extreme compressive fiber and extreme tension fiber. The strain gauge located at 35 mm from the top and bottom of beam's surface as shown in Figure 4.26.

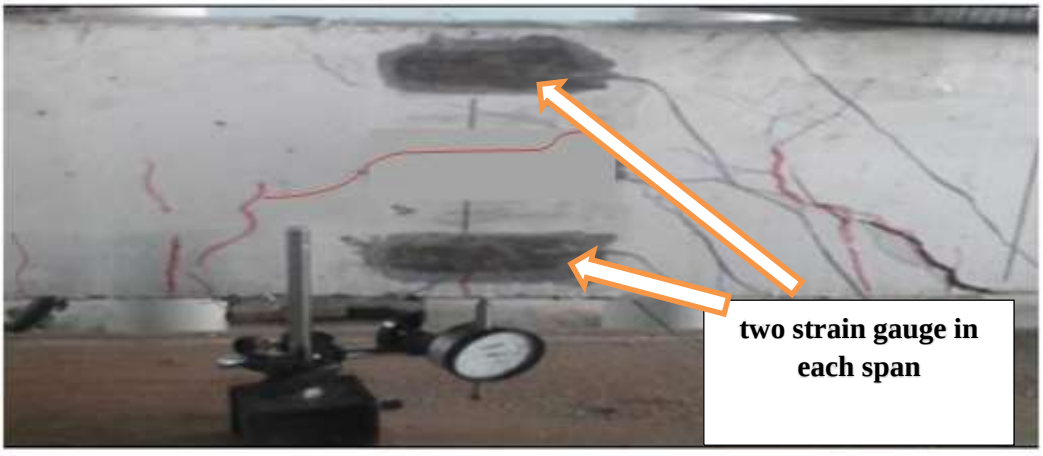

Figure 4.26 Strain Gauges' Distribution.

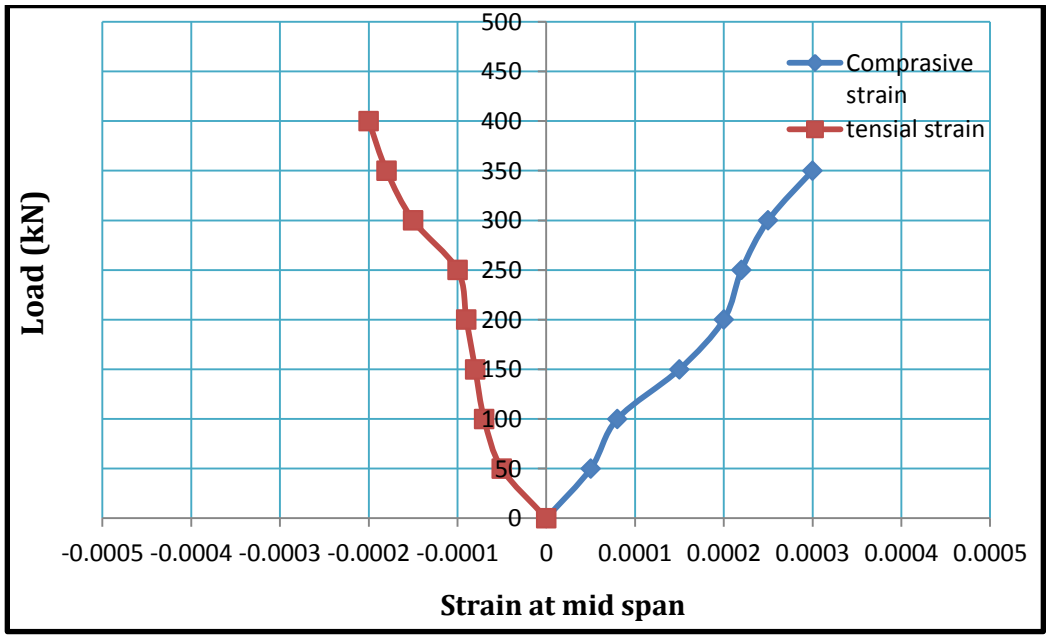

Figure 4.27 Compressive and tensile strain of MXB-4.

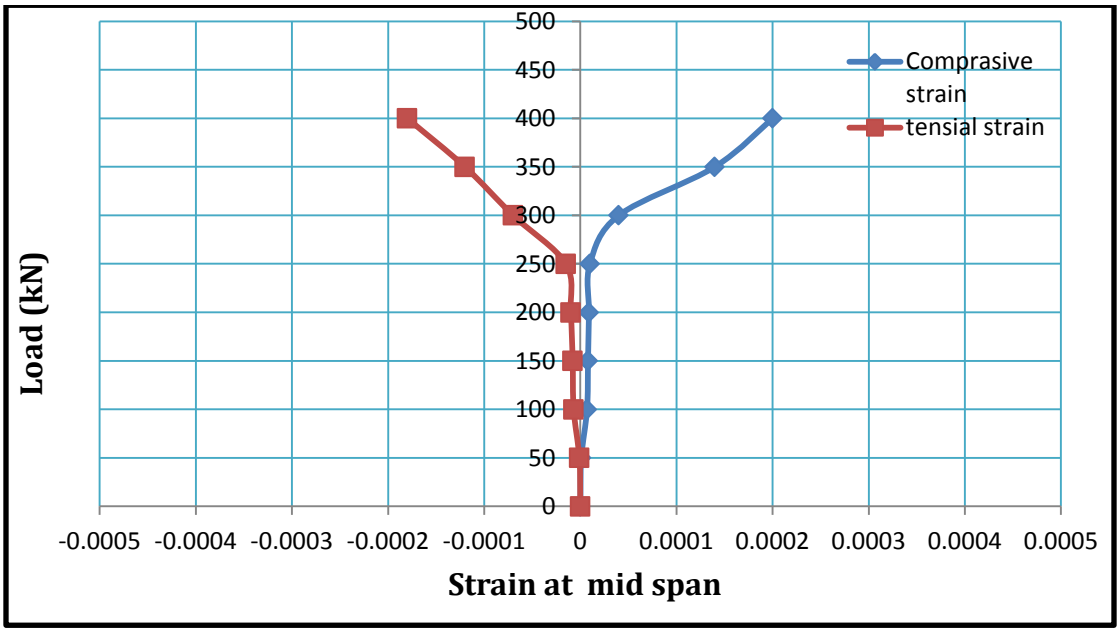

Figure 4.28 Compressive and tensile strain of MXB-5.

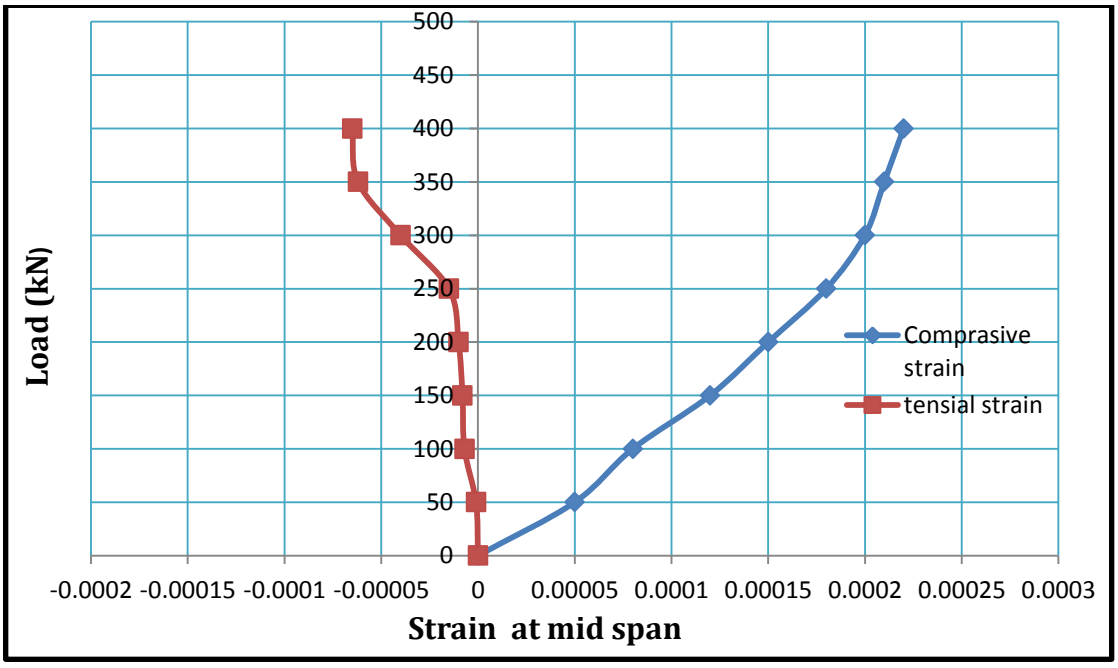

Figure 4.29 Compressive and tensile strain of MXB-6.

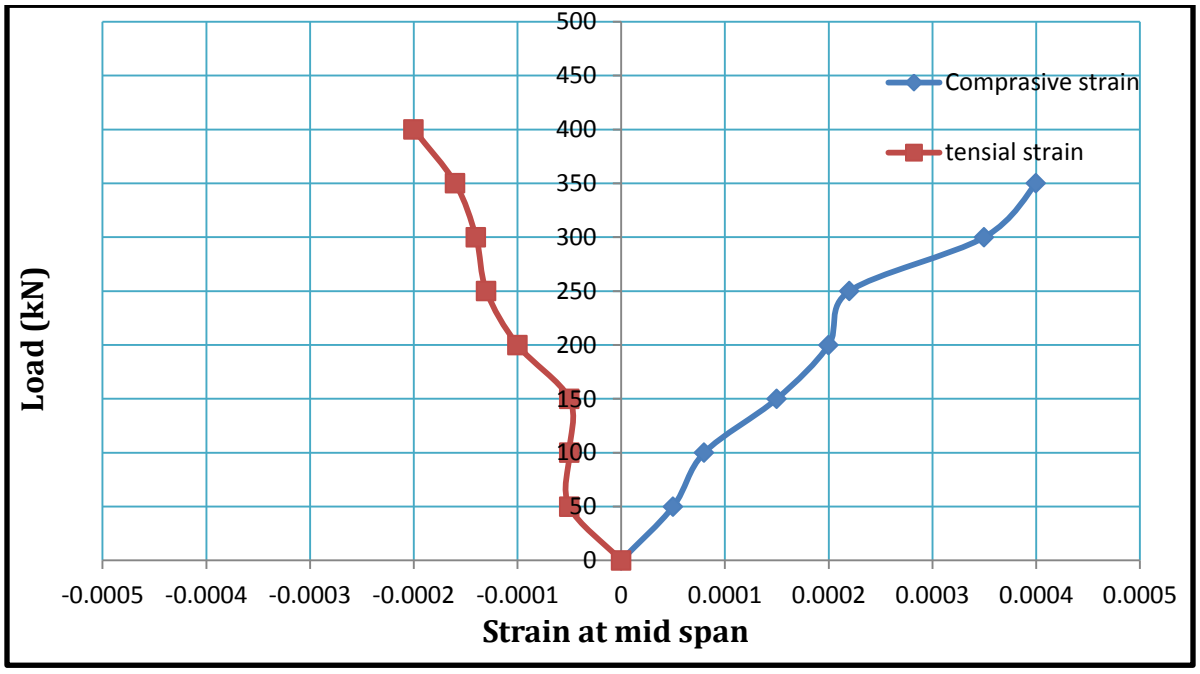

Figure 4.30 Compressive and tensile strain of R.E.-S.

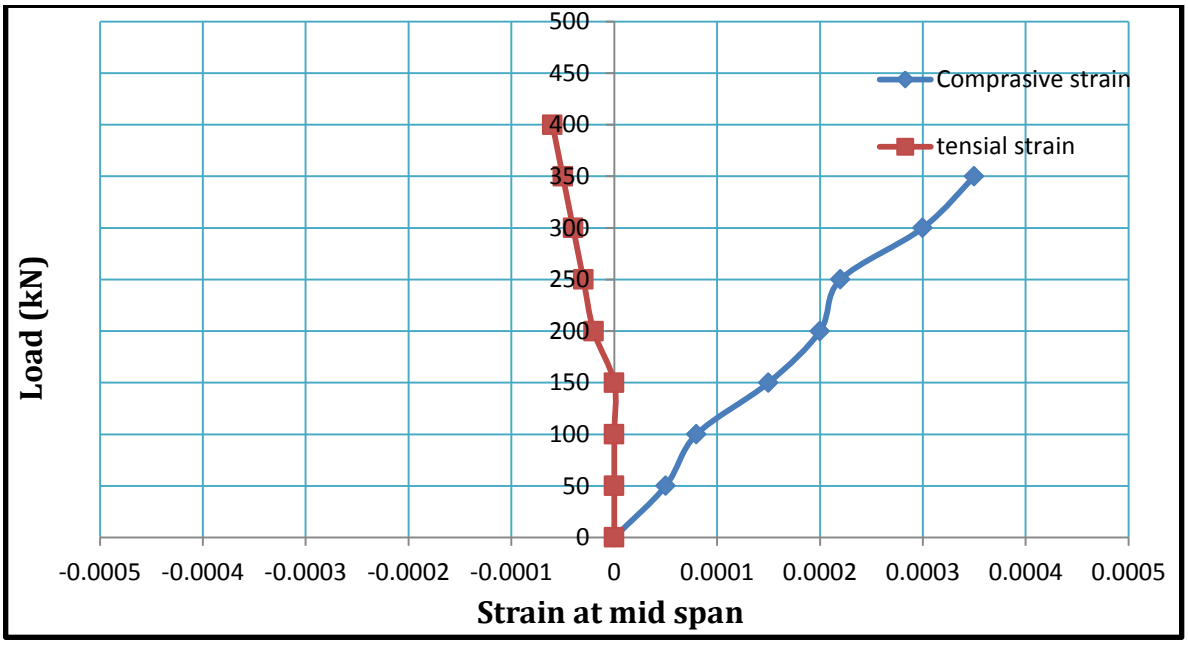

Figure 4.31 Compressive and tensile strain of MXB-7.

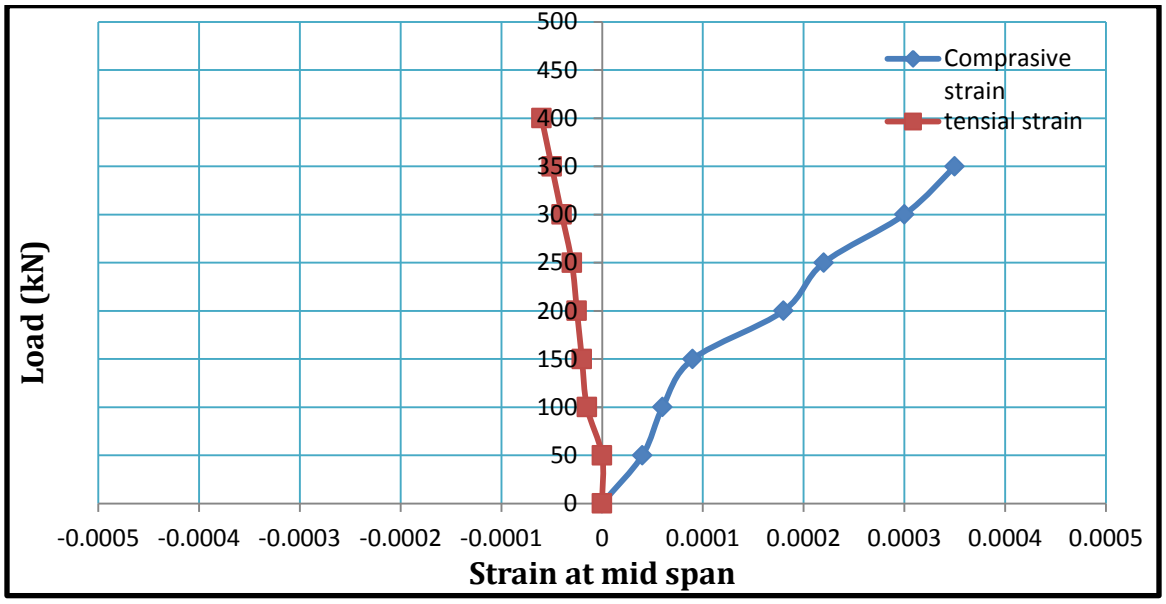

Figure 4.32 Compressive and tensile strain of MXB-8.

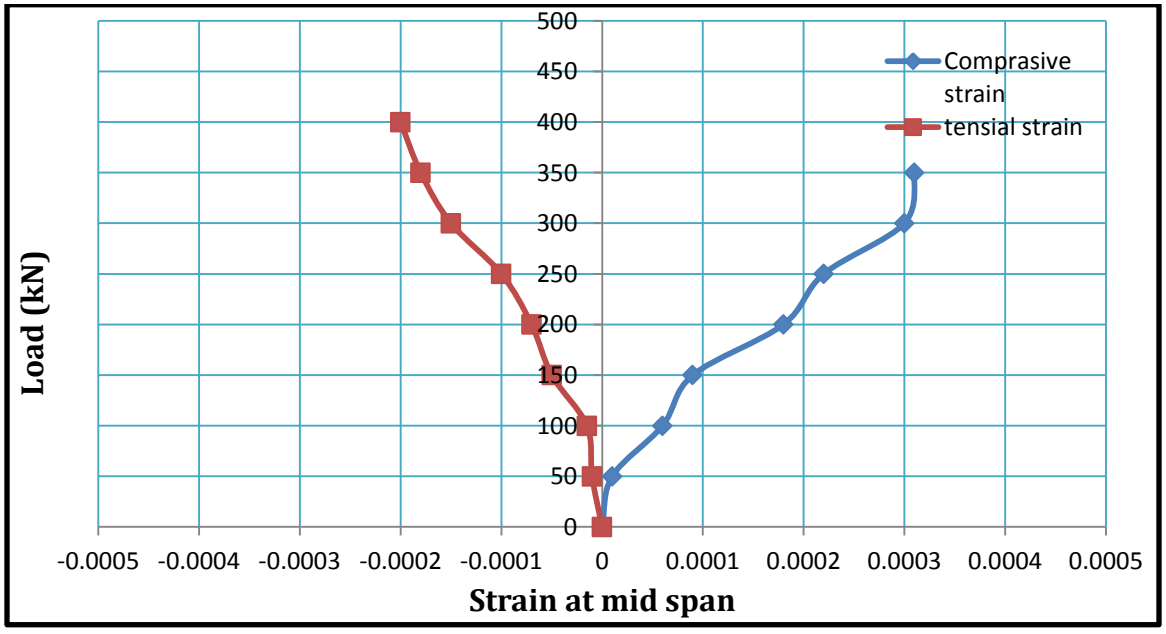

Figure 4.33 Compressive and tensile strain of MXB-9.

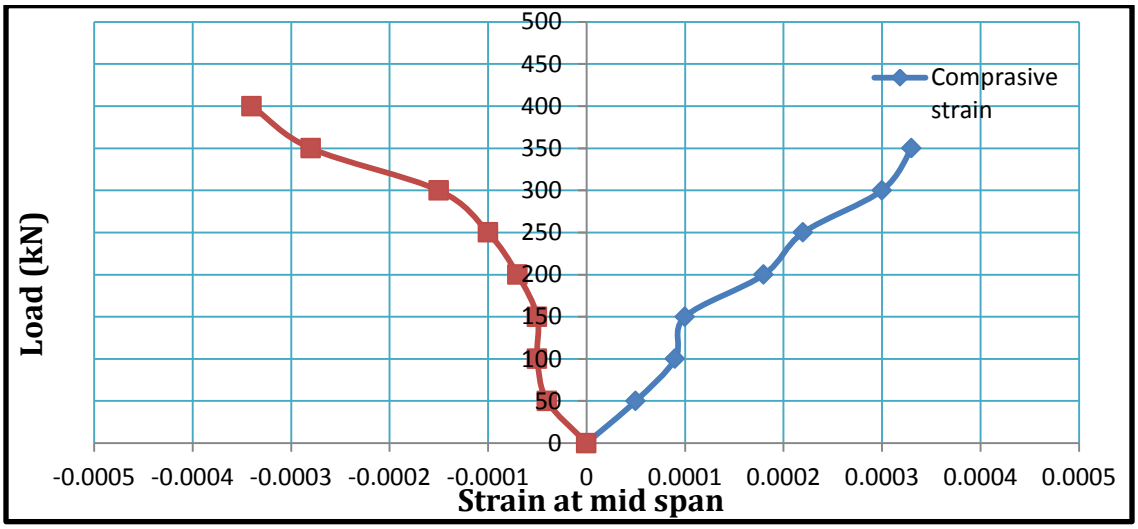

Figure 4.34 Compressive and tensile strain of RE.B.

4.12 MOMENT REDISTRIBUTION

The concept of moment redistribution is used to reduce the absolute magnitudes of moments in critical regions, it is described as the transfer of moment between high moment regions, usually at the supports, to lower moment regions in the member while maintaining the overall structural resistance. This is due to the formation of plastic hinges at the zones where the yielding moment is reached. Phenomenon of moment redistribution. In the design of statically indeterminate structures that occurs at all limit states due to a difference in the relative stiffness of individual cross sections [30], but is typically utilized by designers at the ultimate limit. Moment redistribution allows the designer to reduce both the maximum hogging and sagging elastic moments, thereby reducing the overall moment demanded across a span, enabling a reduction in reinforcement requirements. Additionally, the ability to shift moments away from less efficient cross sections towards other more efficient cross sections may allow for savings in reinforcement costs and the easing reinforcement congestion [28]. These factors may be particularly important for UHPC which has higher material costs than

conventional concrete and has the potential to perform poorly in regions of congested reinforcement if fibres cannot be uniformly distributed around reinforcement.

Moment redistribution is a specific behavior of statically indeterminate reinforced concrete (RC) structures due to the structural redundancy and nonlinear characteristics of the reinforced concrete. However, the evolution of moment redistribution is a complex process moment redistribution in continuous members allows more flexibility in structural design. It is usually carried out by reducing the hogging moments over supports, with corresponding changes in the sagging moments to satisfy equilibrium. Accordingly, reinforcement congestion at beam to column joints in hogging zone regions may be avoided. Alternatively, when moment redistribution is employed in different load combinations, both hogging and sagging moments may be reduced, achieving economic design. Moment redistribution is useful for practical design as it allows some flexibility in the arrangement of reinforcement. It can be used to transfer moment away from congested areas such (beam– column connections) into less congested areas (e.g. mid-spans of beams), thus avoiding the need to detail each beam separately. In addition, useful economies can be achieved when moment redistribution is applied to different load combinations, resulting in a smaller bending moment envelope which still satisfies equilibrium. ACI 318-14 [34] have limited the percentage of the moment redistribution to the maximum value of $20\{1-(\rho-\rho')\rho b\}\%$, where ρ , ρ' and ρb are the ratio of the tensile reinforcement ,$\rho = As\ bd$ the ratio of the compressive reinforcement, $\rho' =$

$As'bd$, and the reinforcement ratio corresponding to the balance condition; respectively. The redistribution is limited to the condition that ρ or $\rho-\rho'$ are not greater than $0.5\rho b$. However the ACI 318-14[34] defines the allowable moment

redistribution in terms of net tensile strain in extreme tensile steel, $\boldsymbol{\varepsilon_t}$, and expresses it as 1000 $\boldsymbol{\varepsilon_t}$ percent. According to this code, the moment redistribution is permitted if the critical sections have adequate ductility; i.e. $\boldsymbol{\varepsilon_t}$ is equal or greater than 0.0075 at the sections under consideration. Using equilibrium equations in a beam section, ACI 318[34] and CAN-A23[22], that have limited the maximum redistribution to the value of 20%.

The advantages of redistribution of moment of the beam can be summarized as:

1- Moment redistribution is useful for practical design as it allows some flexibility in the arrangement of reinforcement.
2- It can be used to transfer moment away from congested areas (e.g. beam–column connections) into less congested areas (e.g. mid-spans of beams)
3- Allowing standard reinforcement layouts where small differences occur in the bending moment distributions for a series of beams, thus avoiding the need to detail each beam separately.
4- Useful economies can be achieved when moment redistribution is applied to different load combinations, resulting in a smaller bending moment envelope which still satisfies equilibrium .
5- Reducing the absolute magnitudes of moments in critical regions.
6- Fully utilize the capacity of non-critical cross sections.

Table 4.9 and Table 4.10 contain on moments value at elastic and experimental case, the elastic moment value produced from excel sheet through equations derived from complex process to become suitable with the present work, especially the concrete type is from Ultra High Performance Concrete that shown in appendix –A . In addition the moment redistribution calculated from Equation (4-3)**,** it is found that moment redistribution it is variable when change amount of steel reinforcement and change values of ultimate failure load in each beam while

the experimental moment in Table (4.9) and (4.10) was calculated from Equations (4-4) and (4-5).

$$\%\text{Redistribution} = \left(\frac{\textit{Elastic Moment} - \textit{Experimental Moment}}{\textit{Elastic Moment}}\right)*100 \quad \ldots (4\text{-}3)$$

$$\text{M negative} = -\left(\frac{3PL}{16}\right) \quad \ldots\ldots\ldots(4\text{-}4)$$

$$\text{M positive} = \left(\frac{5PL}{32}\right) \quad \ldots\ldots\ldots(4\text{-}5)$$

Table 4.9 The moments and % moment redistribution at central support.

Beam Designation	**Ultimate Load (kN)**	**Elastic Moment (kN.m)**	**Experimental Moment (kN.m)**	**% MR β**
MXB-1	240	70.3	63.16	10.18
MXB-2	190	59.1	49.87	15.6
MXB-3	195	68.01	51.18	24.74
RE.M	200	59.1	52.5	11.16

Table 4.10 The moments and % moment redistribution at mid span.

Beam Designation	**Ultimate Load (kN)**	**Elastic Moment (kN.m)**	**Experimental Moment (kN.m)**	**% MR β**
MXB-1	240	62	65.1	5.1
MXB-2	190	49	54.4	11
MXB-3	195	52.3	63	20.45
RE.M	200	51	55.2	8.23

From the test results and according to ACI condition to achieve moment redistribution in continuous beam ($\rho < 0.5\ \rho b$) it's noticed when utilized reinforcement ratio more than 0.5ρb in beam (MXB-3) caused increased in (ß > 20%) in both sagging region(M^+)and hogging region (M^-).

CHAPTER FIVE: CONCLUSIONS AND RECOMMENDATIONS

5.1 General

Ultra High Performance Concrete (UHPC) is a material that is gaining attention in the construction industry due to the high mechanical strength and endurance (durability), which results in structures that required less maintenance. In this work the main purpose is to study the flexural behavior of tubular continuous UHPC beams using different parameters such as effect of steel fiber ratio and bar reinforcement ratio and the important parameter is moment redistribution of continuous beams.

5.2 Conclusions

1. UHPC mixtures are possible to develop from available locally and imported materials, by used sand #4 and heat curing three days at 80°C then remained inside water with room's temperature. The utilized of finer sand leads to increase the compressive strength, even though w/c ratio (0.2%)utilized with it is higher. Used finer sand led to increase the water demand.
2. From the previuos studies and the experimental test results exhibit that optimal steel fiber ratio is 2% and when increase the steel fiber ratio more than 2% producted less effects on compressive strength but is more effect on ultimate load.
3. The solid continuous UHPC beams exhibit more warning before failure than tubular continuous UHPC beams.
4. The presence of longitudinal hole in continuous -beams contributed in decreasing of load carrying capacity, first crack load and deflections, by 5.2%, 18.2% and 13.5%; respectively. Despite of the area ratio of hole was (11.67%) from the whole area, therefore this ratio proper to achieve flexural requirement and economical in the work.

5. The results exhibit clear improvement in compressive strength when increasing steel fiber ratio from 1% to 1.5% to 2% product increasing in fc' at about (9%) and (11%).
6. The results exhibit clear improvement in first cracking load when increasing steel fiber ratio from 1% to 1.5% and 2% at about 11.1% and 66.6% and increasing in ultimate load at about 5.2% and 18.4%. Then when compared MXB-5 (1.5% steel fiber) with reference solid (RE.S ,1.5 % steel fiber) the increasing in ultimate failure load was(20%).
7. There was not found standard method or suitable equation to predict of mix proportion of material to obtain the UHPC. Therefore used trail mixings was essential .
8. The ultimate load was increased at about (2.6%,15.78%and 20.1%) as positive reinforcement ratio increased from 1% to 1.12% ,1.71% and 1% solid beam and when negative reinforcement increased from 0.78% to 1% ,1.4% and 0.78% solid beam respectively.
9. From the test results and according to ACI condition to achieve moment redistribution in continuous beam ($\rho < 0.5\ \rho b$) it's noticed when utilized reinforcement ratio more than $0.5\rho b$ in beam (MXB-3) caused increased in (ß > 20%) in both sagging region(M^+)and hogging region (M^-).
10. It was noticed that strain values of tested beams was not greater than max value of concrete strain (0.0035).
11. The ductility is effected by steel fiber ratio and reinforcement ratio ; therefore, was observed when increasing steel fiber ratio from 1% to 1.5% and 2% the ductility increased by (7.1% and 13.36%) and inverse when increasing steel reinforcement ratio from 1% to 1.12% and 1.71 the ductility decreased by (18.3% and 23.47%) due to brittle failure of beam.

12. It is observed that the increasing in bar reinforcement ratio lead to decreasing in deflection due to high stiffness of the beam ,therefore when increasing steel reinforcement from 1% to 1.12% and 1.71% produced decreasing in deflection by (19.3% and 37%) and when increasing steel fiber ratio from 1% to 1.5% and 2% also noticed decreasing in deflection by (8.6% and 12.9%) due to high stiffness.
13. It was noticed the toughness and stiffness of beams increased when increased both bar reinforcement ratio and steel fiber ratio.
14. It was noticed increasing in number of crack when increasing steel fiber ratio due to good resistance to failure load and give more warning before failure.

5.3 Recommendations and Future Work

1. For this work , the test was performed using two point-loading and static load but is proposed in future studies to test the behavior using different load conditions such as distributed loads, cyclic loads, repeated load .
2. Study the flexural behavior of non-prismatic continuous beams with different inclination angle.
3. Study the effect of longitudinal hole in different position of UHPC beams.
4. Investigate the structura1 behavior of continuous UHPC reinforced with CFRP sheets.
5. Study the structura1 behavior of continuous UHPC beams resistance to fire.

REFERENCES

[1] Arevalo M. and Disefano D. , " design of concrete structures " Conjecture Corporation , (2013-2016).

[2] Dawood, P. M. B., and Abdulkhaleq, M. H., "Structural Behavior of Non-Prismatic Reactive Powder Concrete (RPC) Continuous Members Under Effect of Static and Repeated Loads", International Journal of Scientific & Engineering Research , vol. 8, no. January, pp. 800–806, 2017

[3] Dr. Nazar K. and Qusai K. Hameed, "Flexural Behavior of Partially Pretensioned Continuous Concrete Beams"Number 3 ,vol. 23 , journal of engineering march, 2017.

[4] Alahmari TS, Kennedy CS, Cuaron AM, Weldon BD and Jáuregui DV (2019): Field Testing of a Prestressed Concrete Bridge With High Performance and Locally Developed Ultra-High Performance Concrete Girders. Front. Built Environ. 5:114. doi: 10.3389/fbuil.2019.00114

[5] Shanmukha, "continuous beams introduction"civil engineering cite22 June2017 https://knowledge4civil.wordpress.com/category/structural-analysis-2/.

[6] E. Fehling, M. Schmidt, S. Stürwald, Ultra High Performance Concrete(UHPC) Kassel, Germany March 05-07, 2008.

[7] Nasser H.Tu'ma ,M.R.Aziz, "Flexural Performance of Composite Ultra-High Performance Concrete-Encased Steel Hollow Beams",Master Thesis,Misan University ,2019.

[8] Richard, P., and Cheyrezy , M., "Composition of Reactive Powder Concrete " , Cement and Concrete Research , Vol.25, No.7, 1995 ,pp.2.

[9] Ali Ehsani Yeganeh " Structural Behavior of Reinforced High Performance Concrete Frames Subjected to Monotonic Lateral Loading" , Master Thesis,Toronto, Ontario, Canada, 2015

[10] Moallem, Mohammad Reza. "Flexural Redistribution in Ultra-High Performance Concrete Lab Specimens." Diss. Ohio University, 2010

[11] Ultra-High Performance Concrete: A State-of-the-Art Report for the Bridge Community, Publication No. FHWA-HRT-13-060 June, 2013.

[12] Acker, P. and Behloul, M., 2004, "Ductal Technology: a Large Spectrum of Properties, aWide Range of Applications,", Proceedings of the International Symposium on Ultra High Performance Concrete, Kassel University Press, Kassel, Germany, pp 11-24 .

[13] Buitelaar, Peter. "Heavy reinforced ultra high performance concrete." Proceedings of the Int. Symp. on UHPC, Kassel, Germany. 2004.

[14] Schmidt, M.; Fehling, E.; Teichmann, T.; Bunje, K.; and Bornemann, R., 2003, "Ultrahigh performance concrete: Perspective for the precast concrete industry," Beton und Fertigteil-Technik, 2003, No. 3, pp. 16-29.

[15] Hajar, Z.; Simon, A.; Lecointre, D.; and Petitjean, J., 2004, Design and Construction of the world first Ultra-High Performance road bridges," Proceedings of the International Symposium on Ultra High Performance Concrete, Kassel University Press, Kassel, Germany, pp 39-48

[16] Resplendino, J., 2004, "First Recommendations for Ultra-High-Performance Concretes and examples of Application," Proceedings of the International Symposium on Ultra High Performance Concrete, Kassel University Press, Kassel, Germany, pp 79-90.

[17] Canadian Standards Association (CSA), CSA S6 Annex 8.1 on Fiber Reinforced Concrete, 2019.

[18] Jungwirth, J., "Under-spanned bridge structure in reactive powder concrete (RPC)", Swiss, 2002, pp. 1-6.

[19] Frank Küsel , E.Kearsley, "Effect of steel fibres in combination with different reinforcing ratios on the performance of continuous beams"Construction and Building Materials 227 (2019) 116553.

[20] Maghsoudi, A. A., and H. Akbarzadeh Bengar. "Moment redistribution and ductility of RHSC continuous beams strengthened with CFRP." Turkish Journal of Engineering and Environmental Sciences 33.1 (2009): 45-59.

[21] Mostofinejad, D., Farahbod, F. "Parametric study on moment redistribution in continuous RC beams using ductility demand and ductility capacity concept. Iran J Sci Technol. 2007. 31. Pp. 459.

[22] Visintin, P., Ali, M.A., Xie, T., Sturm, A.B. Experimental investigation of moment redistribution in ultra-high performance fibre reinforced concrete beams. Construction and Building Materials. 2018. 166. Pp. 433–444

[23] Bagge, N., O'Connor, A., Elfgren, L., Pedersen, C. Moment redistribution in RC beams-A study of the influence of longitudinal and transverse reinforcement ratios and concrete strength. Eng Struct. 2014. 80. Pp. 11–23. DOI: org/10.1016/j.engstruct.2014.08.

[24] R. Ehsani, M.K. Sharbatdar Ductility and moment redistribution capacity of two-span RC beams Magazine of Civil Engineering. 2019. 90(6). Pp. 104–118 Инженерно–строительный журнал. 2019. № 6(90). С. 104–118

[25] ACI (American Concrete Institute). 2014."Building code requirements for structural concrete and commentary". ACI 318-14. Farmington Hills, ACI

[26] Scott, R. H., and Whittle, R. T. (2005). “Moment redistribution effects in beams.” Magazine of concrete research, 57(1), 9-20

[27] ACI Committee, & International Organization for Standardization. (2008). Building code requirements for structural concrete (ACI 318-08) and commentary. American Concrete Institute.

[28] ACI 363R-92 (1997), “State-of-the-Art Report on High-Strength Concrete”, American Concrete.

[29] Federal Highway Administration (FHWA) (2006)," Material Property Characterization of Ultra-High Performance concrete", PUBLICATION NO. FHWA-HRT-06-115, USA.

[30] Japanese Society of Civil Engineers. (2008). “Concrete Engineering Series 82: Recommendations for design and construction of high performance fibre reinforced cement composites with multiple fine cracks.” JSCE, Tokyo, Japan

[31] Association Française de Génie Civil (2002) ," Ultra High Performance Fibre-Reinforced-Concretes",Recommendations-provisoires-Interim-Recomm endations. [11] ACI 544.4R-88 (1999), “Design Considerations for Steel Fiber Reinforced Concrete”, American Concrete Institute .

[32] IOSIF BUCHMAN, CĂTĂLIN BADEA, "The Characteristics of Ultra High Performance Concrete" , Politehnica” UniversityTraian Lalescu Street, no. 2 Timisoara ROMANIA ,2015 ,researchgate

[33] Gowripalan N, Ian R Gilbert (2000), "Design Guidelines for Ductal Prestressed Concrete Beams", REFERENCE ARTICLE, VSL (Aust) Pty Ltd, Australia .

[34] Samir P.Y. Hannawayya (2010)," Behavior of Reactive Powder Concrete Beams in Bending" , Ph.D. Thesis, Building and Construction Engineering Department, University of Technology .

[35] Maha M. S. Ridha (2010), "Shear Behavior of Reactive Powder Concrete Beams " , Ph.D. Thesis, Building and Construction Engineering Department, University of Technology

[36] Mahesh Maroliya (2012) ,"Elastic Characteristic of Optimized Composition of Reactive Powder Concrete", International Journal of Emerging Technology and Advanced Engineering , Volume 2,Issue 10,Vadodara,India.

[37] Nasser H. Tu'ma (2016)," behavior of reactive powder concrete beams in bending reinforced with FRP bars" , Ph.D. Thesis, Civil Engineering Department, University of Baghdad.

[38] Danha, L., S., "Tensile Behavior of Reactive Powder Concrete", M.Sc. Thesis, Building and Construction Engineering Department, University of Technology, Baghdad, 2012, 115p.

[39] Suad K. Ibraheem (2008)," Stress-Strain Relationships of Reactive Powder Concrete" , Ph.D. Thesis, Building and Construction Engineering Department, University of Technology.

[40] Haider M. Hekmet (2014)," Analysis and Behavior of RPC T-Beams in Flexure" , MSc. Thesis, Building and Construction Engineering Department, University of

[41] Samir P.Y. Hannawayya (2010)," Behavior of Reactive Powder Concrete Beams in Bending" , Doctorate Thesis, Building and Construction Engineering Department, University of Technology .

[42] Murugesan, A., and Narayanan, A. (2017). “Influence of a longitudinal circular hole on flexural strength of reinforced concrete beams.” Pract. Period. Struct. Des. Constr., 10.1061/(ASCE)SC.1943-5576.0000307, 04016021.

[43] Hadi N. Ghadhban (2013) “Experimental Behavior of Hollow Non-Prismatic Reinforced Concrete Beams” Journal of Engineering and Development, Vol. 17, No.5, November 2013 , ISSN 1813- 7822.

[44] Dr.Ahmed.J.H. Alshimmeri and Dr.Hadi.N.Gh Al-Maliki ,2014, Structual behavior of Reinforced Concrete Hollow Beam Under Partial Uniformly Distributed Load , Journal of Engineering.

[45] Balaji, G., & Vetturayasudharsanan, R. (2020). Experimental investigation on flexural behaviour of RC hollow beams. Materials today: proceedings, 21, 351-356 .

[46] Abbass, A. A., Abid, S. R., Arna'ot, F. H., Al-Ameri, R. A., & Özakça, M. (2020, February). Flexural response of hollow high strength concrete beams considering different size reductions. In Structures (Vol. 23, pp. 69-86). Elsevier

[47] Mazin B. Abdulrahman. Beams, Powder Concrete Hollow. "Strength of reinforced reactive powder concrete hollow beams." Tikrit Journal of Engineering Sciences 26.2 (2019): 15-22.

[48] Specification Test Methods, Practices, Classifications Terminology, 150 – 05 Specification for Portland Cement,1Vol.

[49] IQS 5/1984 “Portland cement Central Organization for Standardization and Quality Control Iraq” (in Arabic).

[50] ASTM C1240-04, “Standard Specification for the Use of Silica Fume as a Mineral Admixture in Hydraulic Cement Concrete, Mortar and Grout”, Vol. 4.2, 2004, 6p.

[51] Standard Specification for Chemical Admixture for Concrete ,ASTM C494/C49M-04.

[52] Standard Specification for steel reinforcement ASTM (A615/615 m).

[53] Benjamin.A.Graybeal,(2008). “Flexural behavior of an ultrahigh-performance concrete I- girder.” Journal of Bridge Engineering, 13(6), pp.602-610.

[54] ASTM C39-86, "Standard Test Method for Compressive Strength of Cylindrical Test Specimens", Annual Book of Standard American Society for Testing and Materials, Vol.04.02, 2003.

[55] ASTM C496/C496M-04, “Standard Test Method for Splitting TensileStrength of Cylindrical Concrete Specimens”, Vol. 04.02, 2004, 5p.

[56] ASTM C78-84, "Standard Test Method for Flexural Strength of Concrete (Using Simple Beam with Two Points Loading", Annual Book of ASTM Standard, Vol. 04.02, 2003.

[57] Strain gauges, TML catalog, Tokyo Sokki Kenkyujo Co., Ltd. www.tml.jp/e.

[58] Mohr, A. W. (2012). “Moment redistribution behaviour of SFRC members with varying fibre content.” Doctoral dissertation, Stellenbosch: Stellenbosch University.

[59] Canh N. Dang and Ali Alsalman , "Evaluation of modulus of elasticity of ultra-high performance concrete" 2017

[60] Kay Wille, Antoine E. Naaman, Gustavo J. Parra-Montesinos, “Ultra-High Performance Concrete with Compressive Strength Exceeding 150 MPa (22 Ksi): A Simpler Way.” ACI Materials Journal 108, no. 1 (2011). doi:10.14359/51664215.

[61] Benjamin Graybeal,2008 "Flexural behavior of an ultra high performance concrete I-girder." Journal of Bridge Engineering ,13(6),pp.602-610

[62] Behzad Nematollahi, Raizal Saifulnaz M. R., Mohd. Saleh Jaafar & Yen Lei Voo" A review on ultra high performance ‘ductile’ concrete (UHPdC) Technology",2010, International Journal oF Civil and Structural Engineering, Volume 2, No. 3, Malaysia .

[63] Graybeal B. and Marshall D. (2008), " Cylinder or Cubes: Strength testing of 80 to 200 MPa (11.6 to 29 ksi) Ultra-High-Performance Fiber-Reinforced Concrete" , ACI Materials Journal, Technical Paper, No. 105-M68 .

[64] Hafeez.Mohammed (2015), " mechanical properties of ultra high strength fiber reinforced concrete" ,Master Thesis, University of Akron, USA.

[65] Leutbecher T.; E. Fehling , (2004) ," Structural Behaviour of UHPC under Tensile Stress and Biaxial Loading ", Ultra High Performance Concrete (UHPC), International Symposium on Ultra High Performance Concrete ,PP: 435- 448, Kassel University, Germany.

[66] Mostafa El-Mogy; Amr El-Ragaby; and Ehab El-Salakawy, (2010), “Flexural Behavior of Continuous FRP-Reinforced Concrete Beams”, Journal of composites for construction, ASCE,Vol.14, No.6, pp. 669-680.

[67] Schmidt M. , E. Fehling, C. Geisenhanslüke " Ultra High Performance Concrete (UHPC)"2004, Proceedings of the International Symposium on Ultra High Performance Concrete, No. 3, University of Kassel , Germany .

[68] Xinhua Zhang and Hongzhuan Zhang , "Experimental Research on Ultra-High Performance Concrete (UHPC)" Shanghai Normal University, Shanghai, 201418, China, 2019

[69] Srinivas Allena1and Craig M. Newtson (2010), "Ultra-High Strength Concrete Mixtures Using Local Materials", Concrete Sustainability Conference, National Ready Mixed Concrete Association, New Mexico.

[70] Yang, I.H., Joh, C. and Kim, B.S. (2010). 'Structural behavior of ultra high performance concrete beams subjected to bending.' Engineering Structures, 32(11), pp.3478-3487.

[71] Mattock, A. H. (1959) Redistribution of design bending moments in reinforced concrete continuous beams, Proceedings, Institution of Civil Engineers (London), Vol. 13, pp. 35-46.

[72] Lin, Chien-Hung, & Chien, Yu-Min. (2002). Effect of section ductility on moment redistribution of continuous concrete beams, Journal of Chinese Institute of Engineers, Transactions of the Chinese Institute of Engineers, Vol. 23, No. 2, pp. 131-141.

[73] do Carmo, R., Lopes, S. Ductility and linear analysis with moment redistribution in reinforced high strength concrete beams. Canadian Journal of Civil Engineering. 2005a. 32(1). Pp. 194–203. DOI:10.1139/l04-080.

[74] Lou, T., Lopes, S.M.R., Lopes, A.V. Evaluation of Moment Redistribution in Normal-Strength and High-Strength Reinforced Concrete Beams. J Struct Eng. 2014. 140. 04014072. DOI: 10.1061/(ASCE)ST.1943-541X.0000994.

APPENDIX (A)

MegaAdd MS(D)

Densified Microsilica

DESCRIPTION

MegaAdd MS(D) is a very fine pozzolanic, ready to use high performance mineral additive for use in concrete. It acts physically to optimize particle packing of the concrete or mortar mixture and chemically as a highly reactive pozzolan.

MegaAdd MS(D) in contact with water, goes into solution within an hour. The silica in solution forms an amorphous silica rich, calcium poor gel on the surface of the silica fume particles and agglomerates. After time the silica rich calcium poor coating dissolves and the agglomerates of silica fume react with free lime ($CaOH_2$) to form calcium silicate hydrates (CSH). This is the pozzolanic reaction in cementitious system.

STANDARDS

ASTM C1240

USES

MegaAdd MS(D) can be used in a variety of applications such as concrete, grouts, mortars, fibre cement products, refractory, oil/gas well cements, ceramics, elastomer, polymer applications and all cement related products.

ADVANTAGES

- High to ultra high strength
- High resistance to chlorides and sulfates
- Protection against corrosion
- Increased durability, longer service life for structures
- Enhanced rheology, control of mixture segregation and bleed
- Greater resistance to chemicals

TYPICAL PROPERTIES at 25°C

PROPERTY	TEST METHOD	VALUE
State	Amorphous	Sub-micron powder
Colour	-	Grey to medium grey powder
Specific Gravity	-	2.10 to 2.40
Bulk Density	-	500 to 700 kg/m^3
Chemical Requirements		
Silicon Dioxide (SiO_2)	-	Minimum 85%
Moisture Content (H_2O)	-	Maximum 3%
Loss on Ignition (LOI)	-	Maximum 6%
Physical Requirements		
Specifi Surface Area	-	Minimum 15 m^2/g
Pozzolanic Activity Index, 7 days	-	Maximum 105% of control
Over size particles retained on 45 micron sieve	-	Maximum 10%

COMPATIBILITY

MegaAdd MS(D) is suitable for use with all types of cement and cementitious materials.

With Admixtures :

MegaAdd MS(D) is compatible to use with all types of water reducing plasticisers / superplasticisers and poly carboxylate based superplasticiser.

DOSAGE

The normal dosage of **MegaAdd MS(D)** is 5 - 8% by weight of cement, but it can be used up to 10%. Site trials should be carried out to establish the optimum dosage for the mix to be used as the dosage varies depending on application.

A

MegaAdd MS(D)

BATCHING	Batch **MegaAdd MS(D)** into the concrete mixer and mix thoroughly with the other mixture ingredients, adopting a procedure that ensures full dispersion of the product.	
PACK SIZE	600 Kgs and 1200 Kgs Jumbo bags	
GENERAL INFORMATION	**Shelf Life**	12 months from date of manufacture when stored under warehouse conditions in original unopened packing. Extreme temperature / humidity may reduce shelf life.
	Cleaning	Clean all equipments and tools with water immediately after use.
HEALTH and SAFETY	**PPE's**	Gloves, goggles and suitable mask must be worn.
	Precautions	Contact with skin, eyes, etc. must be avoided.
	Hazard	Regarded as non-hazardous for transportation.
	Disposal	Do not reuse bags. To be disposed off as per local rules and regulations.
	Additional Information	Refer MSDS. (Available on request.)
TECHNICAL SERVICE	**CONMIX Technical Services** are available on request for onsite support to assist in the correct use of its products.	

Manufacturer:
CONMIX LTD.
P.O. Box 5936, Sharjah
United Arab Emirates
Tel: +971 6 5314155
Fax: +971 6 5314332
Email: conmix@conmix.com www.conmix.com

Sales Office:
Tel: +971 6 5682422
Fax: +971 6 5681442

ISO9001 CERTIFIED VINÇOTTE

B

Hyperplast PC260

High performance concrete superplasticiser (Formerly known as Flocrete PC260)

Description

Hyperplast PC260 is a high performance super plasticising admixture based on polycarboxylic polymers with long chains specially designed to enable the water content of the concrete to perform more effectively.

This effect can be used in high strength concrete and flowable concrete mixes, to achieve highest concrete durability and performance.

Applications

- High strength and high performance concrete.
- Structures with congested reinforcement.
- Pre-cast concrete.
- Improved cohesion allow for use in mass concrete pours and piling.
- Self compacting concrete.

Advantages

- Optimizes cement utilization.
- High density and impermeable concrete through very high water reduction.
- Improves shrinkage and creep behaviors.
- Minimises segregation and bleeding problems by improving cohesion.
- Higher early and ultimate compressive strengths.
- Increases durability and resistance to aggressive atmospheric conditions thorough reduced permeability.

Compatibility

Hyperplast PC260 can be used with all types of Portland cement and cement replacement materials.

Hyperplast PC260 should not be used in conjunction with other admixtures unless DCP Technical Department approval is obtained.

Standards

Hyperplast PC260 complies with ASTM C494, Type A and G, depending on dosage used.

Method of Use

Hyperplast PC260 should be added to the concrete with the mixing water to achieve optimum performance.

Technical Properties @ 25°C:	
Colour:	Yellowish to brownish liquid
Freezing point:	≈ -7°C
Specific gravity:	1.1 ± 0.02
Air entrainment:	Typically less than 2% additional air is entrained above control mix at normal dosages

An automatic dispenser should be used to dispense the correct quantity of Hyperplast PC260 to the concrete mix.

Dosage

The guidance dosage of Hyperplast PC260 is 0.5 - 3.0 litre per 100 kg of cementitious materials in the mix, including GGBFS, PFA or microsilica.

Representative trials should be conducted to determine the optimum dosage of Hyperplast PC260 to meet the performance requirements by using the materials and conditions in actual use.

Effects of Over Dosage

Over dosing of Hyperplast PC260 will cause the following:

- Significant increase in retardation.
- Increase in workability.

Ultimate concrete strength will not be adversely affected and will generally be increased provided that proper concrete curing is maintained.

Cleaning

Hyperplast PC260 can be washed with fresh cold water.

Packaging

Hyperplast PC260 is available in 25 litre pails, 210 litre drums and 1000 litre bulks supply.

Hyperplast PC260

Storage

Hyperplast PC260 has a shelf life of 12 months from date of manufacture if stored at temperatures between 2°C and 50°C.

If these conditions are exceeded, DCP Technical Department should be contacted for advice.

Cautions

Health and Safety

Hyperplast PC260 is not classified as hazardous material. Hyperplast PC260 should not come into contact with skin and eyes.
In case of contact with eyes wash immediately with plenty of water and seek medical advice promptly.

For further information refer to the Material Safety Data Sheet.

Fire

Hyperplast PC260 is nonflammable.

More from Don Construction Products

A wide range of construction chemical products are manufactured by DCP which include:

- Concrete admixtures.
- Surface treatments
- Grouts and anchors.
- Concrete repair.
- Flooring systems.
- Protective coatings.
- Sealants.
- Waterproofing.
- Adhesives.
- Tile adhesives and grouts.
- Building products.
- Structural strengthening.

Antislip Aggregate

Non slip flooring aggregate

Description

Non-slip, chemically inert, graded, hard wearing aggregate available in four grades to suit most site requirements,

they are identified as follows:

Antislip Aggregate No. 1 coarse
For use with Strongcoat SL, Strongcoat HB range and Gripdeck systems or any other coating systems to produce a coarse textured, non-slip floor topping.

Antislip Aggregate No. 2 medium
For use with Strongcoat HB, Strongcoat SL range and Gripdeck systems or any other coating systems to produce a medium coarse textured floor finish.

Anti-slip Grain No.3 fine aggregate
For use with Strongcoat HB, Strongcoat SL range and Gripdeck systems or any other coating systems to produce a non-slip floor with a fine textured finish.

Anti-slip Grain No. 4 extra fine aggregate
For use only with Strongcoat WD or Strongcoat EC10 to provide a fine textured non-slip finish with thin floor coatings.

Applications

Antislip Aggregateare designed for use with Strongcoat resin products to produce non-slip industrial floors. Ideally suited for wet work areas in abattoirs, breweries,
dairies, chemical industries, food processing areas,
loading bays, ramps and walkways.

Advantages

- Range of products to suit most applications.
- Special grading to suit Strongcoat range products.
- Pre-packed ready for immediate site use.

Method of Use

Application Instructions

- All Antislip Aggregatesshould be clean and dry prior to application.
- Antislip AggregateNo. 1, No. 2 and No. 3 are designed
for use with Strongcoat HB, solvent free, resin based, roller applied floor coating and Strongcoat TC2, and Strongcoat SL self-smoothing, solvent free epoxy floor
toppings.
- In the case of application onto the Strongcoat products, a final coat of Strongcoat HB is applied.
- Antislip Aggregate No. 4 is used in conjunction with Strongcoat WD and Strongcoat EC10 floor coatings.

Application

The specially graded aggregates are scattered onto the first rolled coat of Strongcoat resin flooring whilst it is still wet. Sufficient Antislip Aggregate should be applied to
completely cover or "blind" the surface.

The selected anti-slip grain should be allowed to fall vertically onto the resin coating rather than be thrown across the surface as this may cause bridges or scour the
coatings, and damage the continuous film of the resin flooring.

When the first coat has dried, the excess aggregate can be brushed or vacuumed off the substrate and provided it is still clean and dry can be re-used.

The final roller coat of Strongcoat EC can then be applied to produce a hard wearing, chemically resistant non-slip floor. The texture and thickness of the floor is determined
by the choice of the anti-slip grain.

Anti-slip grain	Finished floor	Finished floor thick- ness for Strongcoat HB
No. 1	Coarse	2.0 – 2.5 mm
No. 2	Medium	1.0 – 2.0 mm
No. 3	Fine	0.75 – 1.5 mm
No. 4	Extra Fine	0.3 – 0.6 mm

Packaging

Antislip aggregate is available in 25 kg bags.

Storage

Antislip aggregate has a shelf life of 12 months from date of manufacture if stored in dry conditions in the original unopened bags

If these conditions are exceeded, DCP Technical Department should be contacted for advise.

Antislip Aggregate

Cautions

Health and Safety

Antislip aggregate is non hazardous

Fire

Antislip aggregate is nonflammable.

More from Don Construction Products

A wide range of construction chemical products are manufactured by DCP which include:

- Concrete admixtures.
- Surface treatments
- Grouts and anchors.
- Concrete repair.
- Flooring systems.
- Protective coatings.
- Sealants.
- Waterproofing.
- Adhesives.
- Tile adhesives and grouts.
- Building products.
- Structural strengthening.

APPENDIX (B)

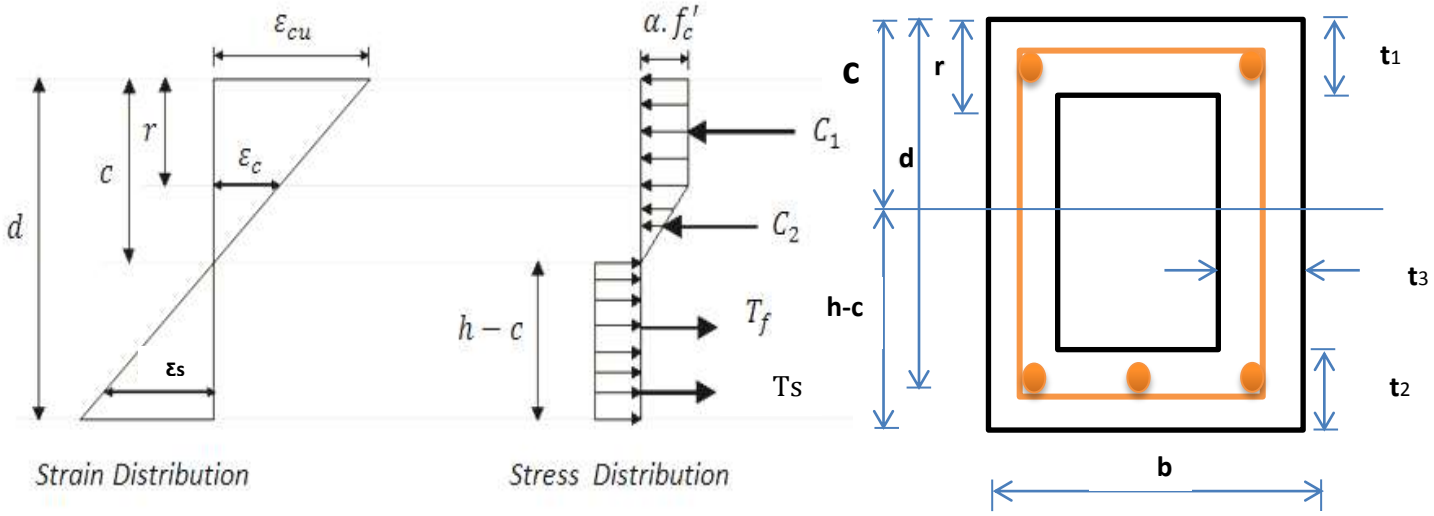

$$\mathbf{C_1} = \propto . \mathbf{f_c'} . [\, \mathbf{b} . t_1 + 2t_3\,(r - t_1)]$$

$$C = \frac{\varepsilon_{cu} \cdot}{\left(\varepsilon_{cu} + \frac{f_s}{E_s}\right)} d$$

$$\mathbf{r} = \left[1 - \frac{\propto . \mathbf{f_c'} .}{\varepsilon_{cu} . \mathbf{E_c}}\right] \frac{\varepsilon_{cu} \cdot}{\left(\varepsilon_{cu} + \frac{f_s}{E_s}\right)} . d$$

$$\mathbf{C_2} = \frac{1}{2}(\mathbf{c} - \mathbf{r}) * 2t_3 * \propto . \mathbf{f_c'}$$

$$\mathbf{C_2} = \propto . \mathbf{f_c'} * (\mathbf{c} - \mathbf{r}) * t_3$$

$$\mathbf{T_s} = \mathbf{A_s} . \mathbf{f_s}$$

$$\mathbf{T_f} = 0.4 . \sqrt{\mathbf{f_c'}} . (\, \mathbf{b} . t_2 + (\mathbf{h} - \mathbf{c} - t_2) * 2t_3)$$

$$\mathbf{T_f} = 0.4 . \sqrt{\mathbf{f_c'}} . [\, \mathbf{b} . t_2 + 2t_3 \mathbf{h} - 2t_3 \mathbf{c} - 2t_3 t_2]$$

$$(\sum \mathbf{T} = \sum \mathbf{C})$$

$$\sum \mathbf{C}$$

$$(\propto . \mathbf{f_c'})[\, \mathbf{b} . t_1 + 2t_3\,(r - t_1)] + (\propto . \mathbf{f_c'}) * (\mathbf{c} - \mathbf{r}) * t_3$$

Multiplying by $(\boldsymbol{\varepsilon_{cu}} + \frac{\mathbf{f_s}}{\mathbf{E_s}})$

G

$$(\propto.\mathbf{f_c'}).\mathbf{b}.\boldsymbol{t_1}\left(\boldsymbol{\varepsilon_{cu}}+\frac{\mathbf{f_s}}{\mathbf{E_s}}\right)+(\propto.\mathbf{f_c'}).\mathbf{2}\boldsymbol{t_3}.\left[\mathbf{1}-\frac{\propto.\mathbf{f_c'}.}{\boldsymbol{\varepsilon_{cu}}.\mathbf{E_c}}\right](\boldsymbol{\varepsilon_{cu}}*\mathbf{d})-(\propto.\mathbf{f_c'}).\mathbf{2}.\boldsymbol{t_1}.\boldsymbol{t_3}.\left(\boldsymbol{\varepsilon_{cu}}+\frac{\mathbf{f_s}}{\mathbf{E_s}}\right)$$

$$+(\propto.\mathbf{f_c'}).\boldsymbol{t_3}.(\boldsymbol{\varepsilon_{cu}}*\mathbf{d})-(\propto.\mathbf{f_c'}).\boldsymbol{t_3}.\left[\mathbf{1}-\frac{\propto.\mathbf{f_c'}.}{\boldsymbol{\varepsilon_{cu}}.\mathbf{E_c}}\right].(\boldsymbol{\varepsilon_{cu}}*\mathbf{d})$$

$$(\propto.\mathbf{f_c'}).\mathbf{b}.\boldsymbol{t_1}.\boldsymbol{\varepsilon_{cu}}+\left[\frac{\propto.\mathbf{f_c'}.\mathbf{b}.\boldsymbol{t_1}.}{\mathbf{E_s}}\right]\mathbf{f_s}+(\propto.\mathbf{f_c'}).\mathbf{2}\boldsymbol{t_3}.\left[\mathbf{1}-\frac{\propto.\mathbf{f_c'}.}{\boldsymbol{\varepsilon_{cu}}.\mathbf{E_c}}\right].(\boldsymbol{\varepsilon_{cu}}*\mathbf{d})-(\propto.\mathbf{f_c'}).\mathbf{2}.\boldsymbol{t_1}.\boldsymbol{t_3}.\boldsymbol{\varepsilon_{cu}}$$

$$-\left(\frac{\propto.\mathbf{f_c'}.\mathbf{2}.\boldsymbol{t_1}.\boldsymbol{t_3}.}{\mathbf{E_s}}\right)\mathbf{f_s}+(\propto.\mathbf{f_c'}).\boldsymbol{t_3}.\boldsymbol{\varepsilon_{cu}}.\boldsymbol{d}-\left(\propto.\mathbf{f_c'}\right).\boldsymbol{t_3}.\boldsymbol{\varepsilon_{cu}}.\boldsymbol{d}\left[\mathbf{1}-\frac{\propto.\mathbf{f_c'}.}{\boldsymbol{\varepsilon_{cu}}.\mathbf{E_c}}\right]$$

$$\left[\frac{\propto.\mathbf{f_c'}.\boldsymbol{b}.\boldsymbol{t_1}.}{\mathbf{E_s}}\right]-\left[\frac{\propto.\mathbf{f_c'}.\mathbf{2}.\boldsymbol{t_1}.\boldsymbol{t_3}.}{\mathbf{E_s}}\right]\mathrm{fs}+\left\{\begin{array}{l}\propto.\mathbf{f_c'}.\,2\boldsymbol{t_3}.\left[\mathbf{1}-\frac{\propto.\mathbf{f_c'}.}{\boldsymbol{\varepsilon_{cu}}.\mathbf{E_c}}\right].\mathrm{d}.\boldsymbol{\varepsilon_{cu}}\\ -(\propto.\mathbf{f_c'}).\,\mathbf{2}.\boldsymbol{t_1}.\boldsymbol{t_3}.\boldsymbol{\varepsilon_{cu}}\\ +(\propto.\mathbf{f_c'})\boldsymbol{t_3}.\boldsymbol{\varepsilon_{cu}}.\boldsymbol{d}\\ -(\propto.\mathbf{f_c'}).\boldsymbol{t_3}.\boldsymbol{\varepsilon_{cu}}.\mathbf{d}.\left[\mathbf{1}-\frac{\propto.\mathbf{f_c'}.}{\boldsymbol{\varepsilon_{cu}}-.\mathbf{E_c}}\right]\end{array}\right\}$$

ΣT and multiplying by $(\boldsymbol{\varepsilon_{cu}} + \frac{\mathbf{f_s}}{\mathbf{E_s}})$

$$\mathbf{A_s} \,.\, \mathbf{f_s}\left(\boldsymbol{\varepsilon_{cu}} + \frac{\mathbf{f_s}}{\mathbf{E_s}}\right) + \mathbf{0.4}.\sqrt{\mathbf{f_c'}}.\left[\,\mathbf{b}.t_2\left(\boldsymbol{\varepsilon_{cu}} + \frac{\mathbf{f_s}}{\mathbf{E_s}}\right) + 2t_3.\mathbf{h}\left(\boldsymbol{\varepsilon_{cu}} + \frac{\mathbf{f_s}}{\mathbf{E_s}}\right) - \; 2t_3.\boldsymbol{\varepsilon_{cu}}.d - 2t_3t_2\;\left(\boldsymbol{\varepsilon_{cu}} + \frac{\mathbf{f_s}}{\mathbf{E_s}}\right)\right]$$

$$\mathbf{f_s}^2\mathbf{A_s} \,.\, \mathbf{f_s}.\boldsymbol{\varepsilon_{cu}} + [\,\frac{\mathbf{A_s}}{\mathbf{E_s}}\,]\mathbf{f_s}^2 + \mathbf{0.4}.\sqrt{\mathbf{f_c'}}\,\mathbf{b}.t_2.\boldsymbol{\varepsilon_{cu}} + \left[\frac{\mathbf{b}.t_2.0.4.\sqrt{\mathbf{f_c'}}}{\mathbf{E_s}}\right]\mathbf{f_s} + \mathbf{0.4}.\sqrt{\mathbf{f_c'}}\,2t_3.\boldsymbol{\varepsilon_{cu}}.\boldsymbol{h} + \left[\frac{2t_3.\mathbf{h}.0.4.\sqrt{\mathbf{f_c'}}}{\mathbf{E_s}}\right]\mathbf{f_s} \; - \mathbf{0.4}\sqrt{\mathbf{f_c'}}.\mathbf{d}.2t_3.\boldsymbol{\varepsilon_{cu}} - \mathbf{0.4}\sqrt{\mathbf{f_c'}}.2t_3.\boldsymbol{\varepsilon_{cu}}t_2 - \left[\frac{2t_3t_2.0.4.\sqrt{\mathbf{f_c'}}}{\mathbf{E_s}}\right]\mathbf{f_s}$$

$$\left[\frac{\mathbf{A_s}}{\mathbf{E_s}}\right]\mathrm{fs}^2$$

$$+\left\{\mathbf{A_s} \,.\, \boldsymbol{\varepsilon_{cu}} \; + \left[\frac{2t_3.\mathbf{h}.0.4.\sqrt{\mathbf{f_c'}}}{\mathbf{E_s}}\right] - \left[\frac{2t_3.t_2.0.4.\sqrt{\mathbf{f_c'}}}{\mathbf{E_s}}\right] + \left[\frac{\mathbf{b}.t_2.0.4.\sqrt{\mathbf{f_c'}}}{\mathbf{E_s}}\right]\right\}\;\mathbf{f_s}$$

$$+\left\{\mathbf{b}.t_2.\boldsymbol{\varepsilon_{cu}} \,.\, \mathbf{0}.\mathbf{4}.\sqrt{\mathbf{f_c'}} \; + 2t_3.\mathbf{h}.\boldsymbol{\varepsilon_{cu}}.\mathbf{0}.\mathbf{4}.\sqrt{\mathbf{f_c'}} - 2t_3.\mathbf{d}.\mathbf{0}.\mathbf{4}.\sqrt{\mathbf{f_c'}} - 2t_3.\boldsymbol{\varepsilon_{cu}}.t_2.\mathbf{0}.\mathbf{4}.\sqrt{\mathbf{f_c'}}\right\}$$

$$\left[\frac{A_s}{E_s}\right] fs^2 +$$

$$\left\{ A_s \cdot \varepsilon_{cu} + \left[\frac{0.8\sqrt{f_c'}\, t_3 .h.}{E_s}\right] - \left[\frac{0.8\sqrt{f_c'}\, t_3 . t_2 .}{E_s}\right] - \left[\frac{t_1 .b. \propto . f_c' .}{E_s}\right] + \left[\frac{2 t_3 . t_1 . 0.4 . \propto . f_c' .}{E_s}\right] + \left[\frac{b . t_2 . 0.4 . \sqrt{f_c'}}{E_s}\right] \right\} f_s$$

+

$$\left\{ \begin{array}{l} 0.4.\sqrt{f_c'}.b.t_2.\varepsilon_{cu}.+ 0.8\sqrt{f_c'}\, t_3 .h..\varepsilon_{cu} - 0.8\sqrt{f_c'}\, t_3 .d..\varepsilon_{cu} - 0.8\sqrt{f_c'}\, t_3 .\varepsilon_{cu}.t_2 \\ -\propto . f_c'). 2. t_3 . [1 - \frac{(\propto . f_c')}{E_c . \varepsilon_{cu}}] \varepsilon_{cu} . d - (\propto . f_c'). \varepsilon_{cu} . d . t_3 + (\propto . f_c'). \varepsilon_{cu} . d . t_3 [1 - \frac{(\propto . f_c')}{E_c . \varepsilon_{cu}}] + \\ (\propto . f_c'). \varepsilon_{cu} . 2 . t_1 . t_3 \end{array} \right\} = 0$$

$AX^2 + bX + C = 0$

$A = \frac{A_s}{E_s}$

b= ✓

C= ✓

} to find $fs \leq fy$

J

الخلاصة

تعتبر مسارات الخدمة جانبًا مهمًا لأي منشأ. لذلك فأن أستخدام العناصر الأنشائية الأنبوبية (ذات فتحات طولية) طريقة جيدة لتغطية الطلب على هذه المسارات مع ما لها من فوائد أقتصادية . لذلك فأن الخصائص الأنشائية والأقتصادية التي تتمتع بها الأعتاب المجوفة هي أثنان. الأولى هي أيجابية وذات فائدة من حيث إنقاص الوزن الميت للعتبة والثانية سلبية لأنها تقلل من قوة العتبة وحمل الفشل الأقصى للعتبة. وعليه، تهدف الدراسة الحالية إلى معالجة هذه المشكلة عن طريق تقليل كمية الخرسانة المستخدمة مع الحفاظ على زيادة و مقاومة المقطع عن طريق أختيار أبعاد مناسبة للتجويف الطولي من خلال حسابات خاصة أعدت لهذا الغرض .

هذه الدراسة هو التحقيق في تصرف الأنثناء للأعتاب الخرسانية المستمرة فائقة الأداء (UHPC). تم أختبار أثنتا عشر عتبة أنبوبية مستمرة ومسّندة تحت حملين مركزين في منتصف كل فضاء . ثلاث عتبات من كل مجموعة كانت أنبوبية ، بينما كانت العتبة الرابعة مصمتة بمثابة عتبة مرجعية لغرض المقارنة. تم تقسيم الحزم إلى ثلاث مجموعات ، المجموعة الأولى لدراسة ظاهرة إعادة التوزيع العزوم ، والمجموعة الثانية لدراسة تأثير تغيّر نسبة الألياف الفولاذية والمجموعة الثالثة لمعرفة تأثير تغيّر نسبة حديد التسليح. جميع الأعتاب لديه نفس الطول الإجمالي (٣٠٠٠)ملم ، ويبلغ الطول الصافي لكل فضاء(١٤٠٠) ملم ، والعرض(١٥٠) ملم ، والعمق(٢٠٠) ملم. كان هدف الدراسة هو معرفة متى يظهر الشق الأول ،تحديد حمل التشقق الأول (Pcr) ، الحمل الأقصى (Pu) ، الهطول الخدمي (Δs) ،أقصى هطول (Δu) ، أنماط الفشل ، منحنيات الحمل – الهطول ، عرض التشققات ،أنماط التشققات ، الليونة وتوزيع الإنفعال على مدى عمق الأعتاب ، وتحديد الخواص الميكانيكية لخرسانة فائقة الأداء. وتأثير المعالجة الحرارية حيث يلعب دورًا رئيسيًا في تحسين الخواص الميكانيكية بواسطة خزان مُصنَّع بثلاثة سخانات متصلة بالكهرباء لمعالجة الحزم في الأيام الثلاثة الأولى.

ان استخدام نسب مختلفة من حديد التسليح ، ثم مقارنة العزوم المرنة والتجريبية عند الفشل لتقييم نسبة إعادة التوزيع وفقًا لمتطلبات الكود الأمريكي ACI. أثبتت النتائج التجريبية أنه عند استخدام نسبة تسليح أكثر من (٠.٥)من نسبة حديد التسليح المتوازنة في العتبة تسبب في زيادة (20 <نسبة اعادة التوزيع) في كل من منطقة التدلي (M +) ومنطقة التحدب (M-) ، وأظهرت النتائج أيضًا أن دائمًا ما يكون إعادة توزيع العزوم السالبة على المسند الأوسط أكبر منه في منتصف الفضاء وكمية اعادة توزيع العزوم فيه كانت بحدود ١٥% وهي اقل من نسبة ال ٢٠% المسموح بها في شروط الكود الامريكي.

أظهرت النتائج تحسنًا واضحًا في حمل التشقق الأولي عند زيادة نسبة الألياف الفولاذية من (١٪)إلى (١.٥٪ و ٢٪) حوالي(١١.١٪ و ٦٦.٦٪)وزيادة في الحمل الأقصى بحوالي(٥.٢٪ و ١٨.٤٪). ثم عند مقارنة (١.٥% ألياف فولاذية) بالعتبة المرجعية الصلدة (1.5٪ ألياف فولاذية) ،كانت الزيادة في حمل الفشل الأقصى بحدود (٢٠٪)، بالإضافة إلى زيادة مقاومة الانضغاط. وزاد الحمل الأقصى بحوالي (٢.٦٪ و ١٥.٧٨٪ و ٢٠.١٪) عندما تزداد نسبة التسليح الموجب من(١٪ إلى ١.١٢٪ و ١.٧١٪ و ١٪ عتبة صلدة) وعند زيادة التسليح السالب من(٠.٧٨٪ إلى ١٪ ١.٤ ٪ و ٠.٧٨٪ عتبة صلدة) على التوالي.

حيث ساهم وجود التجويف الطولي في الأعتاب المستمرة في تقليل القدرة الاستيعابية للحمل وحمل التشقق الأولي والهطول بنسبة(٥.٢٪ و ١٨.٢٪ و ١٣.٥٪)؛ على التوالى. بالرغم من أن نسبة مساحة التجويف كانت (١١.٦٧٪) من المساحة الكلية للمقطع ، فإن هذه النسبة مناسبة لتحقيق متطلبات الإنثناء واقتصادية في العمل. أخيرًا ، تم حساب العزم الاسمي ومقاومة الإنثناء من خلال الصيغ المقترحة والمعادلة المشتقة للتنبؤ بحمل الفشل العزوم في كل عتبة .

جمهورية العراق
وزارة التعليم العالي والبحث العلمي
جامعة ميسان
كلية الهندسة
قسم الهندسة المدنية

سلـوك الإنثـناء للعتبـات الأنبوبيـة المستمرة لخرسانة فائقـة الأداء

رسالة
مقدمة الى كلية الهندسة في جامعة ميسان كجزء من متطلبات الحصول على درجة الماجستير
في علوم الهندسة المدنية
(هندسة الإنشاءات)

من قبل

محمد شناوه جاسم

(بكالوريوس هندسة مدنية-٢٠١٢)

بإشراف

م.د. ناصر حكيم طعمة

آذار ٢٠٢٢ مـ رجب ١٤٤٣ هـ